Characterising Southern Ocean CO_2 Flux Variability

By

Andrew Allan Lenton BSc BAntStud (Hons)

Submitted in fulfilment of the requirements for the
Degree of Doctor of Philosophy

Antarctic Climate and Ecosystems Cooperative Research Centre and the
Institute of Antarctic and Southern Ocean Studies, University of Tasmania

November 2006

Declaration

This is to certify that the material composing this thesis has never been accepted for any other degree or award in any tertiary institution and, to the best of my knowledge and belief, is solely the work of the author, and contains no material previously published or written, except where due reference is made in the text.

Andrew Allan Lenton

Authority of Access

This thesis may be available for loan and limited copying in accordance with the Copyright Act 1968.

Andrew Allan Lenton

Abstract

The Southern Ocean, defined in this study as south of 40°S, plays an important role in mitigating climate change by sequestering atmospheric CO_2, which has continued to rise at unprecedented rates due to anthropogenic activities. The Southern Ocean is a highly variable net sink of atmospheric CO_2, but remains globally the most under-sampled ocean region for quantifying CO_2 uptake. Therefore Southern Ocean CO_2 flux estimates are subject to large uncertainties and hence the carbon budget remains poorly determined in this region. Consequently any prediction about how the Southern Ocean responds to climate change is also highly uncertain.

To compensate for limited Southern Ocean observations, a coarse-resolution (1° x 2°) prognostic, biogeochemical ocean general circulation model, driven with NCEP R-1 atmospheric forcing, was used to simulate variability in the carbon cycle. My model simulations of the ocean carbon cycle were used to tackle two important questions: 1) *What level of sampling is required to minimise uncertainty in the annual net uptake of CO_2 in the Southern Ocean?* ; and 2) *Does the large amount of interannual variability that has been simulated as well as observed have its origin in the large scale variation of atmospheric pressure in the region known as the Southern Annular Mode (SAM)?*

A sampling strategy was developed by applying 2D Fourier transforms and signal-to-noise ratios to the daily-simulated air-sea CO_2 fluxes and ΔpCO_2 between 1990-1999. Oceanic pCO_2 observations were used to validate the statistical properties of the model and to estimate the mesoscale variability not captured by the model resolution. The results showed that a sampling strategy of measuring 3-monthly, at every 30° in longitude and 3° in latitude was sufficient to determine the net annual Southern Ocean CO_2 uptake. Applying this strategy to the total simulated air-sea fluxes, the net annual mean CO_2 uptake was estimated to be 0.6 ±0.1 PgC/yr (1990-1999).

The estimated uncertainty in the sampling strategy developed was dominated by the simulated interannual variability, and not by errors in the sampling or unresolved mesoscale variability. Therefore, sampling at higher resolutions in space and time would not reduce the uncertainty in the Southern Ocean annual mean uptake any further. The results showed that a doubling of the current Southern Ocean sampling (in longitude) would be required to constrain the net annual mean air-sea CO2 fluxes to within the natural variability of the system.

The Southern Annular Mode (SAM), identified as the leading mode of atmospheric variability, has been suggested to be the driver of this large interannual variability. To explore what role the SAM played in driving Southern Ocean CO_2 fluxes between 1980-2000, the simulated air-sea CO_2 flux and its drivers were regressed against the SAM. The results showed that the change in CO_2 uptake was 0.18 PgC/yr per unit change in SAM and that 47% of the variance in interannual air-sea CO_2 fluxes in the Southern Ocean was explained by the SAM with a 4-month phase lag. This region acted as region of decreased CO_2 uptake during the positive SAM phase and increased CO_2 uptake during the negative SAM phase.

The response of the Southern Ocean to the SAM was governed by changes in ΔpCO_2 and not by changes in the gas exchange co-efficient. Component analyses showed that changes in ΔpCO_2 were due to SAM-induced changes in ocean physics controlling the supply of nutrients, primarily DIC, to the upper ocean. The SAM is predicted to become stronger and more positive in response to climate change; suggesting that this would in turn result in a net decrease in Southern Ocean CO_2 uptake.

Acknowledgments

Firstly my thanks go to my three academic advisors Richard J. Matear, Bronte Tilbrook and Tom W. Trull, who each played a unique and critical role in the supervision of this thesis. In particular I single out Richard Matear for his excellent training, friendship and the constant challenging of my science that has resulted in my development as a scientist. Many others, too numerous to list at CSIRO, ACE CRC and other scientific institutes also deserve thanks, but suffice it to say I know who you are and offer my heartfelt thanks.

To my wife Marta, my thanks could never be enough, for without your support, patience and love none of this would ever have been possible. Finally I would like to thank also my family, family-in-law and friends for your understanding and support through this thesis.

1. INTRODUCTION

1.1 Background

The increase in atmospheric greenhouse gases over the last two centuries is believed to be responsible for a detectable warming of the oceans e.g. (Levitus et al. 2000) and a net global warming of 0.6°C over the 20th century (Prentice et al. 2001). The impact that this global warming will have on our climate system is only now beginning to be understood (Prentice et al. 2001; Boyd and Doney 2004; Sarmiento et al. 2004; Orr et al. 2005).

Carbon dioxide (CO_2) in the atmosphere is the second most abundant and potent of the greenhouse gases after water vapour (H_2O). The rise in atmospheric CO_2 concentration mirrors the increased anthropogenic CO_2 emissions due to the use of fossil fuels, cement production and land use changes over the last two centuries. Prior to the industrial revolution, the rate of atmospheric CO_2 emission was balanced by oceanic and terrestrial uptake. Atmospheric CO_2 levels remained relatively stable at around 280±10 parts per million (ppm) for several thousand years (Prentice et al. 2001; Figure 1.1). Following the start of the industrial revolution, the rate of annual CO_2 emission quickly exceeded the uptake by the ocean and terrestrial biospheres, and therefore atmospheric concentrations quickly began to increase. Current projections suggest that the atmospheric value of CO_2 maybe exceed 800 ppm by 2100 (Prentice et al. 2001).

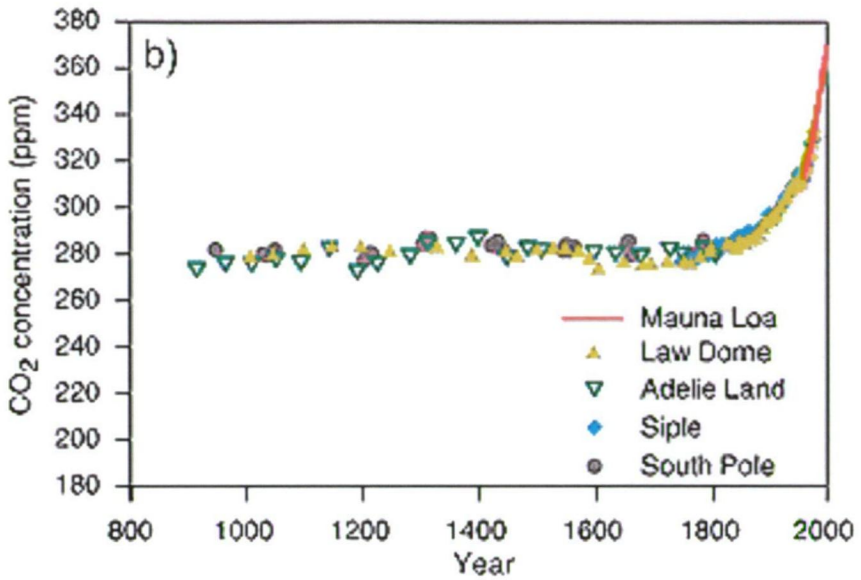

Figure 1.1 CO_2 concentration in Antarctic ice cores for the past millennium (Siegenthaler and Sarmiento 1993; Barnola et al. 1995; Netfel et al. 1995; Etheridge et al. 1996). Recent atmospheric measurements at Mauna Loa (Keeling and Whorf 2003) are shown for comparison (Prentice et al. 2001)

1.2 The Role of Oceanic Uptake

Only about 50% of the CO_2 emitted annually remains in the atmosphere. The oceans and land take up the remainder, 70% and 30% respectively. The primary pathway for CO_2 to be taken up and sequestered into the deep ocean is through surface air-sea CO_2 fluxes (Gruber and Sarmiento, 2002). It has been estimated from modeling and observational studies that the annual oceanic uptake of anthropogenic of CO_2 was ~ 2 PgC/yr during the 1990s (Watson and Orr 2003); (McNeil et al. 2003) compared with an estimated annual atmospheric emission of 6.4 ± 0.2 PgC/yr (Marland et al. 2005).

CO_2 fluxes are highly variable in space and time (Volk and Hoffert 1985; Mahadevan et al. 2004) but balance to within 2% when integrated over the earth's surface (Watson and Orr 2003). It is this 2% difference (presently ~2PgC/yr), termed the net air-sea CO_2 flux, that plays an important role in reducing the rate of climate change by slowing the rate of increase in atmospheric CO_2. The magnitude of this air-sea CO_2 flux is a function of the difference between the partial pressures of CO_2 of the atmosphere minus that of the ocean, across the boundary layer (ΔpCO_2), and the gas exchange coefficient (K), which is in turn proportional to wind speed:

$$CO_2FLUX_{AIR-SEA} = K(pCO_{2AIR} - pCO_{2SEA}) = K(\Delta pCO_{2AIR-SEA}) \qquad (1.1)$$

The concentration of CO_2 in the seawater is calculated through the equations of carbonate chemistry and is a function of dissolved inorganic carbon (DIC), total alkalinity (TALK), salinity and temperature. The concentration of each of these components depends on ocean physics, biology as well as chemical thermodynamics.

1.3 The Carbon Budget and the Southern Ocean

The energetic interactions between the atmosphere, ocean and sea ice in the Southern Ocean (Figure 1.2), result in the formation of key water masses that play a critical role ventilating deep waters of thr entire ocean and in regulating the climate system through the uptake and storage of atmospheric CO_2 (Rintoul et al. 2001; Sarmiento et al. 2004). The Southern Ocean is a region of high air-sea CO_2 flux variability and uptake (Sabine and Key 1998; Louanchi et al. 1999; McKinley et al. 2004). Recent studies have suggested the formation of SubAntarctic Mode Water (SAMW) may be responsible for as much as 40% of the annual uptake of anthropogenic CO_2 flux taken up by the oceans annually (Sabine et al. 2004).

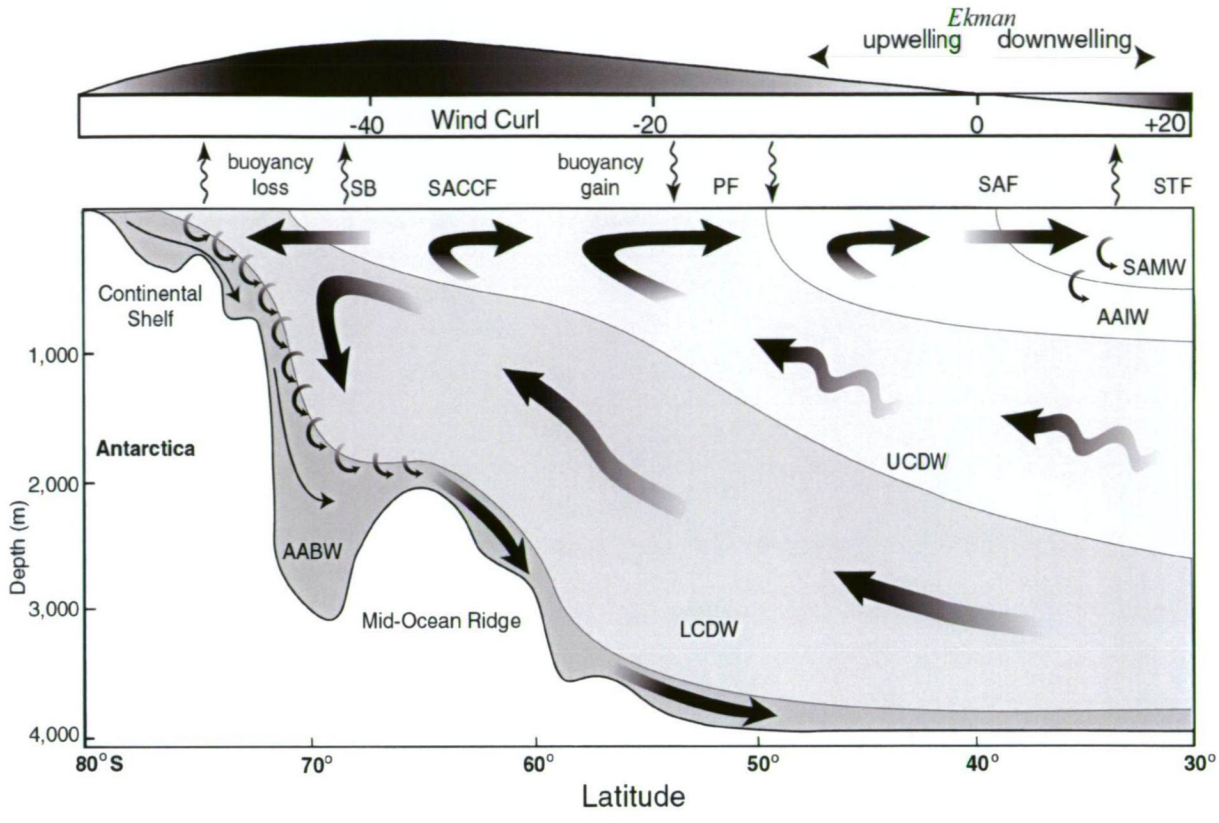

Figure 1.2 Schematic view of the meridional overturning circulation (from (Speer et al. 2000)). The upper cell is formed by northward Ekman transport and represents the formation of Antarctic Intermediate Water (AAIW) and Subantarctic Mode Water (SAMW); the lower cell results from the formation of dense AABW along the continent occurring primarily in the Ross, Weddell and Adelie Seas. Upper and Lower Circumpolar Deep Water (UCDW) and (LCDW) provide return flow (southward) and nutrients to the surface (Trull et al. 2001).

Despite the importance of the Southern Ocean in the global carbon budget, the combination of sparse sampling and high variability make characterising variability and determining the magnitude of CO_2 uptake challenging.

Estimates of the annual Southern Ocean uptake obtained from model and observational studies range between 0.2 and 0.8 PgC/yr for the 1990s (Matear and Hirst 1999; Metzl et al. 1999; Rayner et al. 1999; Takahashi et al. 2002; Roy et al. 2003; Rödenbeck et al. 2003). Interannual variability has proved even more difficult to constrain, with estimates from modeling studies showing large variations both spatially and temporally in uptake (Le Quéré et al. 2000; McKinley et al. 2004; Peylin et al., 2005).

The large uncertainties and poor characterisation of Southern Ocean air-sea CO_2 flux variability imply that predictions of its response to climate change will also be prone to the same large uncertainties. Understanding air-sea CO_2 flux, characterising its variability and balancing the Southern Ocean CO_2 budget, are necessary to predict and understand how the Southern Ocean carbon cycle will respond to climate change. The goal of this thesis study was to contribute to the characterisation of Southern Ocean air-sea CO_2 flux variability.

1.4 Approach and Overview

The lack of Southern Ocean observations is compensated for by simulating the carbon cycle, using a Biogeochemical Ocean General Circulation Model (BOGCM). The observations and model simulations are combined to address two important questions: 1) What level of sampling is required to constrain the net seasonal Southern Ocean CO_2 uptake?; and 2) Does the large amount of interannual variability CO_2 uptake simulated have its origin in large scale variations in atmospheric pressure known as the Southern Annular Mode (SAM)?

This thesis is structured in the following way:

Chapter 2. Describes the formulation of the physical and biogeochemical model. The chapter also summarises the initialisation, forcing and restoration used in the model simulations. The chapter concludes with a comparison of the simulated fields with observational and modelling studies available in the Southern Ocean.

Chapter 3. To answer the first question: What level of sampling is required to constrain the net seasonal Southern Ocean CO_2 uptake? A sampling strategy of every 3 months, every 30° in longitude and 3° in latitude, was developed by applying 2D Fourier transforms and signal-to-noise ratios to the daily-simulated air-sea CO_2 fluxes and ΔpCO_2 between 1990-1999. Oceanic pCO_2 observations were used to validate the statistical properties of the model and to estimate the mesoscale variability not captured by the model resolution. This strategy was applied to the total simulated air-sea fluxes to estimate the net annual mean CO_2 uptake (1990-1999). This chapter concludes with an estimate of the present observational uncertainty was determined by applying the current sampling strategy to the daily-simulated CO_2 fluxes

Chapter 4. The second question of this thesis is to explore whether the large interannual variability simulated in the Southern Ocean, that dominates non-seasonal variability, can be attributed to the leading mode of atmospheric variability, the SAM. To explore what role the SAM played in driving Southern Ocean CO_2 fluxes between 1980-2000, the simulated air-sea CO_2 flux and its drivers, gas exchange co-efficient and ΔpCO_2, were regressed against the SAM. A component analysis of ΔpCO_2 and its drivers: Dissolved Inorganic Carbon (DIC), alkalinity (TALK), salinity and temperature was undertaken to evaluate the relative importance of each in response to the SAM. This analysis is extended to explore what drives changes in DIC and TALK in response to the SAM. To conclude an assessment is made of how Southern Ocean CO_2 uptake may respond to the predicted changes in the SAM.

2. MODELLING THE SOUTHERN OCEAN CARBON CYCLE

2.1 Introduction

In terms of the ocean carbon system measurements the Southern Ocean remains one of the most poorly carbon sampled regions on earth. To compensate and interpolate between the limited measurements, a model of the carbon cycle was used. To explore and characterise the uptake of CO_2 in the Southern Ocean a global, prognostic, 3D biogeochemical ocean general circulation model was chosen. A global rather than regional model was chosen to avoid problems related to the parameterisation of open boundary conditions. The model we chose to simulate the components of the carbon cycle was one of the current class of coarse-resolution, global biogeochemical ocean models.

This chapter is structured in the following way:

i) Model formulation and parameterisations are described by separating the model into its physical and biogeochemical components;

ii) Initialisation, forcing and restoration used in these experiments are summarised;

iii) A comparison with the limited Southern Ocean observations is made;

iv) To conclude, a brief discussion of the suitability of the model is given.

2.2 The Physical Ocean Model

The physical component of the biogeochemical ocean model was the Commonwealth Scientific and Industrial Research Organisation (CSIRO) Mk3 ocean model. This model was based on the GFDL Z-coordinate Modular Ocean Model (MOM) - Version 3.1 (Pacanowski and Griffies 1999) that originated from the original Bryan-Cox model (Cox 1984). This model was not coupled to a sea-ice model, instead relying on the atmospheric fluxes and surface restorating, discussed later, to simulate ocean physics.

2.2.1 Model Resolution

The horizontal resolution of the model was 1.88° in longitude x 0.94° in latitude at the equator with a cosine tapering in longitude, as a function of latitude, toward the poles e.g. nominally 1°x1° at 60°S, hereafter denoted as T63_2. The vertical resolution was non-regular with 31 levels (Table 2.1), 15 in the top 500m. This resolution was sufficient to reproduce large scale features in the Southern Ocean, such as the Antarctic Circumpolar Current (ACC) and basin gyre systems (see Section 2.6). While eddies and frontal dynamics were not resolved in detail, their contributions to tracer transport were accounted for by the sub-grid scale parameterisation of Gent and McWilliams (1990) (see Section 2.2.7).

Model level k	Depth of layer (*m*)	Layer thickness (*m*)
1	5.00	10.00
2	15.00	11.62
3	28.25	13.51
4	42.02	15.71
5	59.66	18.26
6	78.54	21.22
7	102.11	24.67
8	127.88	28.68
9	159.47	33.34
10	194.56	38.75
11	236.97	45.04
12	284.65	52.36
13	341.69	60.87
14	406.38	70.75
15	483.19	82.24
16	570.87	95.83
17	674.86	111.45
18	793.76	129.61
19	934.08	150.73
20	1095.21	175.29
21	1284.65	203.85
22	1502.91	237.06
23	1758.77	275.69
24	2054.29	320.61
25	2400.00	372.85
26	2800.00	400.00
27	3200.00	400.00
28	3600.00	400.00
29	4000.00	400.00
30	4400.00	400.00
31	4800.00	400.00

Table 2.1 Vertical resolution of the CSIRO Mk3 biogeochemical model (Gordon et al. 2002)

2.2.2 Domain and Bathymetry

The model domain was global, thereby avoiding issues inherent in using open boundary conditions. The bathymetry was based on the ETOPO5 5° x 5° dataset (NOAA 1988), averaged onto the horizontal model grid. The bathymetry was then smoothed to reduce numerical noise and the sill depths were modified to ensure that important outflows such as the Baltic Sea, Hudson Sea, Persian Gulf, Red Sea and the Strait of Gibraltar were well represented (Gordon et al. 2002). This modified bathymetry reasonably reproduced the location and features of the Antarctic Circumpolar Current, discussed later.

A rigid lid version of the MOM3 model was implemented. The advantage of fixing the sea surface height was that a relatively large momentum time step could be taken and hence the speeds of the model spin up increased. This was because the fast external gravity waves and/or Kelvin waves associated with displacements of the water column under a free surface were eliminated (Pacanowski and Griffies 1999).

2.2.3 Numerical Grid Implementation

The horizontal discretisation was on the rectangular Arakawa staggered B grid (Bryan 1969) containing U and T cells. Velocity was defined as on the U grid while tracers e.g. temperature and salinity were defined on the T grid. At the centre of each T cell there was a T grid point representing the locations of the tracer quantities, likewise at the centre of each U cell there was a U grid-point that defined the location of the zonal and meridional velocities (Pacanowski and Griffies 1999; Figure 2.1).

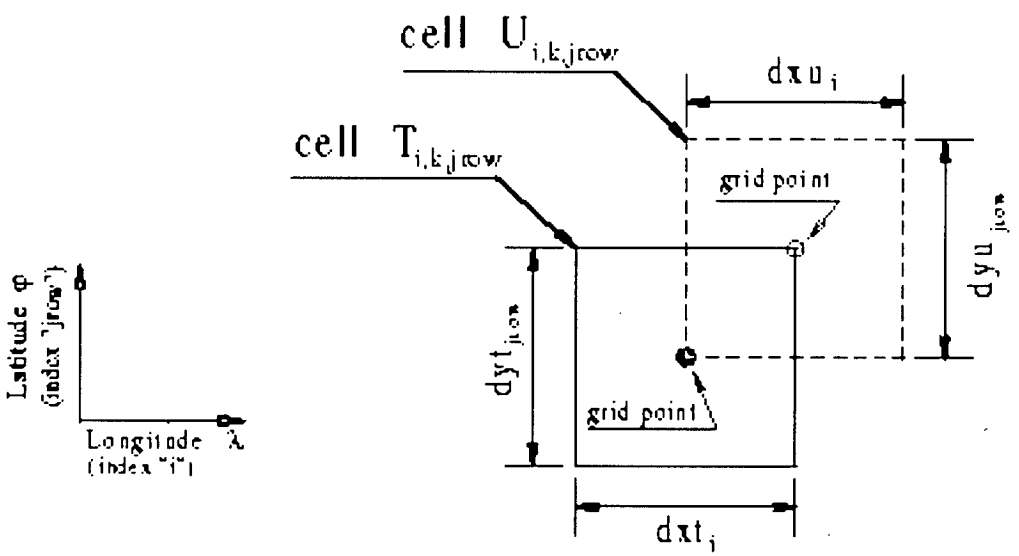

Figure 2.1 The Arakawa B grid (from Pacanowski and Griffies (1999))

In the vertical plane the U and T grids were not staggered, thus these cells were both at the same Z level and located at the centre of each grid box. This B grid has historically been most commonly implemented coarse-resolution grid for Z-coordinate ocean models, although recent model have moved toward implementing C grid. For a discussion of grids, their implementation and advantages see Griffies et al. (2000).

2.2.4 Advection

Horizontal tracer advection was implemented using the Pacanowski (1996) implementation of the third order accurate 'Quicker' scheme (Leonard 1979). This scheme was not positive definite, but it did have the advantage that it conserved tracer properties i.e. it did reduce the level of numerical dispersion (Gordon et al. 2002).

2.2.5 Background Vertical Diffusivity

From the surface to k=14 (~450m) the vertical diffusivity was prescribed to produce a more realistic thermocline in the tropics (Gordon et al. 2002) and was modified by the Chen mixed layer scheme (Chen et al. 1994) described in Section 2.2.8.

Vertical diffusivity for k > 14 (κ_v) was parameterised with a depth-dependent hybrid scheme (Bryan and Lewis 1979) shown below (Equation 2.1). This provided for a reasonable representation of the deep-water vertical property gradients.

$$\kappa_v = 0.8 + \left(\frac{1.05}{\pi}\right)\tan^{-1}\left[4.5\times10^{-5}(z-2500m)\right] \qquad (2.1)$$

2.2.6. Sub-grid Scale (SGS) Mixing and Tracer Mixing: Horizontal Diffusivity

To represent the effect of eddies not explicitly represented in the model, the Griffies (1998) parameterisation of the GM90 scheme (Gent and McWilliams 1990) was implemented. This parameterisation includes mixing along isoneutral surfaces and effective transport velocity. The value of isopycnal or eddy diffusivity thickness (κ_I) was set to 1 x 10^7 cm^2/s, except in regions of steep isopycnal surfaces in which κ_I was tapered according to Gerdes et al. (1991) to avoid numerical instability. The Redi (1982) mixing scheme was used to represent mixing along isopycnal surfaces. This scheme has been shown to improve the stratification and subsurface ventilation of the Southern Ocean (Hirst et al. 2000), aiding in the formation of SubAntarcic Mode Water (SAMW) (Dutay et al. 2002).

2.2.7 Viscosity

Horizontal viscosity parameterisation (a_m) was a function of latitude, shown below (Equation 2.2) where ϕ refers to latitude and the constant of proportionality was set as $a_o = 3 \times 10^8$ cm^2/s.

$$a_m = a_o \cos\phi \tag{2.2}$$

Vertical viscosity (κ_m) was parameterised with a constant background value of 20 cm^2/s.

2.2.8 Mixed Layer Scheme

To represent mixing in the upper ocean the Chen mixed layer scheme (Chen et al. 1994) was implemented. This is a hybrid mixed layer scheme that combines an estimate of mixed layer depth from a bulk mixed layer model, the Kraus-Turner (K-T) scheme (Kraus and Turner 1967), with the dynamic instability model of Price et al. (1986). The implementation used in the physical model followed Pacanowski and Philander (1981), using the Richardson number dependence of Price et al. (1986) as suggested by Chen et al. (1994).

The implementation of the hybrid Chen scheme accounted for differences in the dominant processes that control mixing in high and low latitudes (Godfrey and Schiller 1997). In the Southern Ocean, south of Australia, this scheme despite showing a bias towards too shallow summer mixed layers (Wang and Matear 2001), does produce reasonable seasonal cycles of mixed layer depth, discussed later.

2.3 The Biogeochemical model

The biogeochemical model was a prognostic (non-nutrient restoring) four-component model that included phosphate (PO_4), dissolved inorganic carbon (DIC), alkalinity (TALK) and oxygen (O_2). The O_2, DIC and PO_4 were related to each other via the Redfield ratio P:N:C:O_2 of 1:16:106:-138 (Redfield et al. 1963).

This is a relatively low-order biogeochemical model, with two major advantages: 1) it is efficient to run at high resolution; and 2) unlike higher order models, it can be better constrained in the poorly observed Southern Ocean. This biogeochemical model has been implemented and the limitations evaluated in previously published studies e.g. (Matear and Hirst 1999; Matear 2004).

2.3.1 Tracer Equations

For each of the four biogeochemical tracers (Tr) the following equation can be written:

$$\frac{\partial T}{\partial t} = \nabla.(\vec{u}Tr) + \nabla.(K\nabla Tr) + \frac{\partial}{\partial z}\left(K_z \frac{\partial Tr}{\partial z} \right) + Q(Tr)_{FLUX} + Q(Tr)_{REMIN} + Q(Tr)_{VFLUX} \tag{2.3}$$

The first three terms (Equation 2.3) describe the behaviour of each tracer due to ocean dynamics. The first term is the advection due to Eulerian and GM velocities. The second and third terms refer to horizontal isopycnal and vertical eddy diffusion of the tracer respectively.

The Q_{FLUX} denotes the air-sea exchange of each tracer, Q_{REMIN} denotes the export and remineralisation of material and the Q_{VFLUX} terms refers to the change in tracer concentration due to dilution by freshwater fluxes, also known as virtual flux. There is no air-sea flux term for PO_4 and TALK (i.e. $Q_{FLUX} = 0$). In the following sections the parameterisations of each of the biogeochemical terms (Q_{FLUX} , Q_{VFLUX}, Q_{REMIN}) is discussed.

2.3.2 Air-Sea Fluxes (Q_{FLUX})

The air-sea exchange term (Q_{FLUX}) in O_2 and DIC is driven by the differences in partial pressures across the air and sea boundary layer, shown below (Equation 2.4).

$$Q(Tr)_{FLUX} = K(p(Tr)_{AIR} - p(Tr)_{SEA})) \qquad (2.4)$$

K denotes the gas exchange co-efficient calculated as a function of wind speed, solubility (for CO_2)/saturation (for O_2) and the Schmidt number. The wind speed dependence of the gas exchange co-efficient follows Wanninkhof (1992). Solubility and the Schmidt number for CO_2 were calculated using the formulations of Weiss and Price (1980) and Wanninkhof (1992) respectively. The saturation and Schmidt number for O_2 were calculated from formulations of Garcia and Gordon (1992) and Keeling et al. (1998) respectively.

The partial pressures of CO_2 and O_2 were calculated from standard equations of carbonate chemistry; for a more detailed description refer to Murray (2004). The implementation of the carbonate chemistry in the model was taken from a modified version of the Ocean Carbon Model Intercomparsion Project 2 (OCMIP2) carbonate chemistry routines (Najjar and Orr 1998) as sourced from Dickson and Goyet (1994).

The lack of sea-ice required that the air-sea flux of CO_2 and O_2 were scaled by values between 0 and 1, where 1 represents ice-free conditions, as determined from observed monthly climatological northern and southern hemisphere sea-ice cover from Walsh (1978) and Zwally et al. (1983) respectively.

These parameterisations were chosen to ensure that the model was consistent with the protocols of the Northern Ocean Carbon Exchange Study (NOCES)/Ocean Carbon Model Intercomparsion Project 3 (OCMIP3) (http://www.ipsl.jussieu.fr/OCMIP/) (Aumont et al. 2004). Final model output was submitted for participation in this project.

2.3.3 Virtual Fluxes (Q_{VFLUX})

Implementing a rigid lid model required that ocean volume be conserved. Therefore freshwater fluxes were parameterised as a positive or negative dilution of the surface layer (10m) tracer concentration. Freshwater fluxes in the model were a combination of an imposed surface freshwater flux and a surface restoring flux, discussed later.

To calculate the change in tracer concentration in each grid box, the following equation was used (Equation 2.5). The initial value of the tracer was multiplied by the change in surface salinity divided by the initial concentration of the surface grid cell. In general the virtual flux adjustments to the tracer fields were quite small.

$$Q(Tr)_{VFLUX} = \frac{\Delta SSS}{SSS} \times Tr \qquad (2.5)$$

2.3.4 Remineralisation and Export (Q_{REMIN})

2.3.4.1 Phytoplankton Growth Rate

Biological nutrient transformations and transports were parameterised as a function of physical variables, with no tracking of any of the biological components. Nutrient transformations took place in the euphotic zone (surface to 1% of the incident radiation level) through biological activity. This biological activity was parameterised by the Phytoplankton Growth Rate (*PGR*) and calculated as a function of temperature (^{o}C). An empirical third order polynomial expansion of the Eppley growth rate (Eppley 1976) shown below for *PGR* was used (Equation 2.6). This varied from 0.26 in the cold waters of the sea-ice zone (SIZ; -1.88 °C) to 0.65 in the northern SubAntarctic Zone (SAZ; 15 °C).

$$PGR(T) = 0.29 + 0.015938T + 0.00046195T^2 + 4.3542 \times 10^{-6} T^3 \qquad (2.6)$$

2.3.4.2 Production

Biological Production (*BP*) of particulate organic carbon (*POC*) was calculated as a function of light, nutrients (PO_4), and *PGR*. It was then scaled as a function of the euphotic zone depth (Equation 2.7). *POC* was related to Particulate Inorganic Carbon (PIC) below via the rain ratio of 8.48 following (Yamanaka and Tajika 1996).

$$BP = \sum_{k=1}^{4} S\left(\frac{h_e}{h}\right)\left(\frac{I}{I_o}\right)\left(\frac{P}{P+P_o}\right)PGR(T)\Delta z \qquad (2.7)$$

S was a scaling factor, set to 0.01 to ensure compatibility with observations and Δz was the depth of the model layer. I was the prescribed daily averaged incident radiation, as a function of latitude and time, while I_o was the solar constant. P was the PO_4 concentration from the model and P_o was the half-saturation value of phosphate from (Eppley 1972) set at 0.02 mmolP/l, from the half-saturation of nitrate scaled via the Redfield ratio (Redfield et al. 1963). The mixed layer depth (h) was from the Chen mixing scheme (Section 2.2.8) and the depth of the euphotic zone (h_e) was set to 50m.

2.3.4.3 Export Production

The export production (*EP*) of each tracer (*Tr*) from the euphotic zone is described below (Equation 2.8), where *a* is the Redfield Ratio of 1:16:106:-138 (P:N:C:O_2). The export of calcium carbonate ($CaCO_3$) was fixed at 8% of POC following Yamanaka and Tajika (1996) consistent with Trull et al. (2001).

$$EP = aBPh_e \tag{2.8}$$

2.3.4.4 Remineralisation

Below the euphotic zone, remineralisation of each tracer occurred with no time lag as described below (Equation 2.9).

$$Q(Tr)_{REMIN} = aEP\frac{d[R(z)]}{dz} \tag{2.9}$$

R(z) is the remineralization function described below (Equation 2.10) for POC as a standard profile of downward flux (Yamanaka and Tajika 1996). Remineralisation depth (z_R), was set to 100m, while the value of *n* was set at 0.9 - these values were both deduced from sediment trap data (Suess 1980; Martin et al. 1987).

$$R(z) = \left(\frac{z}{z_R}\right)^{-n} \tag{2.10}$$

Remineralisation of $CaCO_3$ followed Yamanaka and Tajika (1996), shown below (Equation 2.11). The model remained consistent with carbonate chemistry by ensuring that for every mole change in $CaCO_3$, DIC changed by 1 mole and TALK by 2.

$$R(z) = e^{\left(\frac{-z}{3500m}\right)} \tag{2.11}$$

If not all of the POC was remineralised by the time it reached the bottom (of the ocean) it was remineralised in the bottom grid-cell.

2.4 Simulations

2.4.1 Initial Conditions and Integration

The model was initialised from observations of temperature, salinity and phosphate from Conkright et al. (2002). The model was then evolved for > 4300 years. As the model had not yet reached quasi-steady state in accordance with the criteria of (England 1995), and to ensure upper ocean dynamics were well captured, the temperature and salinity fields were reinitialised from Conkright et al. (2002). This was done in accordance with the protocols of the Northern Ocean Carbon Exchange Study (NOCES)/Ocean Carbon Model Intercomparsion Project 3 (OCMIP3) (Aumont et al. 2004).

2.4.2 Atmospheric Forcing

The heat flux, freshwater flux, wind stress and short-wave heat flux used to drive this model were taken from NCAR/NCEP Reanalysis 1 (R1) for the 55-year period between 1948 and 2003 (Kalnay 1996; NOAA 2005). Initially the model was formulated to run with the NCEP R2 atmospheric forcing fields (Kanamitsu et al. 2002). As this dataset only existed between 1979 and the present, the decision was taken to use the earlier R1 dataset. This also enabled participation in the NOCES (OCMIP3) project.

Daily fluxes from NCEP were an average of the six-hourly fields. Wind stresses and net short-wave radiation fluxes were applied directly from NCEP-R1. The net surface heat flux was calculated as the sum of turbulent (sensible, latent) and radiative (short-wave, long-wave) components shown below (Equation 2.12).

$$Q_{HEATFLUX} = Q_{SENS} + Q_{LATENT} + Q_{LONGWAVE} + Q_{SHORTWAVE} \tag{2.12}$$

Freshwater flux was calculated as shown below (Equation 2.13), where P denotes precipitation and E evaporation.

$$Q_{FRESHWATERFLUX} = P - E \tag{2.13}$$

2.4.3 Physical Surface Restoration

To compensate for a lack of sea-ice and ensure the model did not drift too far from the observed temperatures and salinities, the surface fields of temperature and salinity were restored to observed values. Temperature was restored to Reynolds and Smith (1994) (1948-2003) and salinity to annual mean climatological values Conkright et al. (2002).

Surface restorating was applied by calculating the difference between the simulated observed values, and applying this differences as either a freshwater flux or a heat flux over the chosen restoring period (discussed in Section 2.5).

2.5 The Model Experiment

The model experiment was run in accordance with the NOCES protocols (Aumont et al. 2004). These protocols involved prescribing the year 1837 to the model and evolving it from 1837-2003 (165 years) using observed atmospheric CO_2 values from Enting et al. (1994) and from GlobalView2003 MLO data. The evolution of the model was completed in two stages. This was required to allow freshwater fluxes to vary interannually, since no interannually varying time-series of observations were available for the Southern Ocean.

In the first stage, NCEP R-1 atmospheric forcing fields were applied twice, between 1837-1892 and 1893-1947 (110 years). During this period, sea surface temperature (SST) and salinity were restored to observed values over a 30-day time scale.

In the second stage, NCEP-R1 atmospheric forcing fields were applied to the final 55 years of the model (1948-2003), with only SST restored every 30 days to the observed values. Freshwater fluxes were derived by calculating the average difference between the modelled freshwater flux and NCEP-R1 from the previous 55 years (1893-1947). This mean difference was added to the NCEP-R1 forcing to allow salinity to vary interannually. An additional weak 2-year restoring of surface salinity to observations was required to avoid excessive model drift.

2.6 Physical Response of the Southern Ocean.

To assess the suitability of the model for exploring air-sea CO_2 flux variability, the simulated physical response of the Southern Ocean was compared with the observations. The annual means were compared to allow the maximum information to be extracted from the limited observations. In this section:

- the structure of the Southern Ocean is discussed and the locations of the major fronts identified and compared with observations;
- the zonal sections of temperature, salinity and density were compared with those from Conkright et al. (2002);
- the barotropic stream function, the zonally averaged meridional overturning stream functions are assessed against published studies; and
- the summer and winter mixed layer depths are also assessed against published studies.

In simulating the dynamics of the Southern Ocean a 'measurement' was generated for every day over the time period, in this way the true annual mean was generated. In contrast, the observations were in general sparse and biased toward the summer period and hence a potential source of error was introduced in the following comparison.

The Southern Ocean is comprised of four major regions from north to south, the Subtropical Gyre (STG), the SubAntarctic Zone (SAZ), the Polar Frontal Zone (PFZ) and the Antarctic Zone (AZ). These regions are separated by three major fronts, the Subtropical Front (STF), the SubAntarctic Front (SAF) and the Polar Front (PF). These features are identified in Figure 2.2.

To identify the location of Southern Ocean fronts, a variety of definitions based on different combinations of density, temperature and salinity have been used e.g. (Orsi et al. 1995; Belkin and Gordon 1996; Trull et al. 2001). More recently sea surface height (SSH) anomalies have been used to identify water masses and the fronts that separate these (Sokolov and Rintoul 2002). In the Southern Ocean, many of these studies have identified additional fronts between the north, middle and southern parts of each interfrontal zone. As the resolution of the ocean model was only nominally 1° x 2° (NS- EW) only the 3 major fronts were identified, based upon the potential temperature (θ) based definitions using annual mean climatological values. The definitions were:

i) The Subtropical Front (STF) $\theta < 10°C$ at 150m from Orsi et al. (1995)

ii) The SubAntarctic Front (SAF) $\theta > 4°C$ at 400m from Orsi et al. (1995)

iii) The Polar Front (PF) $\theta > 2°C$ at 300m from Trull et al. (2001)

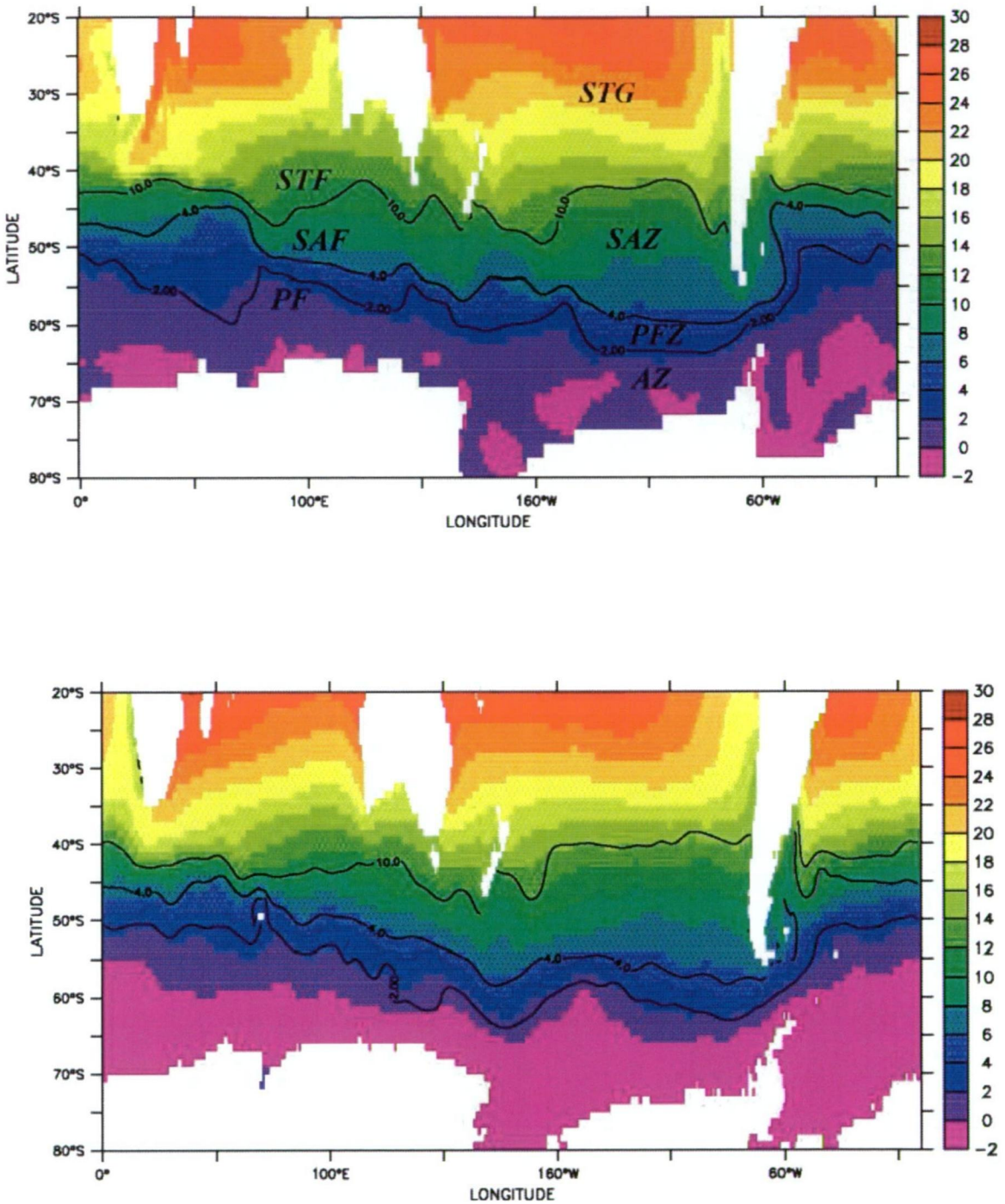

Figure 2.2 Surface temperature maps from the model (top) and WOA observations (bottom), showing the positions of the major Southern Ocean fronts, see text for frontal definitions.

The annual mean positions of the fronts from the model were calculated and compared with those from Conkright et al. (2002) using the same definitions. A good agreement between the modelled and observed frontal position was seen. The exceptions were: south of Kerguelen Island, where the simulated PF showed a significant southward deviation compared with the observations; and on the eastern side of South America where the model did not capture the observed northward frontal excursions.

The modelled positions of these fronts did show large north and south spatial deviations (> 3°) from the mean position. This is consistent with observations from satellite altimetry in the Australian Sector of the Southern Ocean (Sokolov and Rintoul 2002).

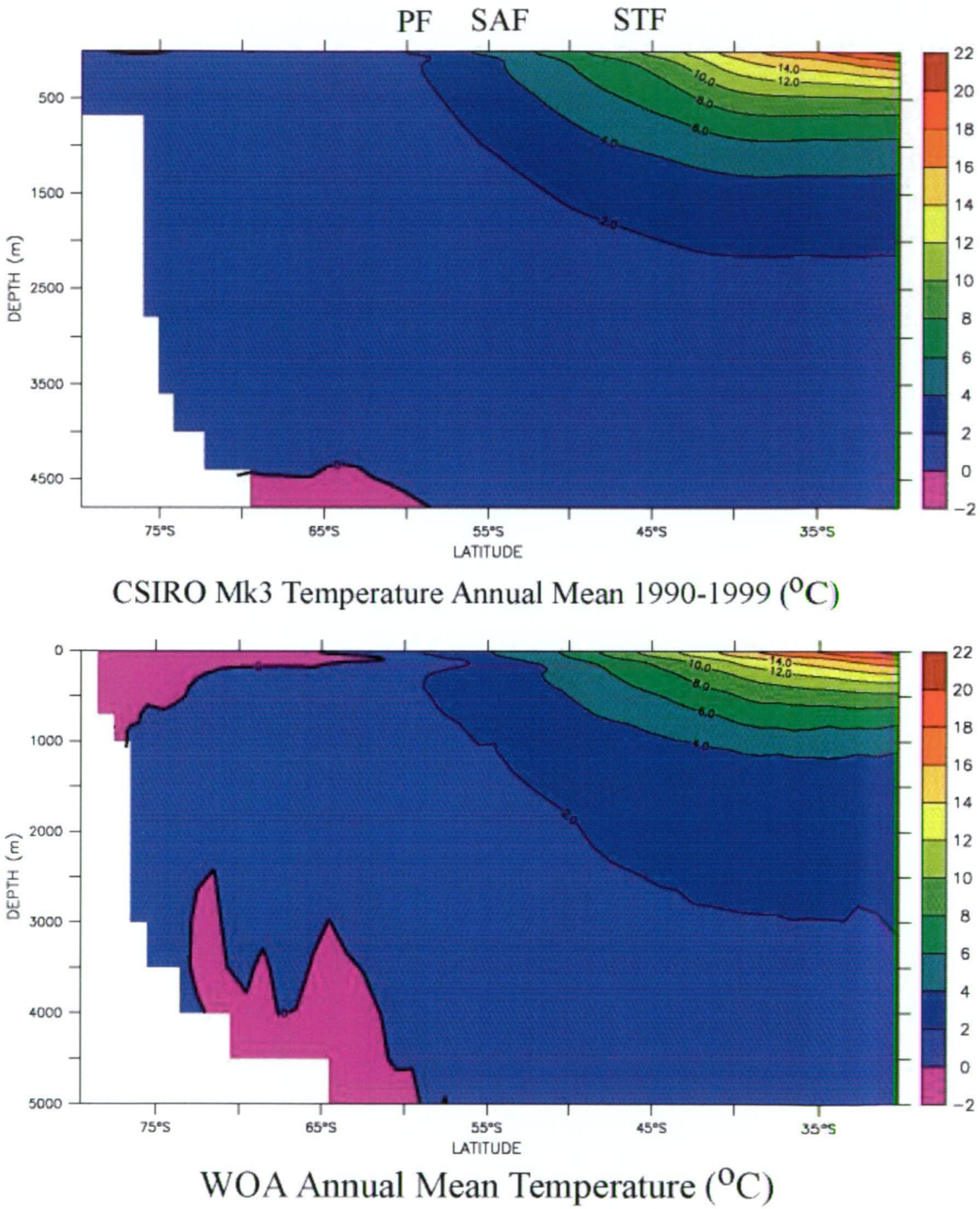

Figure 2.3 Zonal annual mean potential temperature from the model (top) (1990-1999) and from observations (Conkright et al. 2002) (bottom)

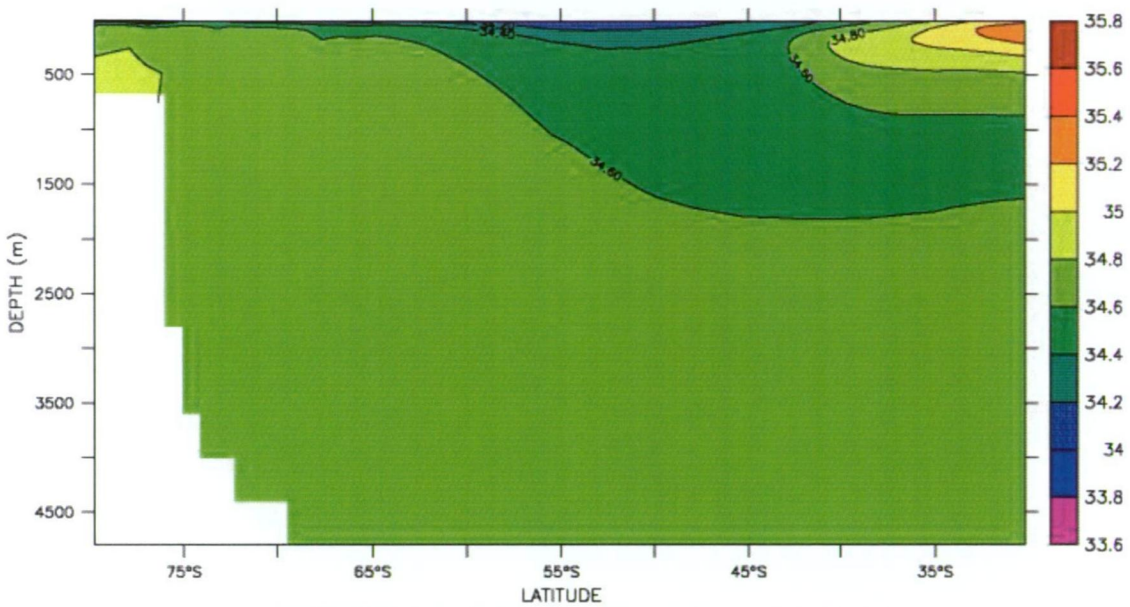

CSIRO Mk3 Salinity Climatology 1990-1999

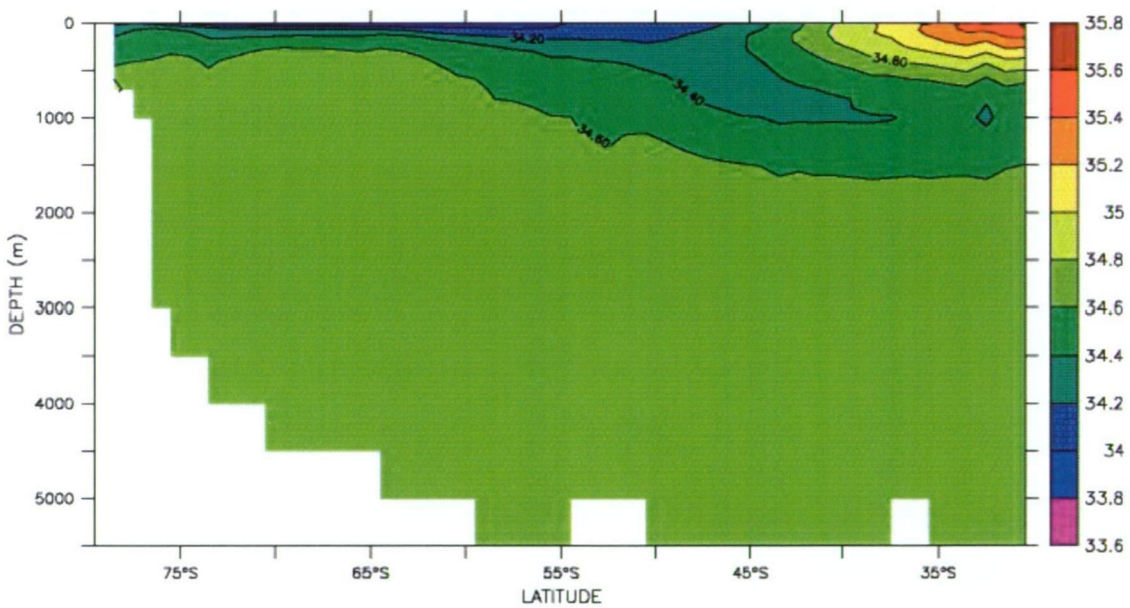

WOA 2001 Salinity Climatology

Figure 2.4 Zonal annual mean salinity (psu) from the model (top) (1990-1999) and from observations (Conkright et al. 2002) (bottom)

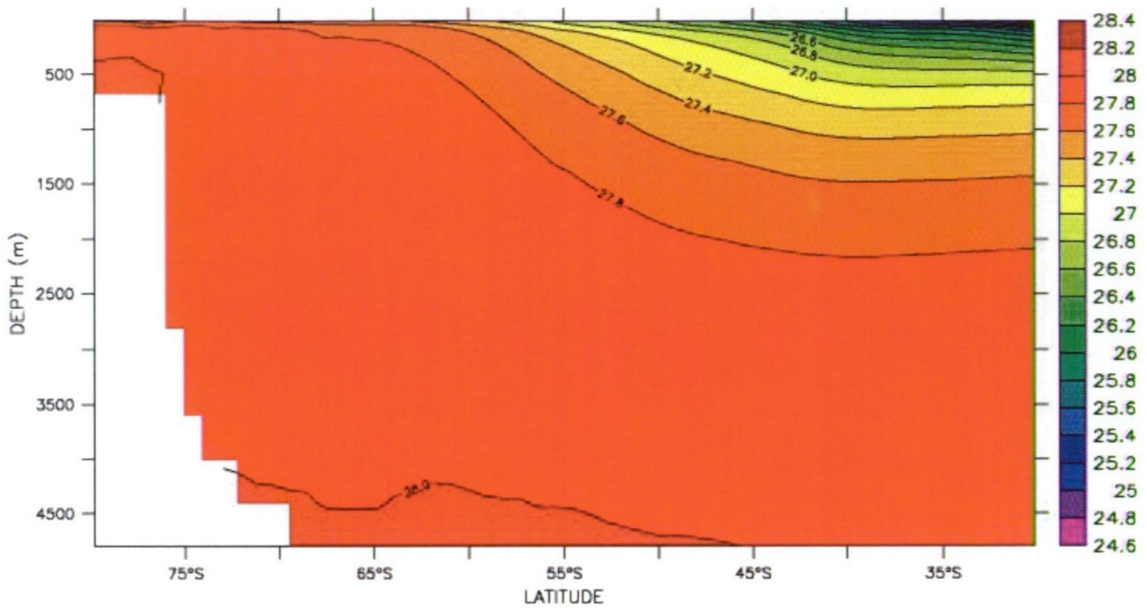

CSIRO Mk3 Climatology Density 1990-1999

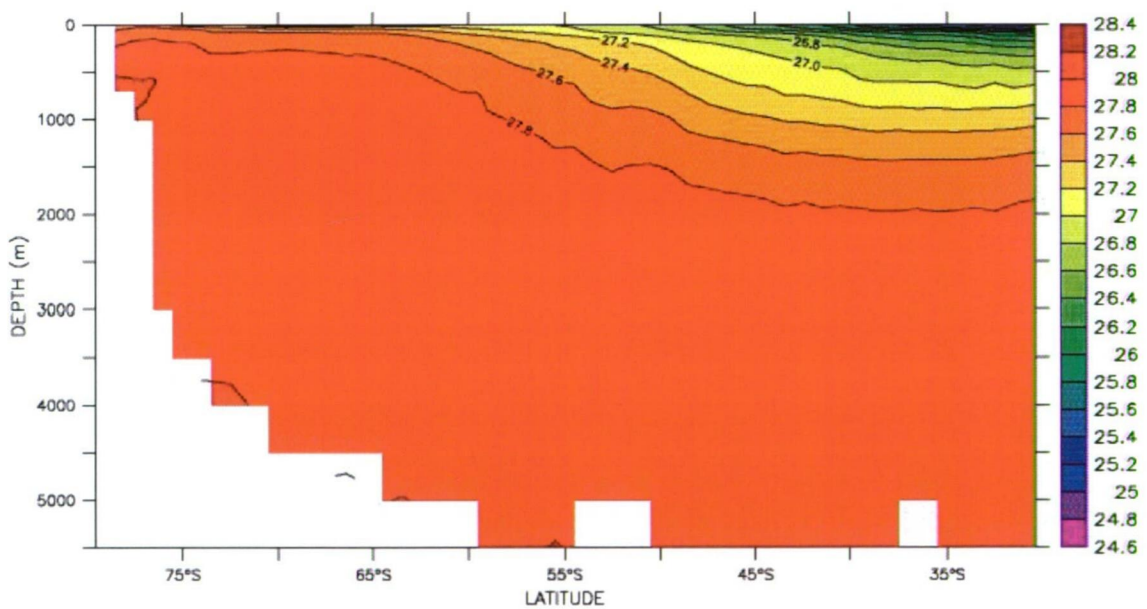

World Ocean Atlas Climatology Density

Figure 2.5 Comparison between the zonal annual mean potential density between the model (top) and the observations (Conkright et al. 2002) (bottom), units are (kg/m^3 – 1000)

The salinities, potential temperatures and potential densities simulated in the model, were compared with those from the World Ocean Atlas 2001 (WOA) (Conkright et al. 2002) (Figures 2.3-5). There was generally good agreement between the model and observations. However at the continental margins, along the Antarctic Slope and near the bottom, the model was in general too warm and too fresh. This was indicative of a poor representation of Antarctic Bottom Water (AABW). There were two reasons for this: firstly the model lacked sea ice and relied on NCEP-R1 fluxes, which in themselves have been suggested to be poorly validated in polar regions (Marshall 2002), and also on surface restoration; secondly AABW formation results in part from polynya processes, which can only be modelled at much higher resolution (Marsland et al. 2004). The good agreement in density suggested that the deviations by the model from observations (in temperature and salinity) appear to have a compensating effect.

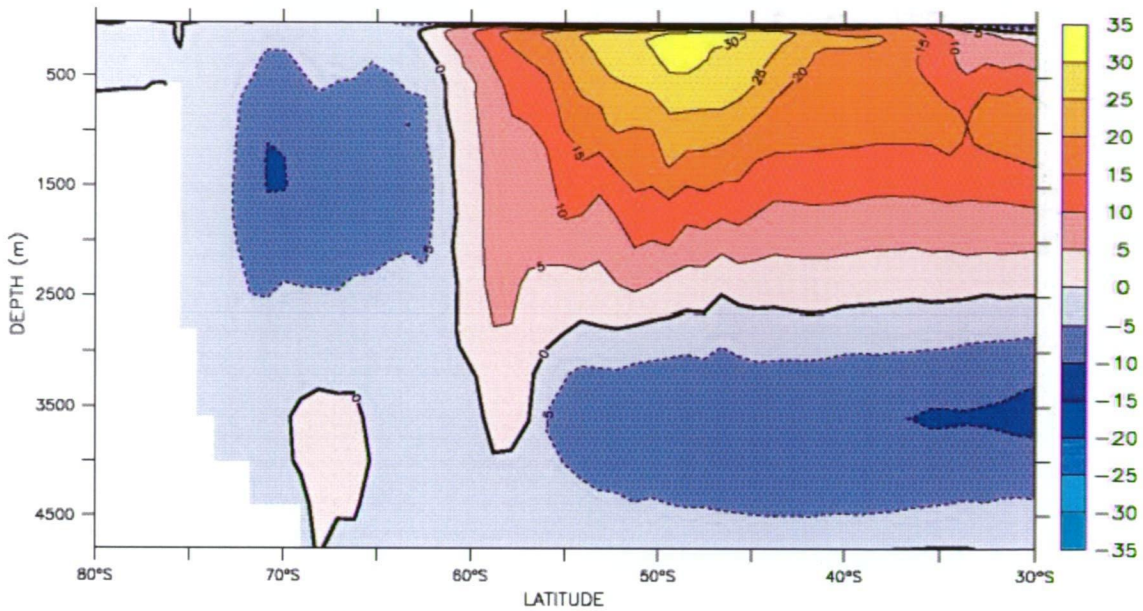

CSIRO Mk3 Model Meridional Stream Function (Sv)

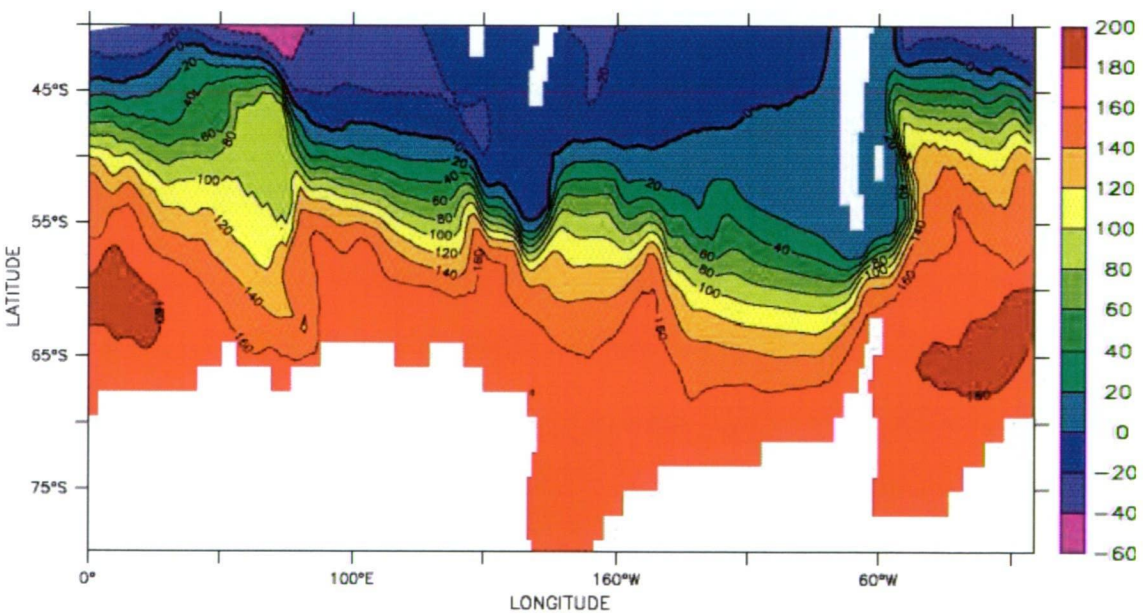

CSIRO Mk3 Model Stream Function (Sv)

Figures 2.6(a) Meridional Overturning Stream Function (Sv; Eulerian+ GM) (top) and 2.6(b) The Barotropic Stream Function (Sv) from the model between 1990-1999 (bottom)

The Southern Ocean meridional stream function included the contribution from both Eulerian and GM velocities (Figure 2.6(a)). The strength of the modelled Southern Ocean cell was -10.5 Sv at 1300 m near 71°S while the maximum strength of the AABW cell was -11.5 Sv near 23°S at 3500 values are consistent biogeochemical ocean models (Doney et al. 2004). The wind-driven Deacon cell with a value of ~32 Sv was also consistent with results from coarse-resolution biogeochemical ocean models of between 18-30Sv (Doney et al. 2004).

The decadal mean barotropic stream function, Figure 2.6(b), showed an estimated Drake Passage transport for the 1990s of ~160 Sv. Although this value was larger than observed 136.7 ± 7.8 Sv (Cunningham et al. 2003), it is also consistent with the current range of values from coarse-resolution biogeochemical ocean models (Doney et al. 2004). To be noted is that few observations exist by which to validate the large-scale circulation, instead by demonstrating that the values from the model fall within the current class of coarse-resolution biogeochemical ocean models, provides both a context and perspective of these results.

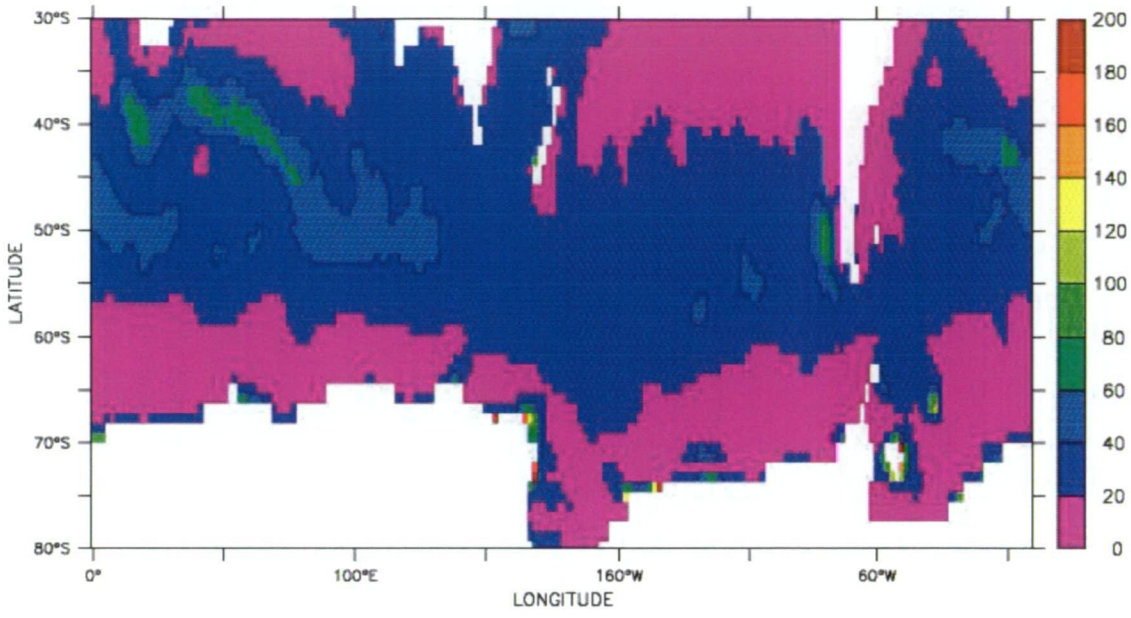

CSIRO Mk3 January Clim Mixed Layer Depth (0.1)

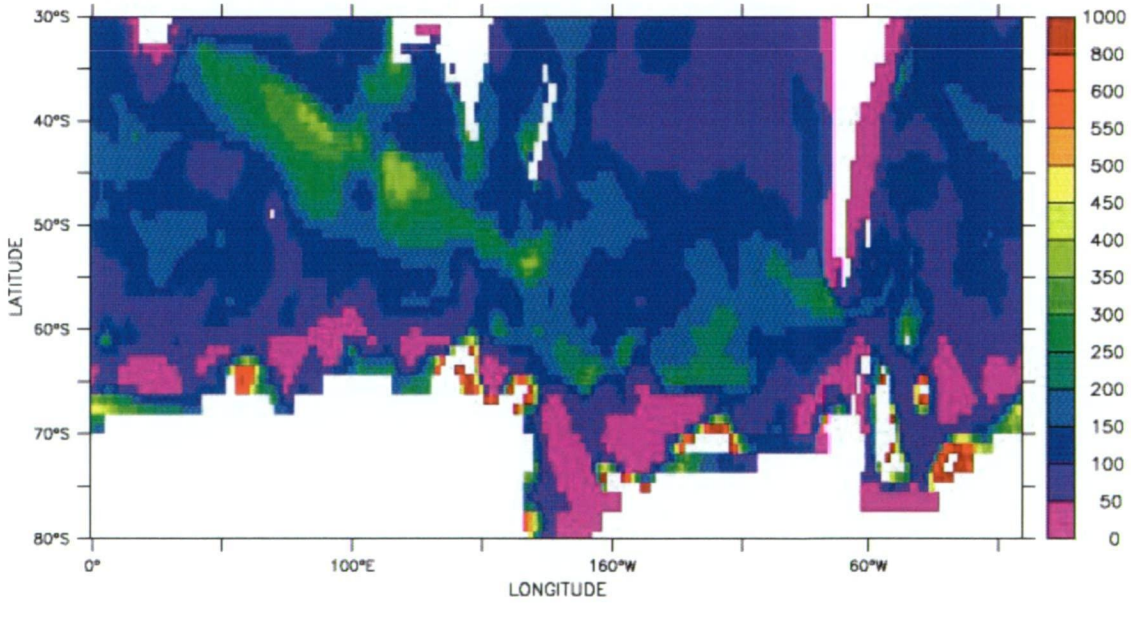

CSIRO Mk3 July Clim Mixed Layer Depth (0.1)

Figures 2.7(a) Summer (top) and 2.7(b) Winter (bottom) mixed layer depths (m) based on the 0.1 (kg/m^3) potential density criterion

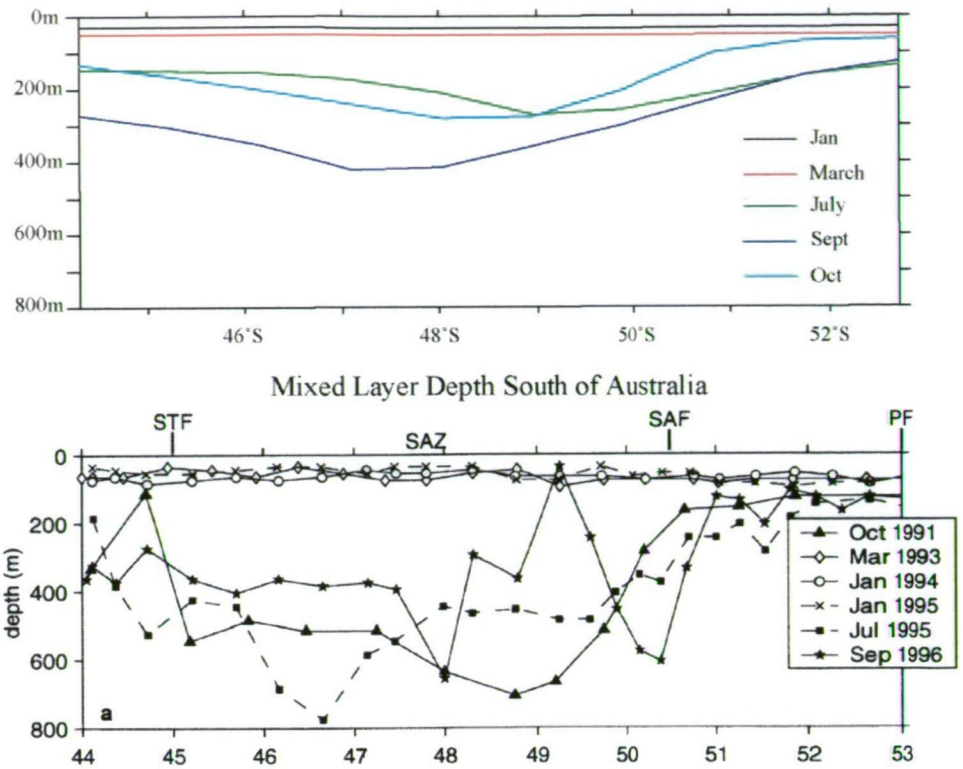

Figures 2.8 Mixed layer depths south of Australia (m) and based on the 0.1 (kg/m^3) potential density criteria from (a) the monthly mean values of model; and (b) monthly observed values from Rintoul and Trull (2001).

Realistic representation of seasonal mixed layer depths (MLDs) is crucial in the Southern Ocean to the simulation of the carbon cycle. In the winter, deep mixing plays a crucial role by bringing nutrients from below the mixed layer to replenish or 'reset' nutrient concentrations that are utilised and reduced over the (more strongly) biologically active summer season. Very few synoptic Southern Ocean observations exist to allow comparison of simulated MLDs. Instead, observations made in the Australian Sector of the Southern Ocean, corresponding roughly to the well-sampled WOCE SR3 line, were used to validate the Southern Ocean MLDs.

The simulated summer values (Figures 2.7(a) and 2.8(a)) were calculated based on the 0.1 kg/m^3 potential density criteria (from the surface). In general, the summer modelled mixed layers were shallower than observed. The PFZ and the SAZ showed similar MLDs, in general < 40m. These were shallower than the observed values of 60-75m (Trull et al. 2001). In the AZ the summer simulated MLD was shallower (< 20 m) than observed (40m - 60m) (Trull et al. 2001; Chaigneau et al. 2004).

Deep winter mixing, which is primarily responsible for bringing up nutrient-rich water, is due to changes in both wind mixing and buoyancy fluxes. The model in general did a good job simulating winter (Figures 2.7(b) and 2.8(b)) mixed layers. The model showed deep winter mixing in the SAZ to depths greater than 450m, consistent with those observed by (Rintoul and Trull 2001) at > 400m. In the PFZ MLDs were between 100 and 250m. This was in broad agreement with observed values of ~ 150m by (Trull et al. 2001). The modelled values of MLD in the AZ were in general between 50m and 150m. This was shallower than the summer MLDs observed in the AZ of 40-60m (Chaigneau et al. 2004). Note that we are comparing observed MLDs to climatological values derived from month fields, this difference may account for the mismatch between observations and simulated MLDs.

The simulated salinity (Figure 2.4) appears to have the elements, although not as strongly pronounced, of the low salinity core visible in the observations (Conkright et al, 2001) that characterises SubAntarctic Mode Water (SAMW)/ Antarctic Intermediate Water (AAIW) (Sloyan and Rintoul, 2001). This in conjunction with deep winter mixing, a prerequisite of SAMW formation (Doney etal, 2004) and reasonable agreement with the observed annual mean density field suggests that SAMW/AAIW is captured in this model. Within this thesis time did not permit to run a CFC simulation e.g. Dutay et al (2002) or bomb and natural radiocarbon simulation e.g. Matusmoto et al. (2004) that would have allowed a more robust assessment of AAIW/SAMW.

2.7 Southern Ocean Biogeochemical Response

To evaluate the modelled biogeochemical response of the Southern Ocean, the simulated fields were compared with PO_4 from Conkright et al. (2002) and ΔpCO2 and air-sea CO_2 flux from Takahashi et al. (2002). These observations suffer from the same poor spatial and temporal resolution as the observations of the physical fields discussed in Section 2.6.

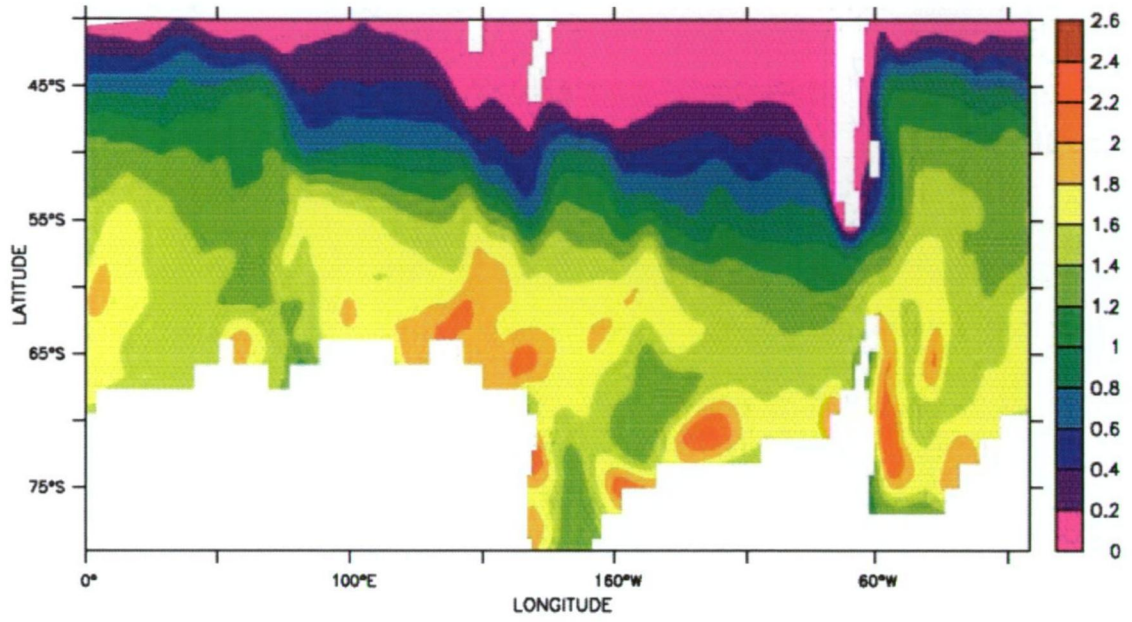

SIMULATED ANNUAL MEAN PO_4 (mmol/m^3)

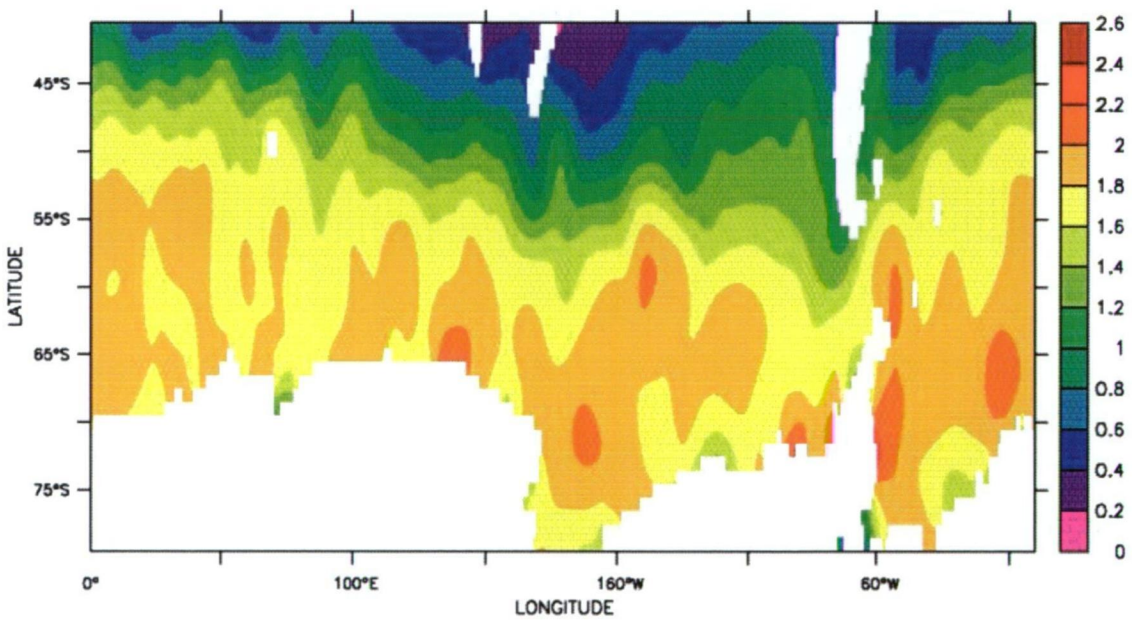

WOA (2001) ANNUAL MEAN PO_4 (mmol/m^3)

Figure 2.9 Comparison between the Phosphate climatology as predicted by the model (top) and the observed WOA climatology (bottom)

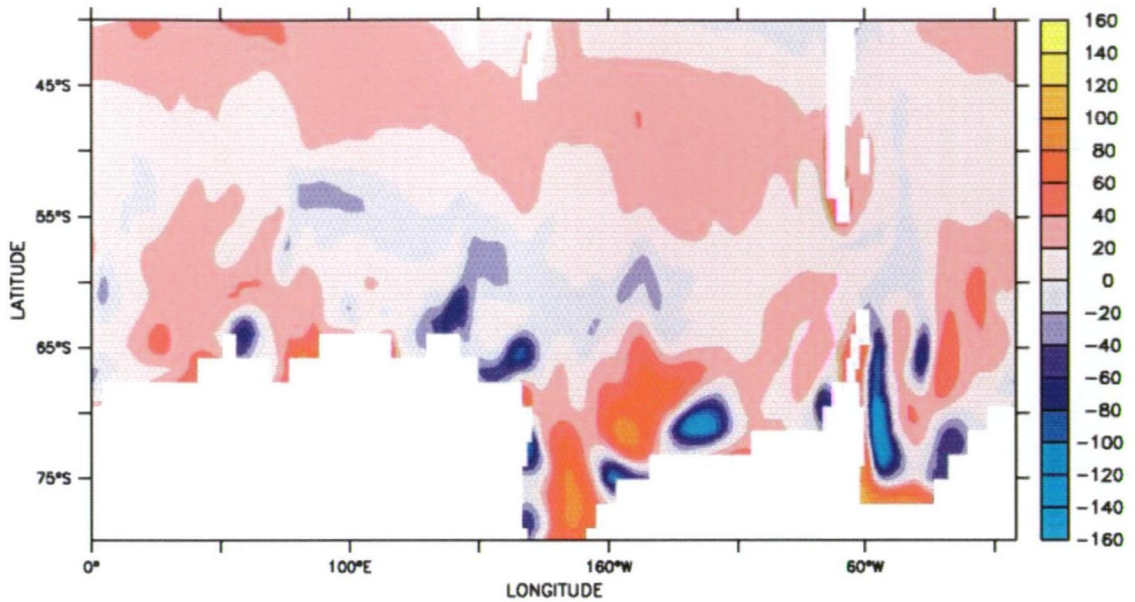

SIMULATED ANNUAL MEAN ΔpCO_2 (uatm)

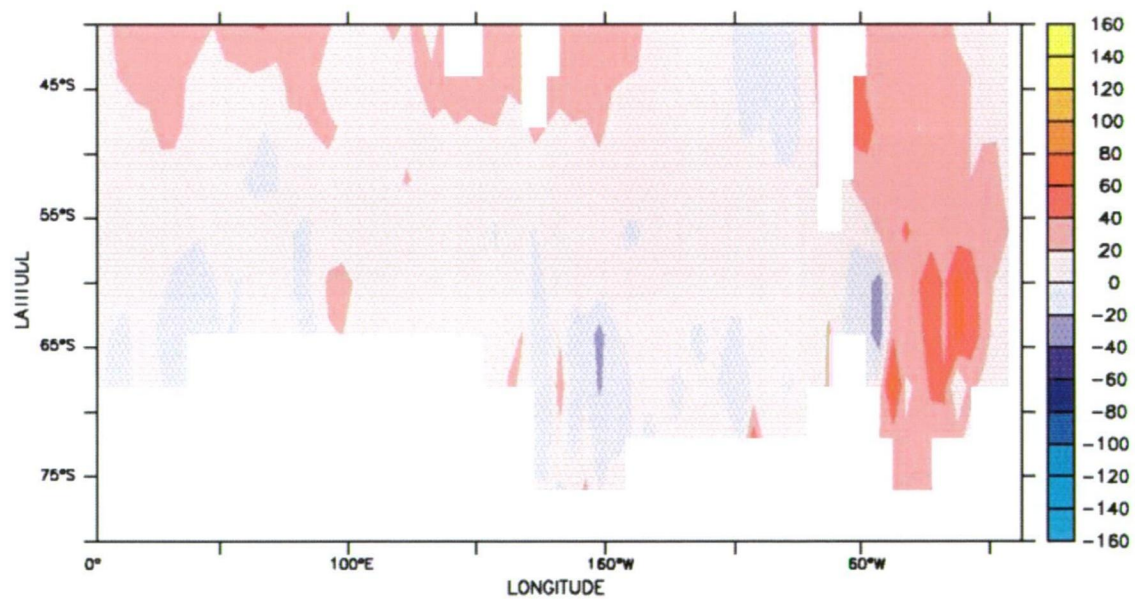

TAKAHASHI ET AL. (2002) ANNUAL MEAN ΔpCO_2 (uatm)

Figure 2.10 Comparison between the ΔpCO_2 climatology as predicted by the model (top) and the observed Takahashi et al (2002) climatology (bottom). Where $\Delta pCO2$ was defined as $pCO_{2atm} - pCO_{2ocn}$

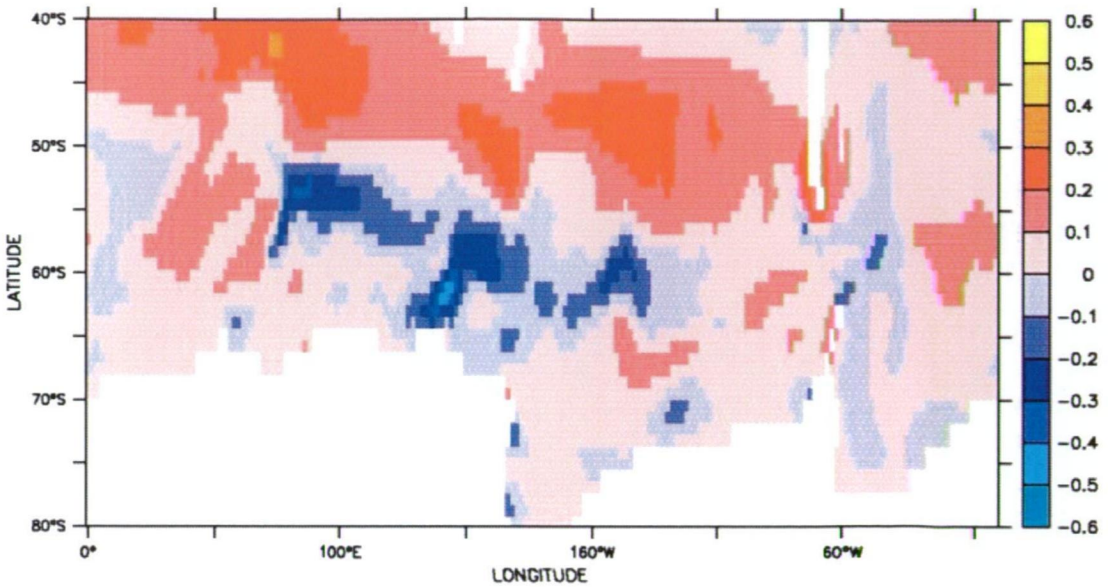

Simulated Air-sea CO_2 flux (mmol/m2/month)

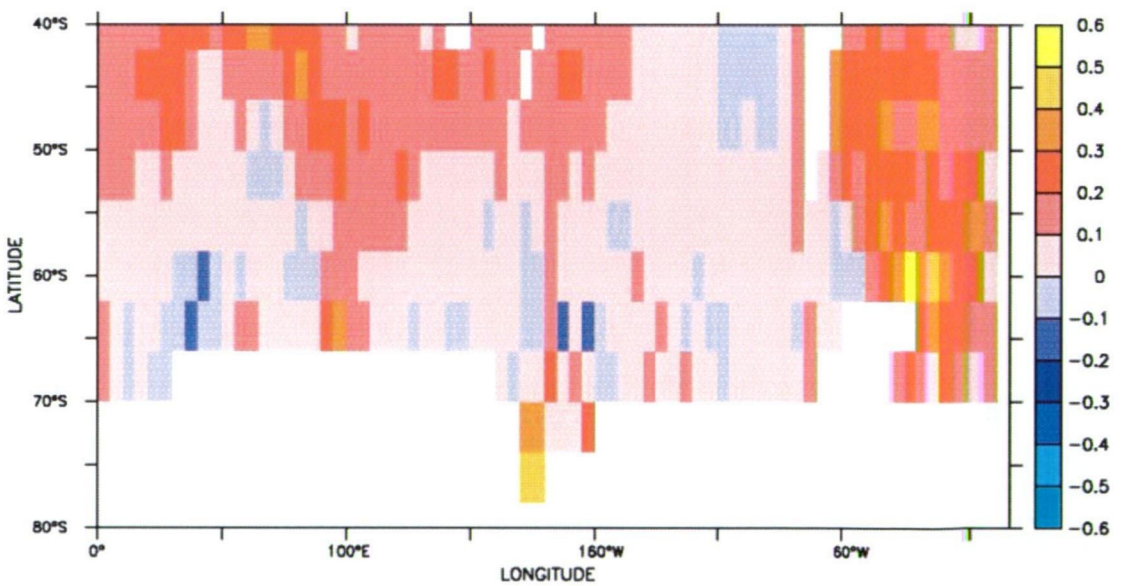

Takahashi (2002) Air-sea CO_2 flux (mmol/m2/month)

Figure 2.11 Comparison between the air-sea CO_2 flux climatology as predicted by the model (top) and observed from Takahashi et al (2002) climatology (bottom). Positive flux is into the ocean

The modelled PO_4 concentration was compared with the observed PO_4 data from (Conkright et al. 2002) (Figure 2.9). The simulated PO_4 captured the broad-scale character and magnitude of the observations. The major differences were: i) in regions south of the Polar Frontal Zone (PFZ; ~55°S) where the simulated PO_4 was less than observed; and ii) in the Subantarctic region where lines of contours (isolines of equal concentration) are shifted further south than observed (i.e. simulated PO_4 was less than observed).

The simulated annual mean ΔpCO_2 and air-sea CO_2 flux were compared with the observed, coarse-resolution, annual mean climatologies of (Takahashi et al. 2002) (Figures 2.10 and 2.11). The simulated ΔpCO_2 captured the complex, large-scale variability that exists in the observations. The major differences between the simulated and observed response were evident in: i) the Southern Indian Ocean sector and the Subantarctic region, where the simulated ocean showed a stronger positive ΔpCO_2 than the observed; and ii) in the region 50°S-60°S where the simulated ΔpCO_2 was opposite in sign but of a similar magnitude to the observations. The large (winter) ΔpCO_2 values simulated along the Antarctic coast cannot not compared to observations nor translated to an air-sea flux (Figure 2.11) as these reflect sea-ice preventing the exchange of CO_2 with the atmospheric. The lack of under ice ΔpCO_2 measurements prevents a comparison with the observations.

The simulated air-sea flux reasonability represents most of the zonal mean variability (average variations between latitudinal bands). The major differences between the simulation and observations were evident in: i) the Southern Atlantic Ocean where the simulated ocean was a weak source (outgassing) of CO_2 while the observations showed it to be a strong CO_2 sink (uptake); ii) the Subantarctic region where the simulated fluxes showed a larger sink of CO_2 than the observations; and iii) in the region 50°S-60°S where the simulated fluxes showed a stronger source of CO_2 than the observations. The differences between the simulated and observed ΔpCO_2 and air-sea CO_2 fluxes may reflect the coarse resolution (4° x 5°) and the limited observations of Takahashi et al. (2002).

2.8 Conclusion

Given the sparse number of carbon system measurements in the Southern Ocean, I relied on a prognostic biogeochemical ocean general circulation model to simulated and characterise large-scale variability CO_2 fluxes. The goal of this chapter was to document the formulation, parameterisations, initialisation and forcing of the CSIRO Mark3 biogeochemical ocean model to simulate the Southern Ocean carbon cycle and to compare the annual mean oceanic physical and biogeochemical fields with the sparse Southern Ocean observations to evaluate the limitations that stem from using this model.

In general the simulated fields did capture the large-scale synoptic behaviour of the Southern Ocean. The major difference was in the region adjacent to the Antarctic continent where the model appeared not capture well AABW formation a common problem in this class coarse resolution biogeochemical ocean models (Dutay et al, 2002; Doney et al., 2004) . This inconsistency does not preclude the use of the model to explore variability in CO_2 uptake, since most of the uptake, as suggested by observations, occurs north of this region (Metzl et al. 2006; Metzl et al. 1999; Takahashi et al. 2002). In Chapter 3 the seasonal behaviour of ΔpCO_2 and air-sea CO_2 flux is explored and further compared with observations. Further discussion of the relevance of the limitations of the model is given with the results presented in Chapters 3 and 4 of this thesis.

3. DESIGN OF AN OBSERVATIONAL STRATEGY FOR QUANTIFYING THE SOUTHERN OCEAN UPTAKE OF CO_2

Andrew Lenton[1,2]

(Andrew.Lenton@csiro.au)

Richard J. Matear[3,2]

(Richard.Matear@csiro.au)

Bronte Tilbrook[3,2]

(Bronte.Tilbrook@csiro.au)

1. Institute for Antarctic and Southern Ocean Studies (IASOS), University of Tasmania, Australia

2. Antarctic Climate and Ecosystem Cooperative Research Centre (ACE CRC), University of Tasmania, Australia

3. CSIRO Marine and Atmospheric Research (CMAR), Tasmania, Australia

Submitted to Global Biogeochemical Cycles *September 2005*

Accepted *June 2006*

3.1 Abstract

A sampling strategy to estimate the annual mean CO_2 uptake by the Southern Ocean was developed by applying 2D Fourier transforms and signal-to-noise ratios to the simulated air-sea CO_2 fluxes and ΔpCO_2 from an ocean biogeochemical model driven with NCEP-R1. Observations of pCO_2 were used to validate the statistical properties of the model and to estimate the mesoscale variability not captured by the model resolution. Sampling regularly every 3-months, at every 30° in longitude and 3° in latitude is sufficient to determine the net Southern Ocean CO_2 uptake. We applied this sampling strategy to the simulated air-sea fluxes to estimate a net annual mean CO_2 uptake of 0.6 ± 0.1 PgC/yr (1990-1999). This uncertainty in the estimate was dominated by the simulated interannual variability, and not by errors in the sampling or unresolved mesoscale variability. Therefore, sampling at higher resolutions in space and time would not reduce the uncertainty in the Southern Ocean annual mean uptake any further. These results show that a doubling of the current Southern Ocean sampling (in longitude) would be required to constrain the net annual mean air-sea CO_2 fluxes to within the natural variability of the system.

3.2 Introduction

Atmospheric CO_2 levels have continued to rise at unprecedented rates as a result of increases in anthropogenic activities such as fossil fuel burning, cement production and land clearing (Keeling and Whorf, 2003). CO_2 in the atmosphere acts as a potent greenhouse gas, and the increase in atmospheric CO_2 is believed to be responsible for increases in global mean temperatures (Prentice et al., 2001). Only about 40% of the CO_2 emitted each year resides in the atmosphere. The remainder is taken by the ocean and terrestrial biosphere. Current estimates suggest that 48% of the anthropogenic CO_2 emitted (1800 -1994) was taken up by the ocean (Sabine et al., 2004). Oceanic uptake of CO_2 slows the rate of atmospheric CO_2 increase and thus illustrates the important role the ocean plays in slowing the rate of climate change.

The primary pathway for atmospheric CO_2 to enter the ocean is through gas exchange at the air-sea boundary. Air-sea CO_2 flux is a function of the differences in partial pressures between the ocean and atmosphere across this boundary (ΔpCO_2), and the gas exchange co-efficient (K) e.g. following Wanninkhof (1992):

$$CO_2FLUX_{AIR-SEA} = K(pCO_{2AIR} - pCO_{2SEA}) = K(\Delta pCO_{2AIR-SEA}) \qquad (3.1)$$

Air-sea CO_2 fluxes are highly variable in space and time (Mahadevan et al., 2004; Volk and Hoffert, 1985) and balance to within 2% when integrated globally (Watson and Orr, 2003). The 2% difference corresponds to a net air-sea CO_2 flux into the ocean of about 1.7 ± 0.5 PgC/yr (1990-1999) (Prentice et al., 2001).

Estimates of Southern Ocean CO_2 uptake obtained from model and observational studies (0.2 to 0.8 PgC/yr for the 1990s, south of 50°S) show that the Southern Ocean is a net sink of CO_2 but that the magnitude of this sink is poorly constrained (Matear and Hirst, 1999;Metzl et al., 1999; Takahashi et al., 2002; Matear and Hirst, 1999; Rayner et al., 1999; Roy et al., 2003; Rödenbeck et al., 2003). Most studies also suggest that the Southern Ocean is a region of high air-sea CO_2 flux variability (Sabine and Key, 1998; Louanchi et al., 1999; McKinley et al., 2004) but with sparse data coverage (Figure 3.1). The lack of observations, particularly during the austral winter (Sweeney et al., 2002), is a function of sampling cost and the remoteness of the Southern Ocean. The combination of high variability and sparse data coverage may explain the large range in estimates of Southern Ocean uptake.

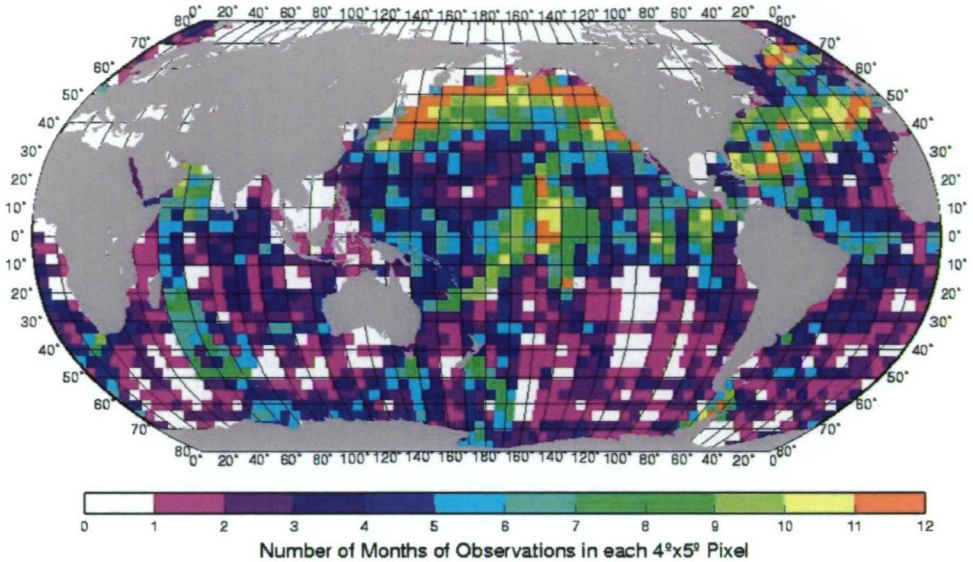

Figure 3.1. The number of different months during the year in which pCO_2 data have been collected. A value of 0 refers to no data while a value of 12 signifies that observations have been collect in all months of the year. This map is a composite of more than 1.1 million observations made since 1958 (Sweeney et al., 2002)

From an observational perspective, it is an important question how the uncertainty in the Southern Ocean uptake may be reduced. Studies have attempted to quantify the sampling frequency required to accurately estimate air-sea CO_2 fluxes. Garçon et al. (1992) in the North Pacific and Mémery et al. (2002) in the Mediterranean Sea both sub-sampled highly resolved observational time-series of air-sea fluxes to estimate the temporal sampling required to constrain the annual net CO_2 flux to ±10%. Their results showed different requirements in each region; 24/year and >70/year in the Pacific and Mediterranean Sea respectively.

Sweeney et al. (2002) use two Southern Ocean north-south transects (winter and summer) to determine the spatial sampling required to constrain the mean ΔpCO_2 to ±4.3 μatm (equating to a ± 0.1PgC/yr for the Southern Ocean using a mean Southern Ocean gas exchange co-efficient, south of 50°S). They show that sampling every 5 ° in latitude in the summer and 10° latitude in the winter is required. Takahashi and Sweeney (2002) sub-sample global, gridded, monthly flux maps (extended from Takahashi et al., 1997)) to determine the sampling needed to capture the net annual CO_2 flux. Sub-sampling the mean monthly flux maps, they suggest sampling 3 times per year is required, but did not develop a specific spatial sampling strategy for the Southern Ocean. Their analysis maybe biased as it assumes that the ocean is in steady-state (for the year 1995) and ignores variability on time scales shorter than monthly.

The goal of this work was to develop and validate a sampling strategy that reduces the uncertainty in the Southern Ocean annual uptake of CO_2 to a target of ± 0.1 PgC/yr. By using a time-evolving-prognostic-high-resolution-biogeochemical model to simulate the fluxes this paper has extended previous analyses by combining spatial and temporal sampling strategies. An accurate representation of the Southern Ocean CO_2 uptake and its uncertainty provides: i) the essential information to resolve the present mismatch between observational and model estimates of the uptake which will reduce the uncertainty in the global budget (Friedlingstein et al., 2003); ii) a reference against which future changes in variability can be assessed; and iii) an observational estimate to assess and validate numerical models.

In Section 3.3 the prognostic biogeochemical ocean model and the observations used to assess the statistical characteristics of our simulated ΔpCO_2 fields are described. In Section 3.4: i) Fourier Transforms with signal-to-noise ratios have been used to investigate the temporal and spatial variability that dominates the simulated Southern Ocean CO_2 air-sea fluxes; and ii) the sampling strategy required to resolve this variability has been developed. Our proposed sampling strategy and the current sampling were also used to estimate the Southern Ocean CO_2 uptake. A strategy to obtain the necessary samples to estimate the Southern Ocean uptake of CO_2 to $\pm$ 0.1 PgC/yr is discussed in Section 3.5.

3.3 Methods

3.3.1 Modelling

To compensate for the lack of observed air-sea CO_2 fluxes, a prognostic 3D Global Biogeochemical Ocean General Circulation Model (BOGCM) was used to simulate daily values of air-sea flux and ΔpCO_2. The ocean general circulation module (OGCM) of the BOGCM was based on the Z coordinate Modular Ocean Model (MOM) - Version 3 (Pacanowski and Griffies, 1999). The OGCM used the T63-2 grid, a grid spacing of 0.94° N-S and 1.9° E-W, with 31 vertical levels - 15 levels in the upper 500m. To represent the effects of eddies not simulated in the model, the eddy parameterisation of Gent and McWilliams, 1990) was implemented, as was the Chen mixed layer scheme (Chen et al., 1994) to parameterise upper ocean mixing.

The biogeochemical module of the BOGCM predicted DIC, alkalinity, oxygen and phosphate. A detailed description of the model is given in Matear and Hirst, 1999; Matear, 2004). Export production in the top 50m was calculated as a function of light, nutrient concentration, temperature and mixed layer depth. $CaCO_3$ production was set at 8% of the export production (Yamanaka and Tajika, 1996). Below the euphotic zone, particulate organic matter and $CaCO_3$ were remineralised as a function of depth according to $(z/100)^{-0.9}$ and $e^{(-z/3500)}$ respectively (Yamanaka and Tajika, 1996). Nutrient uptake and remineralisation of P:N:C:O_2 were related via the Redfield ratio of 1:16:106:-138 in and below the euphotic zone (*Redfield,* 1963) .

The model was forced with daily wind stress, heat and freshwater fluxes from NCEP -R1 (Kalnay, 1996). Sea-ice was not explicitly modeled, but the use of the NCEP -R1 implicitly included the effect of sea ice on heat and freshwater fluxes. The sea surface temperature and salinity were restored to observed sea surface temperatures (SST) (Reynolds and Smith, 1994) and sea surface salinity (Conkright et al., 2002) every 30 days. Air-sea gas exchange of CO_2 was calculated following the short-term wind speed relationship of (Wanninkhof, 1992), using daily wind speed from NCEP-R1. To account for a lack of explicit sea ice, the net CO_2 flux was scaled by the fraction of observed sea-ice cover, interpolated from the monthly-climatological fields of Walsh (1978) and Zwally et al. (1983). A net flux into the ocean was defined as positive.

The model was initialised with the observed fields from Conkright et al. (2002) and evolved for > 4000 years. Following this initial evolution the model had not yet reached quasi-steady state and so to ensure upper ocean dynamics were well captured, we reinitialised the temperature and salinity fields from Conkright et al., 2002) in accordance with the protocols of the Northern Ocean Carbon Exchange Study (NOCES)/Ocean Carbon Model Intercomparsion Project 3 (OCMIP3) (Aumont et al., 2004). The model was then evolved from 1837 to 2002 with observed atmospheric pCO_2 values from Enting et al., 1994) (www.ipsl.jussieu.fr/OCMIP) in accordance with the protocols of NOCES/OCMIP3.

3.3.2 Observations

In the development of a Southern Ocean sampling strategy, observed pCO_2 data was used to characterise the spatial variability of pCO_2 and to estimate model subgrid variability. Observational data chosen was from cruises in the Australian Sector of the Southern Ocean between 80° E and 160° E (Figure 3.2a) (Tilbrook, 2005).

Observational pCO_2 was measured from the seawater intake located approximately 5m below the surface. The seawater was continually equilibrated with a closed loop of air using a 'Weiss' type showerhead equilibrator (*Metzl et al.*, 1999). The xCO_2 of the equilibrated air was dried and measured using a LICOR® 6252 infrared gas analyser. We used the following equation (Equation 2) from Dickson and Goyet, 1994) to convert of xCO_2 to pCO_2; the vapour pressure of seawater ($Vp(H_2O)$) was calculated following Weiss and Price, 1980) and the atmospheric pressure was measured on the ship.

$$pCO_2 = xCO_2 \times P_{ATM}\left(1 - Vp(H_2O)\right) \qquad (3.2)$$

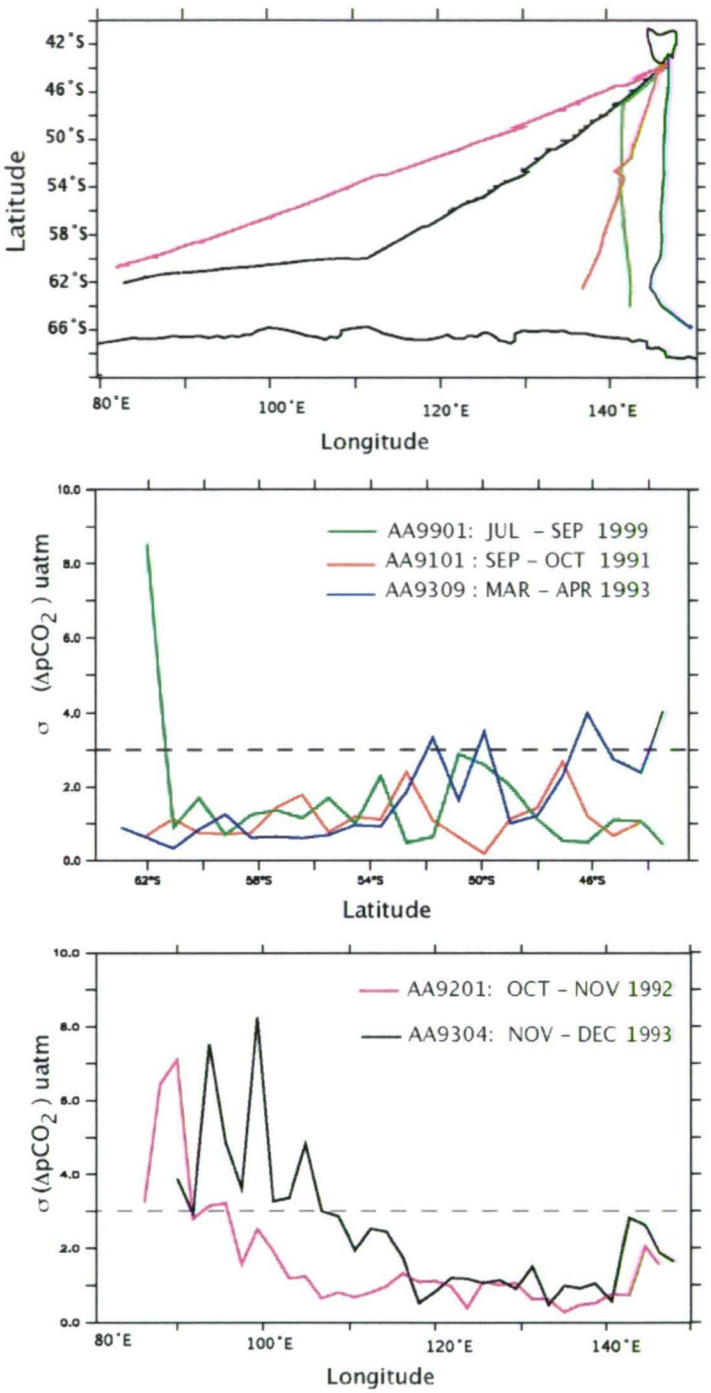

Figure 3.2(a) The location of the observational data used to estimate the variability not captured by the model. Figures 3.2(b) and 3.2(c) show the standard deviation of the subgrid scale variability in pCO_2 not captured by the model resolution. The dashed line represents the 3 μatm value.

The measured warming of less than 1°C between the intake and the equilibrator was corrected following Copin-Montégut (1998; 1989). Surface pCO_2 was calibrated against 3 reference samples every 6 hours. Prior to 1997, data was collected every 4 minutes, and thereafter every minute. Based on inter-comparisons of the system (Körtzinger et al., 2000) and the comparison of air-samples taken at monitoring sites including Cape Grim, Macquarie Island and Mawson Antarctic Base (Francey et al., 2003); the accuracy and precision of pCO_2 was considered to be better than ± 2 µatm.

To account for the subgrid scale variability, which was not captured by our coarse-resolution model simulation, we used the observed variability in the pCO_2 data. This high-resolution cruise data (Figure 3.2a) was first binned by the latitudinal and longitudinal resolution of the model and the standard deviation of the subgrid variability was then calculated (Figures 3.2b and 3.2c). We estimated that a normal distribution with a standard deviation of 3 µatm was adequate to represent the Southern Ocean subgrid-scale variability. We note that by using a normal distribution we may have slightly underestimated the large changes in ΔpCO_2 observed in the seasonal sea ice zone, but may have overestimated the open ocean variability.

3.4 RESULTS AND DISCUSSION

3.4.1 Model Analysis

To better represent the observed variability in the Southern Ocean we defined our simulated ΔpCO_2 and air-sea CO_2 flux as the combination of modelled and subgrid-scale variability between 40° and the Antarctic Continent. In accordance with the observed subgrid-scale variability, we estimated a randomly generated normal distribution with a standard deviation a 3 µatm which was adequate to represent this variability. We added this subgrid-scale variability directly to the modelled ΔpCO_2. For the air-sea CO_2 flux, this variability was first multiplied by the daily gas exchange co-efficient (Equation 3.1) and then added to the modelled air-sea CO_2 flux.

Sparse Southern Ocean sampling meant that existing observational data was too limited (Figure 3.1) to comprehensively assess the simulated air-sea CO_2 fluxes. Instead we separated the simulated air-sea CO_2 flux variability into seasonal and non-seasonal variability. The seasonal cycle was defined as the daily (climatological) air-sea flux of CO_2 over the 1990-1999 period. The non-seasonal variability was defined as the simulated air-sea flux not represented by the seasonal cycle.

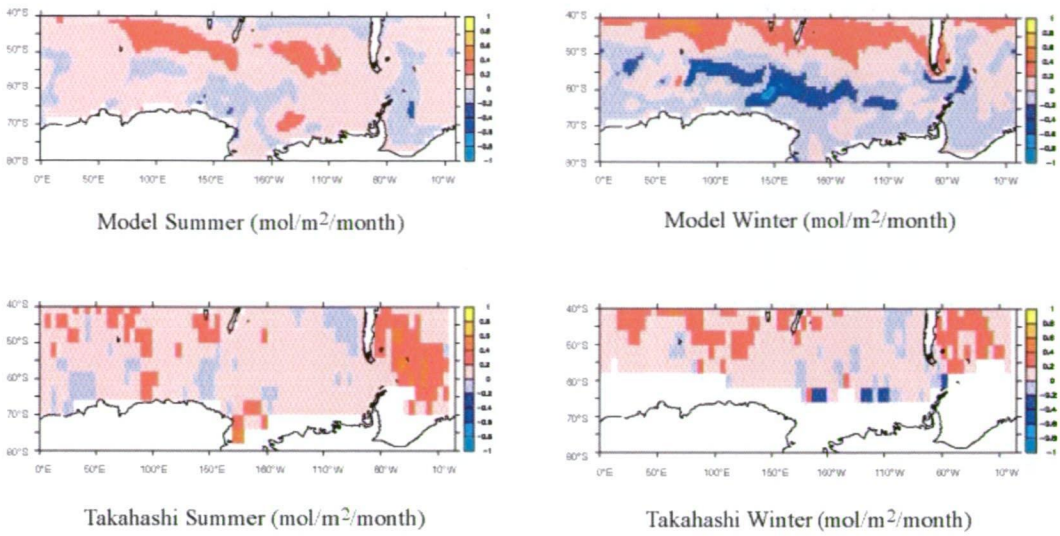

Figures 3.3(a-d) Climatologically summer (Jan, Feb, Mar) and winter (Jul, Aug, Sept) air-sea CO_2 fluxes (mmol/m^2/month); Simulated fluxes from the CSIRO model (top) and from Takahashi et al. (2002), note that positive flux is into the ocean.

The simulated seasonal cycle was compared to the coarse-resolution, monthly climatological maps of Takahashi et al. (2002). The summer (Jan-Mar) and winter (Jul-Sept) comparison showed that the simulated seasonal cycle captured much of the large-scale variability that exists in the Southern Ocean observations (Figures 3.3(a-d)). The major differences between the simulated seasonal cycle and observations were evident in: i) the Southern Atlantic Ocean where the simulated ocean was a weak source (outgassing) of CO_2, while the observations showed it to be a strong CO_2 sink (uptake); ii) the Subantarctic region where the simulated fluxes showed a larger winter sink of CO_2 than the observations; and iii) in the region 50°S-60°S where the simulated fluxes showed a stronger winter source of CO_2 than the observations. These differences may reflect the limited data coverage of Takahashi et al. (2002).

To assess the air-sea flux variability in the Southern Ocean, signal-to-noise ratios (SNR) were calculated following Ballabrera-Poy et al. (2003) and Schiller et al. (2004), where σ^2 denotes variance. We define the seasonal cycle to be the signal and the non-seasonal variability as the noise.

$$SNR = \frac{\sigma^2_{SIGNAL}}{\sigma^2_{NOISE}} = \frac{\sigma^2_{SIGNAL}}{\sigma^2_{ALLDATA} - \sigma^2_{SIGNAL}} \tag{3.3}$$

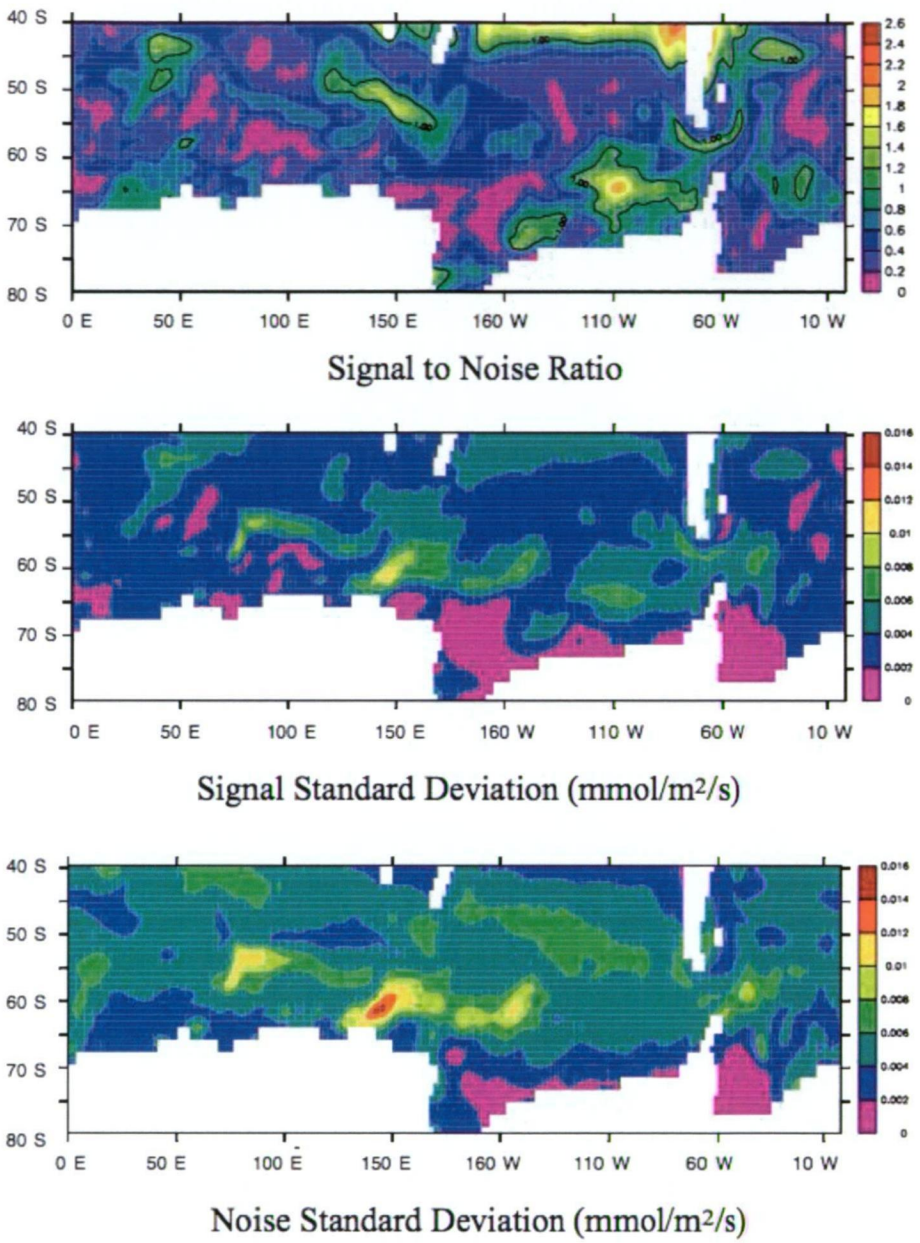

Figure 3.4(a) SNR map of the air-sea fluxes of CO_2 in the Southern Ocean, a contour level representing a SNR of 1 is marked; 3.4(b) shows the standard deviation of the signal; 3.4(c) shows the standard deviation of the noise.

To assess the relative magnitude of the temporal variability in the signal and noise we computed a SNR map for the daily-simulated air-sea CO_2 fluxes (1990-1999; Figure 3.4a). Over most of the Southern Ocean the SNR was less than 1. In these locations it would be difficult observationally, using the 10 years of daily-modelled air-sea fluxes, to separate the seasonal cycle variability from the large non-seasonal variability. The maps of the standard deviation (σ) of the signal and noise are shown in Figures 3.4b and 4.4c. Figure 4.4b showed that the variability in the seasonal flux was not homogenous, consistent with the Takahashi et al., (2002) climatology.

What sampling was required to constrain the Southern Ocean air-sea CO_2 flux given the large variability observed in the model? Two-dimensional Fourier Transforms (2D-FT) in space and time along sections of constant latitude (east-west) and longitude (north-south) were used to characterise the spectrum of the simulated flux variability south of 40°S.

Figures 3.5(a) and 3.5(c) show the log of the variance of the 2D-FT of air-sea flux averaged in latitude (north-south) and in longitude (east-west) in the Southern Ocean. These figures revealed that: i) the Southern Ocean is a net uptake region, i.e. a non-zero value when the wavelength (λ) was zero and the period (T) was equal to the record length (i.e. infinite); ii) at long wavelengths (λ > 5°) there was a more uniform spread of variability across a range of periods; and iii) there was rapid decline in the amount of variance explained by short periods T< 20 days and short wavelengths λ < 5°.

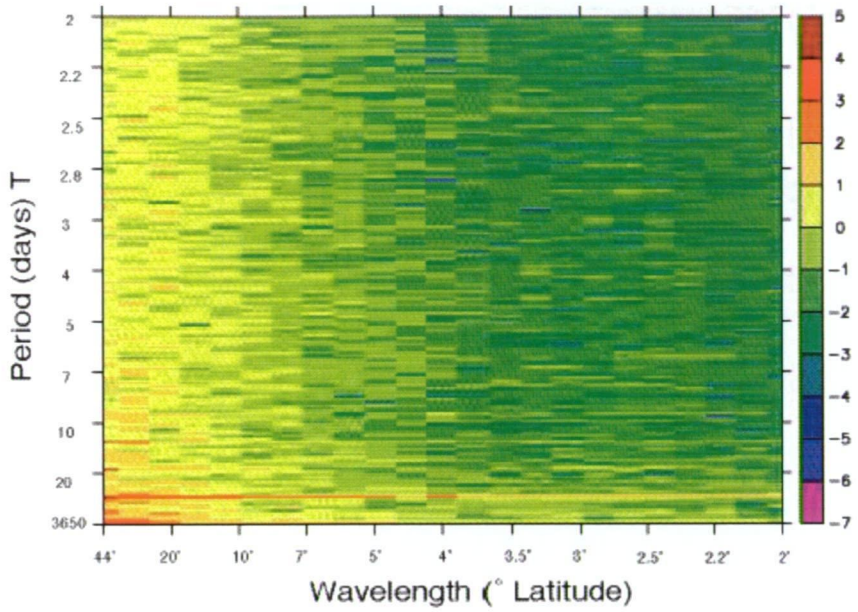
Period (days) T
2
2.2
2.5
2.8
3
4
5
7
10
20
3650
44°
20°
10°
7°
5°
4°
3.5°
3°
2.5°
2.2°
2°
Wavelength (° Latitude)
5
4
3
2
1
0
−1
−2
−3
−4
−5
−6
−7

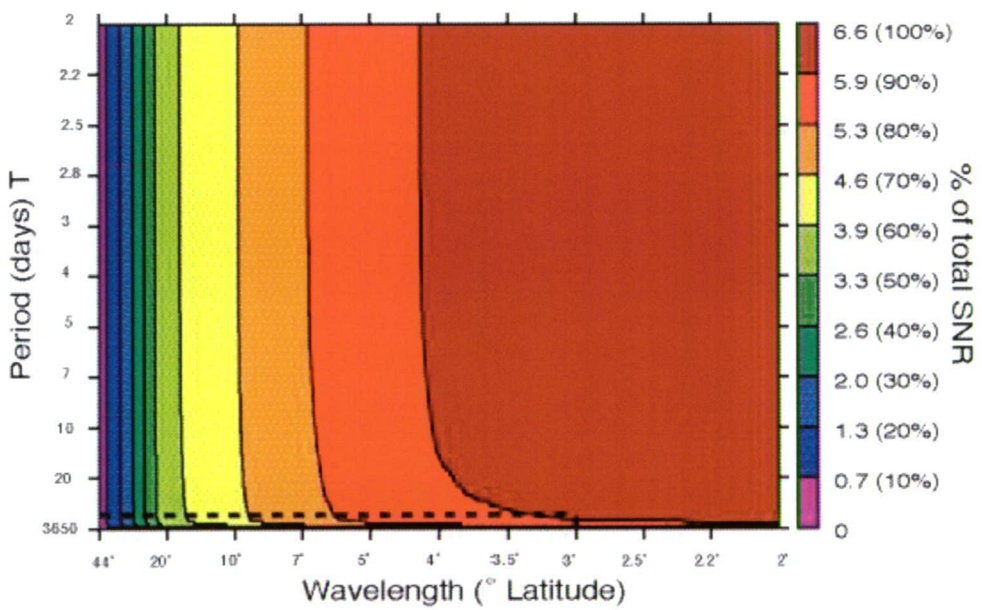
Period (days) T
2
2.2
2.5
2.8
3
4
5
7
10
20
3650
44°
20°
10°
7°
5°
4°
3.5°
3°
2.5°
2.2°
2°
Wavelength (° Latitude)
6.6 (100%)
5.9 (90%)
5.3 (80%)
4.6 (70%)
3.9 (60%)
3.3 (50%)
2.6 (40%)
2.0 (30%)
1.3 (20%)
0.7 (10%)
0
% of total SNR

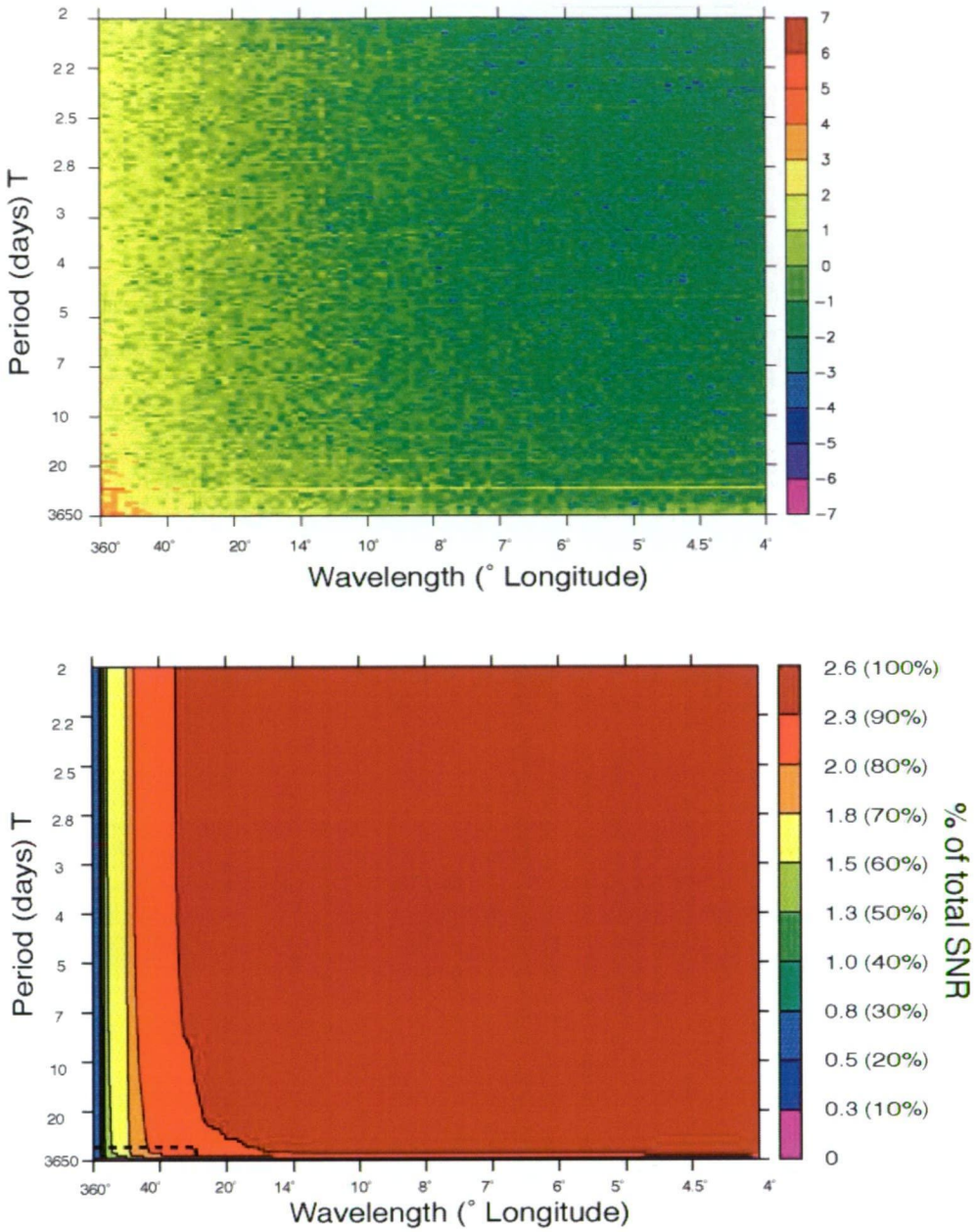

Figures 3.5(a) and 3.5(c) The log 2D Fourier transform in space and time of longitudinally (north-south) and latitudinally (east-west) averaged air-sea fluxes in the Southern Ocean (south of 40°S). Figure 3.5(b) and 5(d) SNR contour plots in the frequency domain of the data in Figure 3.5(a) and 3.5(c) respectively. The sampling point is shown as the intersection of the dashed lines. Please refer to the text for an explanation.

We applied Parseval's Theorem to derive a new relationship for SNR in the frequency domain (Equation 3.4) that is equal to the SNR in the temporal domain (Equation 3.3), see Appendix 3.6. This new SNR describes the variance explained as a function of frequency.

$$SNR(f) = \frac{\sum_{n=1}^{f} H_{signal}(n)^2}{\sum_{n=1}^{f} H_{noise}(n)^2} \tag{3.4}$$

Equation 3.4 was applied to the 2-D Fourier Transform of the air-sea fluxes to investigate how the SNR changed, as higher temporal and spatial sampling frequencies were resolved. Figures 5(b) and 5(d) show the SNR of latitudinally (east-west) and longitudinally (north-south) averaged air-sea fluxes in the frequency domain. We interpret these figures as the SNR resolved at different the sampling frequencies in time and space. The upper right hand corner represented the maximum SNR by sampling at the model resolution.

Once the seasonal cycle is resolved, the amount of variance explained does not continue to increase appreciably. The SNR is shown to asymptote in time and space, as illustrated by the straight vertical and horizontal lines in the contour plots of SNR (figures 3.5b and 3.5d). The most efficient way to increase SNR, after the seasonal cycle has been resolved, is to increase the spatial sampling. Figures 3.5(b) and 3.5(d) also demonstrated that high resolution in time and low resolution in space or high resolution in space and low resolution in time returns a SNR value that is less than 20% of the maximum value. This was consistent with Figure 3.4(a) in which high temporal (daily) sampling and poor spatial sampling produces a SNR < 1.

A sampling strategy for the net air-sea flux of CO_2 that returns the maximum SNR value is ideal. However, with limited sampling resources a strategy was required that best reflected the trade-off between a realistic sampling effort and an acceptable SNR value. We suggest the optimum sampling is the point where the SNR starts to asymptote, i.e. where we can maximise SNR with minimum sampling. From Figure 3.5(b), sampling every 3° in latitude, every three months (~ 91 days) would capture greater than 90% of the maximum SNR. A north-south sampling of every 3° corresponds to approximately 12 samples between 40°S and the Antarctic Continent. From Figure 3.5(d) sampling every 30° in longitude, every three months (~ 91 days) would return more than 85% of the maximum SNR.

Figure 3.5(b) demonstrates that averaging over zonal (north-south) bands, significantly improves the SNR value to 6.6, which is much greater than any point in Figure 3.4(a). This increase in SNR reflects a much greater reduction in the noise than the signal when averaging zonally because the signal is more correlated zonally than the noise. In contrast, no significant improvement in optimal SNR value (2.6) occurs when we average meridionally (east-west).

Figures 3.6(a) and 3.6(b) showed the SNR analyses for ΔpCO_2 and that regular sampling every three months at spatial grid of 3° in latitude and 30° in longitude returned more than 70% of the maximum SNR value. This was very similar to the maximum SNR returned from air-sea fluxes. From Equation 1, any difference in the response between pCO_2 and air-sea CO_2 flux is the gas transfer co-efficient. The similarity in sampling requirements between ΔpCO_2 and air-sea CO_2 flux suggests that it is the longer wavelength changes in ΔpCO_2 that are more important in determining the seasonal fluxes than short-term (high frequency) variability in the gas exchange co-efficient.

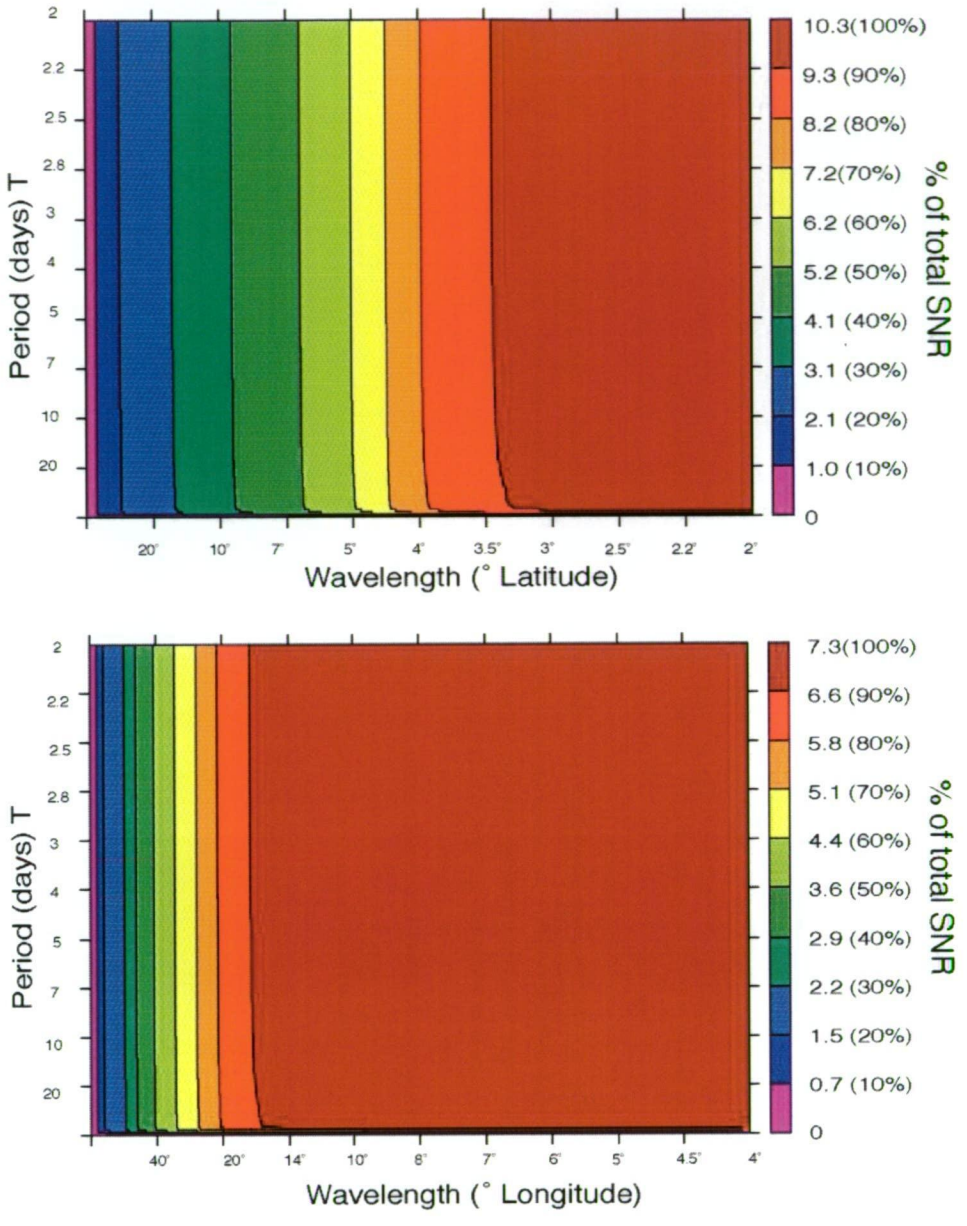

Figure 3.6. ΔpCO_2 SNR contour plots in the frequency domain of (a) longitudinally and b) latitudinally averaged simulated values in the Southern Ocean (south of 40°S). Please refer to the text for an explanation.

3.4.2 Statistical Model Validation

There were not enough observations in the Southern Ocean to validate our sampling strategy directly. We looked instead at the statistical properties of the observations and show these are both consistent with the model and our proposed sampling strategy. As the proposed sampling strategy of ΔpCO_2 is very similar to that for the CO_2 air-sea flux, we only compare ΔpCO_2 from the model with the observations. To aid in the comparison of the statistical properties of the simulated and observed fluxes, the non-zero i.e. mean uptake from both the observations and simulated values were removed.

Figure 7(a) shows the normalised cumulative ΔpCO_2 power spectra from 3 north-south transects, travelling during the austral winter (AA9901), summer (AA9101) and spring (AA9309) between Tasmania (43°S) and Antarctica (66°S) (~ 140°E), Figure 2(a). We have overlain on this plot, the modelled power spectrum corresponding to these transects in time and location. Note the Nyquist frequency from our model was 1.9°, which was much greater than the observations (0.2°). Like the simulated field, the observations had most of the variance in long wavelengths with $\lambda > 3°$ capturing more than 90% of the total variance in the observations. We also saw that the variability that occurs on spatial scales less than what the model resolves (2°) represented less than 5% of the observed variability. Therefore, from the observational data we concluded the variability was dominated by long wavelengths consistent with the model and that the subgrid scale variability not represented in the model did not significantly alter our analysis.

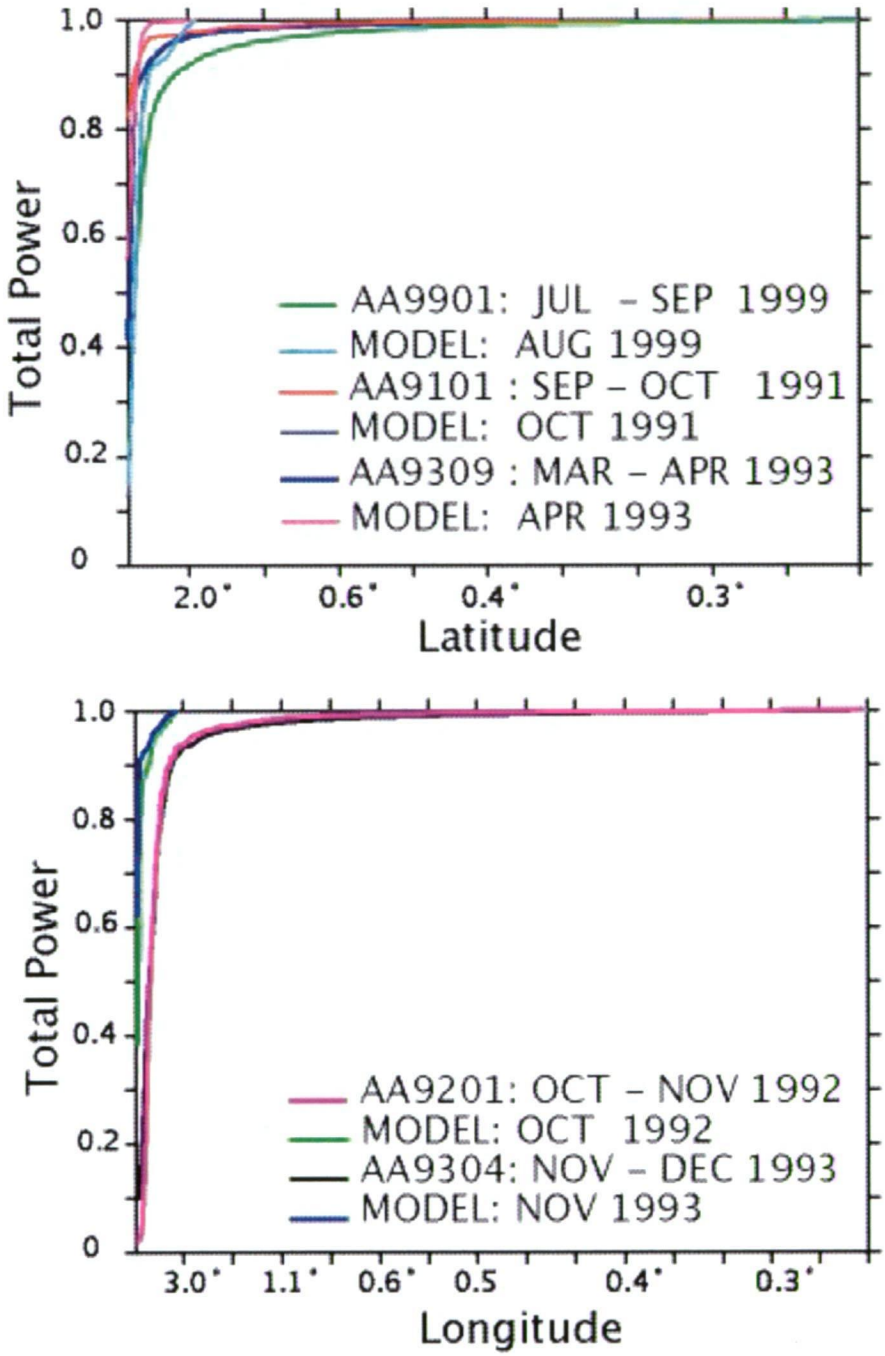

Figure 3.7(a) Cumulative variance plots of ΔpCO_2 from 2 observed transects travelling N-S and the corresponding model transects; Figure 3.7(b) cumulative variance plots of ΔpCO_2, from observed transects travelling E-W (longitude) and the corresponding model transects.

Figure 3.7(b) shows the normalised cumulative ΔpCO_2 power spectra from 3 east-west transects travelling between ~80° and ~150° E. These cruises took place in the Austral summer (AA9304) and spring (AA9201) (Figure 3.2a). Overlain on this plot are the power spectra of the modelled transects, corresponding to the same time and location. The longitudinal Nyquist Frequency from our model was 3.8°, which was much greater than the Nyquist frequency of the observations. The lack of good agreement with the observations may have been due to the ship tracks not being completely truly east-west. The observations did however suggest more than 90% of the variance was captured by $\lambda > 3°$ in longitude. These results suggest the variability was dominated by long wavelengths consistent with the model hence our model resolution of 1.9° in longitude was adequate to capture the statistical characteristics of the observations.

3.4.3 Sensitivity of CO_2 Uptake

To explore how well our sampling strategy performed and to quantify the uncertainty of our estimated annual mean uptake, we applied our sampling strategy to the simulated (modelled + sub grid scale variability) daily fluxes for each year between 1990-1999. We calculated the simulated annual mean uptake to be 0.6 ± 0.1 PgC/yr at the resolution of the model (Table 3.1; column 1). The uncertainty was calculated as $2\sigma_{\overline{Interannual}} = 2\sigma_{Interannual}/\sqrt{10}$ where 2σ denoted two standard deviations (i.e. 95% of the total variability) about the annual mean uptake. The uncertainty in the annual net uptake for the 1990s reflected the magnitude of the simulated interannual variability and was similar to the value reported by Wetzel et al., 2005) in the region between 40°S-60°S (2σ).

Applying our sampling strategy, i.e. sub-sampling every 30° in longitude and 3° in latitude every three months, to our simulated air-sea fluxes, gave more than 4000 (360°/30° x 30°/3° x 365/91 days) realisations (grids) per year. Sub-sampling can change the surface area sampled. Thus, to ensure that the fluxes calculated for each grid could be compared, the air-sea flux was calculated in flux/m^2 and then multiplied by the Southern Ocean surface area. The annual mean uptake and uncertainty that were calculated for the 1990s by applying our sampling strategy are summarised in Table 3.1 (column 2).

Year	Total Simulated Uptake (PgC/yr)	Sub-Sampled estimate of uptake (PgC/yr)	Sampling Uncertainty (2σ) (PgC/yr)
1990	0.67	0.63	0.21
1991	0.76	0.73	0.17
1992	0.99	0.97	0.21
1993	0.71	0.67	0.24
1994	0.56	0.52	0.18
1995	0.54	0.49	0.22
1996	0.53	0.49	0.20
1997	0.49	0.44	0.24
1998	0.38	0.32	0.26
1999	0.40	0.32	0.22
1990-1999	0.60 ± 0.12	0.56 ± 0.13	

Table 3.1. Comparison of the total simulated uptake with the uptake from our proposed sampling and the sampling error introduced, please refer to the text for an explanation. Estimates are of the Southern Ocean (south of 40°S).

We applied our sampling strategy to the simulated fluxes and returned a sampling uncertainty (from > 4000 permutations/yr) of ± 0.2 PgC/yr (2σ) for the Southern Ocean uptake, for any year in the 1990-1999 period (Table 3.1; column 3). This uncertainty level in uptake translates to a global mean oceanic uptake error of approximately ± 10%. For the 1990s, the estimated sampling error was ± 0.07 PgC/yr ($2\sigma_{\overline{Sampling}} = 2\sigma_{Sampling}/\sqrt{10}$).

The annual mean uptake from our sampling strategy was systematically less, as seen in Table 3.1 (column 2), than the total simulated value (column 1). This was due to the bias introduced to the sampling estimate by starting our 3° latitudinal sampling at either 40°, 41° or 42°. The mean values of the annual air-sea fluxes decrease as a function of increasing the latitude (40° to 42°). This error can be as large as ± 0.1 PgC/yr and was included in the sampling error. If we sample our model at every degree N-S, we remove this bias from the estimated uptake, but do not change the estimate of the sampling uncertainty.

The value of interannual variability returned by applying our sampling strategy in the Southern Ocean was ± 0.1 PgC/yr (1990-1999), which is the same value as calculated by sampling at the resolution of the model. Our results showed that even sampling at the maximum model resolution during the 1990-1999 period, would not improve the flux estimate beyond ± 0.1 PgC/yr.

To estimate the total uncertainty we combined our sampling error with the uncertainty due to interannual variability. We assumed these errors were independent and added these accordingly ($2\sigma_{Total} = \sqrt{(2\sigma)^2_{Interannual} + (2\sigma)^2_{Sampling}}$) to estimate an annual averaged uptake for the 1990s of 0.6 ± 0.1 PgC/yr.

The uncertainty calculated when we combined our sampling and interannual variability error estimates was the same as that calculated by sampling at the resolution of the model. This result suggested: i) the uncertainty introduced when we applied our sampling strategy was small compared to the uncertainty due to interannual variability; and further that ii) sampling at a higher resolution that our proposed sampling would not improve the large-scale regional flux estimates.

We repeated this sensitivity study, with the subgrid scale variability calculated from the observations removed. This second analysis showed no change in the annual mean estimate and offered no significant improvement in the sampling error (< 0.002 PgC/yr). These results suggested that the non-seasonal variability was being driven by longer wavelength changes such as interannual variability rather than mesoscale (subgrid scale) variability.

3.4.4 Sensitivity test of the present sampling strategy

To assess the uncertainty of the present Southern Ocean sampling effort on the annual uptake of CO_2 we used the observational effort shown in Figure 3.1 to approximate the current sampling effort. From Figure 3.1 there appear to be 5 north-south sections in the Southern Ocean (~60°E, 120°E, 180°E, 60°W), which are repeated several times a year. We added one more section along 120°W, to approximate additional one-time observations; this allowed Southern Ocean spatial coverage close to every 60° in longitude. We also assumed that this sampling was completed regularly 4 times per year (i.e adequate data coverage in the winter); This was an overestimate of the actual seasonal coverage since there are few observations in the winter season. We chose also to sample every degree in latitude to better represent ship-based measurements. We do not believe this sampling improves on the present sampling of the Southern Ocean but does provide a useful assessment of the uncertainty in the Takahashi et al. (2002) Southern Ocean uptake estimate and an estimate of the uncertainty achievable using the present sampling effort.

Re-applying our sensitivity analysis from section 3.3 to this new, coarser sampling grid, the uncertainty in the uptake for any year in the 1990s was ± 0.4 PgC/yr (2σ) (Table 3.2). These results are derived from more than 2700 grid permutations/yr (360°/60° x 30°/1° x 365/91 days). This sensitivity analysis showed that halving the proposed longitudinal (east-west) sampling doubled the error due to sampling.

Year	Total Simulated Uptake (PgC/yr)	Sub-Sampled estimate of uptake (PgC/yr)	Sampling Uncertainty (2σ) (PgC/yr)
1990	0.67	0.67	0.37
1991	0.76	0.77	0.33
1992	0.99	1.0	0.42
1993	0.71	0.72	0.42
1994	0.56	0.55	0.38
1995	0.54	0.54	0.36
1996	0.53	0.53	0.36
1997	0.49	0.49	0.42
1998	0.38	0.38	0.37
1999	0.40	0.40	0.38
1990-199	0.60 ± 0.12	0.61 ± 0.12	

Table 3.2. Comparison of the total simulated uptake with the uptake from the current sampling and the sampling error introduced, please refer to the text for an explanation.

Estimates are of the Southern Ocean (south of 40°S) Approximating the current Southern Ocean sampling, interannual variability was estimated to be ± 0.1 PgC/yr (1990-1999; column 2). Combining interannual variability with the calculated sampling error (Table 3.2; column 3) we estimated the annual uptake for the Southern Ocean to be 0.6 ± 0.2 PgC/yr (1990-1999). The error introduced by the present sampling was double the error of our recommended strategy. Taking into account our initial assumptions of data and seasonal coverage, the error estimate of ±0.2 PgC/yr can be considered a lower bound uncertainty of the Takahashi et al. (2002) estimate of the Southern Ocean CO2 uptake for the 1990s.

3.4.5 Comparison with Other Studies

We compare our sampling strategy to those published by Garçon et al., 1992) and Mémery et al., 2002). Both these studies used high-resolution 1-D time-series data of air-sea CO_2 fluxes to recommend temporal sampling of 24 and >70 annually (respectively). The findings of Garçon et al. (1992) and Mémery et al. (2002) are consistent with the results shown in Figures 3.5(b) and 3.5(d). These figures demonstrate that for a very small wavelength (λ), i.e. sampling spatially at very few points, the increase in SNR is small with increasing temporal resolution: therefore many temporal samples are needed to maximise the SNR.

Sweeney et al., 2002) using Southern Ocean observations along 170°W, suggested sampling every ~2.5° of latitude in summer and every ~7.5° of latitude in winter. Their sampling strategy was based on determining the number of samples required to constrain the mean ΔpCO_2 to within ± 4.3 μatm (equating to an uncertainty of ± 0.1 PgC/yr over the entire Southern Ocean). Although they use a different criterion for determining the required sampling, their results based on Southern Ocean observations are consistent with our analysis of the simulated fluxes. The agreement further supports the assertion that the model does simulate the spectral characteristics of the observations and the model-derived sampling strategy is applicable to the real ocean.

Takahashi and Sweeney (2002) explored the uncertainty introduced by subsampling in time and space, the coarse resolution (4° x 5°) monthly climatological maps of air-sea flux of CO_2 (extended from Takahashi et al., 1997)). Although Takahashi and Sweeney (2002) did not identify specific Southern Ocean sampling requirements, their global analysis suggests that measurements every three months is sufficient to determine the net CO_2 air-sea flux. They saw no significant improvement in the basin scale net air-sea flux by increasing temporal sampling. Although the monthly climatological data does not include variability on time-scales of less than a month, their results are consistent with our conclusion that most of the variance in the signal of the air-sea fluxes is resolved by three-monthly sampling.

Our sampling strategy suggests different sampling requirements when moving zonally (east-west) and meridionally (north-south) through our study area, consistent with the results of Takahashi and Sweeney (2002). Our sampling strategy is also consistent with the results of Sweeney et al. (2002) and Takahashi and Sweeney (2002) who demonstrated that regular sampling - spatially and temporally - produced better flux estimates than irregular sampling. A comprehensive understanding of the spatial and temporal characteristics of the real ocean would be needed to allow an irregular sampling approach to be exploited.

3.5. Conclusion

We used a BOGCM model simulation driven by NCEP-R1 forcing in conjunction with subgrid-scale estimates of variability to investigate the sampling required to constrain annual uptake in the 1990s of CO_2 by the Southern Ocean. The results showed that a regular three-monthly sampling every 30° in longitude and 3° in latitude would return the annual mean air-sea CO2 flux to within ± 0.1 PgC.

The comparison between observations and the model suggests that the model does represent the statistical properties of the real ocean and captures much of the large-scale variability that exists in the Southern Ocean. A more complex biological model or higher resolution model may better represent high frequency, non-seasonal variability but would not change the accuracy or precision of the large-scale flux estimates. However, this result is specific to resolving the large-scale fluxes, and finer scale sampling may be important for understanding biogeochemical cycling and its drivers.

The proposed sampling of ΔpCO_2 was independent of the error due to uncertainty in gas transfer in air-sea CO_2 fluxes. Therefore, the equivalence between the sampling strategies for air-sea CO_2 flux and for ΔpCO_2, suggest that the strategy we developed is independent of the uncertainty in gas transfer. As the uncertainty in gas transfer can be very large e.g. Nightingale et al. (2000) it is important that the uncertainty calculated by implementing our sampling strategy account for the (additional) uncertainty due to gas transfer.

The goal of determining the Southern Ocean net seasonal air-sea flux to within the natural variability of the system is achievable by augmenting the existing measurements to improve data coverage. The opportunities to make measurements in the Southern Ocean are limited and a number platforms need to be utilised, including additional underway ship observations, time-series moorings and potentially, the use of CO_2 sensors mounted on drifters or profiling floats. An example is the development of a CO_2 sensor on a profiling drifter like *ARGO* (Gould et al., 2004) to utilise its' spatial coverage. *ARGO* drifters have a proposed coverage of 3° x 3° globally (*ARGO Science Team, 1998*); only10% of these in the Southern Ocean would need to be instrumented to satisfy the sampling requirements proposed from our study.

3.6 Appendix

To derive the equation that describes the variance explained as a function of frequency we derived this relationship in one-dimension as follows. The variance in the time domain of time-series, *h(k)*, of *N* observations is given by:

$$\sigma^2_{time} = \frac{1}{N}\sum_{k=0}^{N-1}\left|(h(k)-\overline{h(k)})\right|^2 = \frac{1}{N}\sum_{k=0}^{N-1}\{h(k)^2 - \overline{h(k)}^2\} \qquad \text{(A3.1)}$$

Using the discrete Fourier Transform, the times-series to frequency-series, *H(n)*, is related as follows:

$$h(k) = \frac{1}{N}\sum_{n=0}^{N-1} H(n)e^{2\pi ikn/N} \quad \text{and} \quad H(n) = \sum_{k=0}^{N-1} h(k)e^{-2\pi ikn/N} \qquad \text{(A3.2)}$$

By Parseval's Theorem the total power in the time domain to the total power in the frequency domain are related (as shown in any textbook on spectral analysis e.g. Hzu (1970)) by:

$$\sum_{k=0}^{N-1} h(k)^2 = \frac{1}{N}\sum_{n=0}^{N-1} H(n)^2 \qquad \text{(A3.3)}$$

Using the definition of the mean of the time-series:

$$H(0) = \sum_{k=0}^{N-1} h(k) = N\overline{h(k)} \qquad \text{(A3.4)}$$

and substituting (A3.4) and (A3.3) into equation (A3.1), the relationship between variance in the time domain to variance in .the frequency domain is:

$$\sigma^2_{time} = \frac{1}{N^2}\sum_{n=0}^{N-1}\{H(n)^2 - H(0)^2\} = \frac{1}{N^2}\sum_{n=1}^{N-1} H(n)^2 = \sigma^2_{freq} \qquad \text{(A3.5)}$$

We use equation (A3.5) to define the SNR resolved by frequencies below *f* as:

$$SNR(f) = \frac{\sum_{n=1}^{f} H_{signal}(n)^2}{\sum_{n=1}^{f} H_{noise}(n)^2} \qquad \text{(A3.6)}$$

4. THE ROLE OF THE SOUTHERN ANNULAR MODE (SAM) IN SOUTHERN OCEAN CO_2 UPTAKE

Andrew Lenton[1,2]

(Andrew.Lenton@csiro.au)

Richard J. Matear[3,2]

(Richard.Matear@csiro.au)

1. Institute for Antarctic and Southern Ocean Studies (IASOS), University of Tasmania, Australia

2. Antarctic Climate and Ecosystem Cooperative Research Centre (ACE CRC), University of Tasmania, Australia

3. CSIRO Marine and Atmospheric Research (CMAR), Tasmania, Australia

Submitted to Global Biogeochemical Cycles *March 2006*

Revised and submitted *October 2006*

4.1 Abstract

A biogeochemical ocean general circulation model, driven with NCEP-R1 and observed atmospheric CO_2 history, is used to investigate and quantify the role that the Southern Annular Mode (SAM), identified as the leading mode of climate variability, has in driving interannual variability in Southern Ocean air-sea CO_2 fluxes between 1980 and 2000. The SAM has been shown to induce circulation changes that include altering the strength of both the upwelling of circumpolar deep water along the Antarctic Coast and the northward Ekman transport. The Southern Ocean is shown to be a region of decreased CO_2 uptake during the positive SAM phase and increased CO_2 uptake during the negative SAM phase. The SAM is shown to induce a change in Southern Ocean CO_2 uptake of 0.18 PgC/yr per unit change in the SAM with a 4-month phase lag, and to explain 47% of the variance in the total interannual variability in air-sea CO_2 fluxes. The analysis shows that the response of the Southern Ocean to the SAM is governed by changes in ΔpCO_2 and not by changes in the gas exchange co-efficient. We demonstrate that it is through changes in ocean physics that control the supply of nutrients to the upper ocean, primarily Dissolved Inorganic Carbon (DIC) that air-sea CO_2 fluxes respond to the SAM. The SAM is predicted to become stronger and more positive in response to climate change and our results suggest this will decrease the Southern Ocean CO_2 uptake.

4.2. Introduction

The Southern Ocean, with its energetic interactions between the atmosphere, ocean and sea ice, plays a critical role in ventilating the global oceans and regulating the climate system though the uptake and storage of heat, freshwater and atmospheric CO_2 (Rintoul et al., 2001; Sarmiento et al., 2004). Recent studies suggest that the formation of Sub-Antarctic Mode Water (SAMW) alone may be responsible for as much as 40% of the uptake of anthropogenic CO_2 by the oceans (Sabine et al., 2004). The uptake of CO_2 in the Southern Ocean is primarily through air-sea fluxes which are both poorly sampled and highly variable (Sabine and Key, 1998; Louanchi et al., 1999; McKinley et al., 2004). Consequently, the carbon budget remains poorly constrained with large uncertainties in the global carbon budget and hence in the predicted response to climate change.

Air-sea CO_2 fluxes can be described as a combination of seasonal and non-seasonal variability. In the Southern Ocean seasonal variability - a complex interplay between biological production and deep winter mixing - is the dominant mode of variability. The mechanisms that drive seasonality are well known but the magnitude remains poorly constrained (Metzl et al., 2006; Metzl et al., 1999; Metzl et al., 1995; Louanchi and Hoppema, 2000; Louanchi et al., 1999; Roy et al., 2003). In the Southern Ocean the non-seasonal variability, particularly interannual variability, can also be large (Jabaud-Jan et al., 2004; Metzl et al., 2006); but the interannual changes in biological production, ocean dynamics and thermodynamics that drive these changes are poorly understood and therefore poorly quantified at the interannual timescales. The sampling study in Chapter 3 showed that the non-seasonal variability, dominated by interannual variability, was responsible for the largest component of the uncertainty in the annual mean uptake of CO_2 by the Southern Ocean.

Studies have identified the Southern Annular Mode, which is characterised by changes in atmospheric mass between 20°S and 90°S, as the dominant mode of climate variability in the Southern Hemisphere e.g. (Thompson and Solomon, 2002; Visbeck and Hall, 2004). The SAM induces changes in the strength of westerly winds which have been shown to induce significant changes in ocean circulation (Hall and Visbeck, 2002; Oke and England, 2004). These include: (1) changes in the strength of northward Ekman Flow and increased upwelling along the Antarctic Continent; (2) changes in the vertical tilt of the isopycnals; (3) downwelling around 45°S and (4) changes in the strength of the Antarctic Circumpolar Current (ACC) resulting in changes in mixed layer depth and oceanic heat transport. The SAM is also known as the Antarctic Oscillation (AAO) (Gong and Wang, 1999) and the High Latitude Mode (HLM) (Rogers and van Loon, 1982).

The Northern Annular Mode (NAM), also known as the North Atlantic Oscillation (NAO) or Arctic Oscillation (AO) has been shown to play an important role in driving interannual variability in air-sea CO_2 fluxes in the Northern Hemisphere (Gruber et al., 2002). It is logical then to explore and quantify whether the SAM plays a similarly important role in driving interannual variability in Southern Ocean CO_2 fluxes. This study is unique; no previous studies exist that quantify the air-sea CO_2 flux in the Southern Ocean and the relative importance of its drivers in response to the SAM.

Hall and Visbeck (2002), using a physical only ocean model, hypothesised that in its positive phase the SAM would drive a strong decrease in the CO_2 uptake, due to the increased upwelling of Dissolved Inorganic Carbon (DIC). This predicted response appears to contradict a recent study based on remotely sensed observations (Lovenduski and Gruber, 2005) that looked at the effect of the SAM on the entire carbon cycle over non-seasonal time scales. Lovenduski and Gruber (2005) suggested that when integrated over the entire Southern Ocean between the Subtropical Front (STF) and the Antarctic Continent, the SAM would elicit only a moderate net CO_2 flux response. They suggested that while upwelling of nutrient rich waters did occur in response to the SAM, this effect was offset by changes in export production and solubility.

Present climate change projections suggest that the amplitude of the SAM will increase and become more positive in future decades (i.e. stronger and more sustained increases in zonal wind stress) (Cai et al., 2003; Kushner et al., 2001). If we can understand and quantify the interannual variability in CO_2 air-sea fluxes explained by the SAM from 1980-2000, this relationship may be able to be used to predict the response of the Southern Ocean carbon cycle to climate change.

As the Southern Ocean remains one of the most poorly carbon sampled regions globally, we used a prognostic Biogeochemical Ocean Global General Circulation Model (BOGCM). In this study we used the Commonwealth Scientific Industrial Research Organisation (CSIRO) Mark 3.1 model, driven with NCEP-R1 atmospheric forcing and observed CO_2 history, to simulate the interannual variability of the Southern Ocean carbon cycle, for the period 1980-2000. We defined the Southern Ocean to be the region of ocean bounded by 40°S and the Antarctic Continent.

This paper examines and quantifies the response to the SAM of CO_2 fluxes in the Southern Ocean and in each of its ocean sectors. This paper is structured as follows: in Section 4.3 we describe our methodology; Section 4.4 presents our results; and Section 4.5 gives our conclusion and discussion. In this final section we compare our results to other studies and suggest what impact the predicted role of the SAM under climate change may have on Southern Ocean CO_2 uptake.

4.3 Simulation and Approach

4.3.1 Modelling the Southern Ocean

To compensate for the lack of observed air-sea CO_2 fluxes, a prognostic 3D Biogeochemical Ocean General Circulation Model (BOGCM) was used. A global domain model thereby avoiding any problems related to open boundary conditions. The ocean general circulation module (OGCM) of the BOGCM was based on the Z coordinate Modular Ocean Model (MOM) - Version 3 (Pacanowski and Griffies, 1999). The model grid has a horizontal resolution of 0.94° N-S and 1.9° E-W at the equator with a tapering of longitude as a function of cosine (T63-2) and 31 non-regular vertical levels - 15 levels in the upper 500m. To represent the effects of eddies not simulated in the model, the eddy parameterisation of Gent and McWilliams (1990) was implemented, as was the Chen mixed layer scheme (Chen et al., 1994) to parameterise upper ocean mixing.

The biogeochemical module of the BOGCM predicted DIC, alkalinity, oxygen and phosphate. What follows is brief description of this model: a more detailed description of the model is given in Matear and Hirst (1999) and Matear (2004). Export production in the top 50m was calculated as a function of light, phosphate, temperature and mixed layer depth. $CaCO_3$ production was set at 8% of the export production following Yamanaka and Tajika (1996) and consistent with Trull, et al. (2001). Below the euphotic zone, particulate organic matter was remineralised as a function of depth according to $(z/100)^{-0.9}$ following values deduced from observations Suess (1980) and Martin et al. (1987); and $CaCO_3$ according to $e^{(-z/3500)}$ following Yamanaka and Tajika (1996). Nutrient uptake and remineralisation of P:N:C:O_2 were related via the Redfield ratio of 1:16:106:-138 (Redfield et al., 1963) in and below the euphotic zone.

The model was forced with daily wind stress, heat and freshwater fluxes from NCEP-R1 (Kalnay, 1996). The model was not coupled to sea-ice model, but the effects of sea-ice on heat and freshwater fluxes were accounted for by the use of NCEP-R1 forcing that does contain sea-ice. To avoid excessive model drift, sea surface temperature and salinity were restored to observed sea surface temperatures (SST) (Reynolds and Smith, 1994) and observed sea surface salinity (Conkright et al., 2002) every 30 days. Air-sea gas exchange of CO_2 was calculated following the relationship of Wanninkhof, 1992), using daily wind speed from NCEP-R1. To account for a lack of explicit sea ice, the net CO_2 flux was scaled by the fraction of observed sea-ice cover, interpolated from the monthly-climatological fields of Walsh (1978) and Zwally et al., (1983). A net flux into the ocean was defined as positive and ΔpCO_2 as atmosphere minus ocean.

The model was initialised with the observed fields from Conkright et al. (2002) and evolved for > 4000 years. Following this initial evolution the model was reinitialised with the temperature and salinity fields from Conkright et al., 2002) in accordance with the protocols of the Northern Ocean Carbon Exchange Study (NOCES)/Ocean Carbon Model Intercomparison Project 3 (OCMIP3) (Aumont et al., 2004). The model was then evolved from 1837 to 2002 with observed atmospheric pCO_2 values from Enting et al. (1994) in accordance with the protocols of NOCES/OCMIP3. The protocols of NOCES were designed to best simulate variability in global biogeochemical ocean models on interannual to interdecadal timescales.

To isolate the simulated interannual variability in the monthly averaged biogeochemical fields, we calculated for the 1980-2000 period the seasonal climatology and subtracted this from the simulated fields. The remaining non-seasonal variability was smoothed with a 12-month running-mean filter to ensure that only interannual variability was extracted.

4.3.2 Positions of the Fronts

The Southern Ocean south of 40°S is made up of a series of major fronts and interfrontal zones: each of these zones has its own unique set of biogeochemical and physical properties. To facilitate our later discussion of the response of each region, the mean positions (1980-2000) of the major fronts of the Southern Ocean were identified based on temperature definitions (θ). These major fronts and their definitions were the Subtropical Front (STF) θ<10°C at 150m (Orsi et al., 1995), the SubAntarctic Front $\theta > 4$°C at 400m (Orsi et al., 1995) and the Polar Front (PF) $\theta > 2$°C at 300m (Trull et al., 2001). These fronts separate the four major interfrontal zones of the Southern Ocean: the Subtropical Gyre (north of the STF); the SubAntarctic Zone (SAZ; between the STF and SAF); the Polar Frontal Zone (PFZ; between the SAF and PF); and the Antarctic Zone (south of the PF). These fronts and interfrontal zones are displayed on subsequent spatial maps.

4.3.3 The Southern Annular Mode (SAM)

The SAM is assessed in terms of the SAM index, defined as the time-series of the 1st EOF of the 850 hPa geopotential height anomaly. We use the NCEP-R1 reanalysis (Kalnay, 1996) to calculate the geopotential height anomaly (1980-2000) by subtracting the mean climatology between 1979-2000. In the calculation of the mean we neglected data prior to 1979 because it is not well validated over Antarctica (Marshall, 2002). The SAM index was then smoothed with a 12-month running-mean filter to ensure that only interannual variability in the SAM was captured. The SAM index (1980-2000; Figure 4.1) showed a definite positive trend consistent with other SAM indices calculated using other techniques and datasets (Marshall, 2002). The spatial pattern of the SAM is also displayed in Figure 4.1.

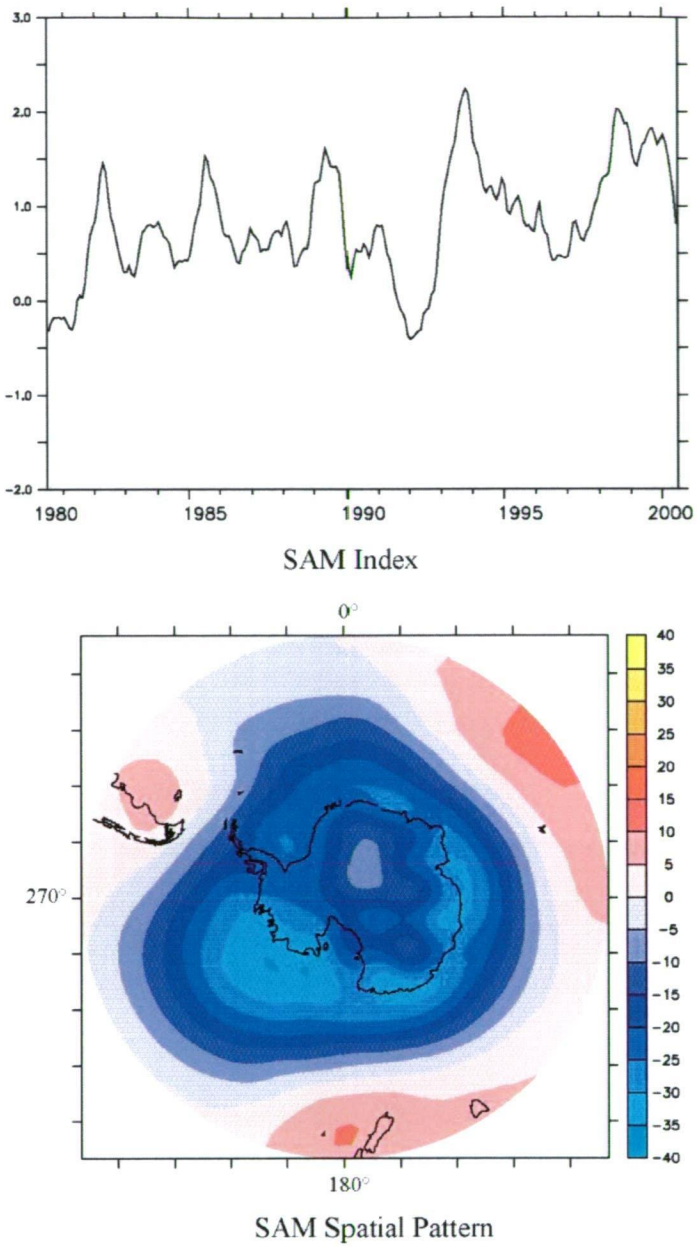

Figure 4.1. The SAM index and spatial pattern as calculated from the NCEP-R1 850hPa geopotential height anomaly

4.3.4 Statistical Approach

To quantify the response to the SAM of the Southern Ocean air-sea CO_2 flux and its components, we regressed these components against the SAM, which allowed us to estimate the response of each component per unit of change in the SAM. We also calculated the square of the corresponding correlation co-efficient or R^2. The R^2 value quantified how much of the simulated variability was explained by the SAM (0 = not at all and 1= totally). This approach is consistent with recent SAM studies e.g. (Lovenduski and Gruber, 2005; Lefebvre et al., 2004; Hall and Visbeck, 2002).

To evaluate the statistical significance of our results we determined the autocorrelation length scale for the time series of 12 months translating to 20 degrees of freedom (n=20). At the 95% significant level, values of $R^2 > 0.1296$ were determined to be statistically significant. In subsequent analyses only the statistically significant part of the spatial maps are included.

4.4 Results

4.4.1 Southern Ocean Fluxes and the SAM

The Southern Ocean's high variability and paucity of sampling make it impossible to validate large-scale interannual variability from observations. Instead we rely on the interannual variability imposed on the model by using NCEP-R1 atmospheric forcing in conjunction with the protocols of NOCES (Aumont et al., 2004). As we chose to restore sea surface temperature to Reynolds and Smith (1994) we can not use this dataset to validate interannual variability following Le Quéré et al. (2000). We do not believe that validating the model at the North Atlantic Bermuda Time Series Station (BATS) nor North Pacific Hawaii Ocean Time Series (HOTS) would elucidate the processes controlling air-sea CO_2 fluxes in the Southern Ocean. Hence, we are forced to rely on model simulations to investigate interannual variability. We note also that in assessing the response of the Southern Ocean to the SAM we use the SAM index as calculated from NCEP-R1, which is entirely internally consistent.

From our simulation the interannual variability for the study area (south of 40°S: 1980-2000) was calculated as ± 0.15 PgC/yr. This variability was regressed against the SAM and the R^2 value was calculated using different temporal phase lags. Integrating the total response of the Southern Ocean to the SAM we see a net decrease in uptake of CO_2 of 0.15 PgC/yr per unit change in the SAM with no phase lag to a maximum value of 0.18 PgC/yr per unit change in the SAM with a lag time lag of 4-months (Figure 4.3).

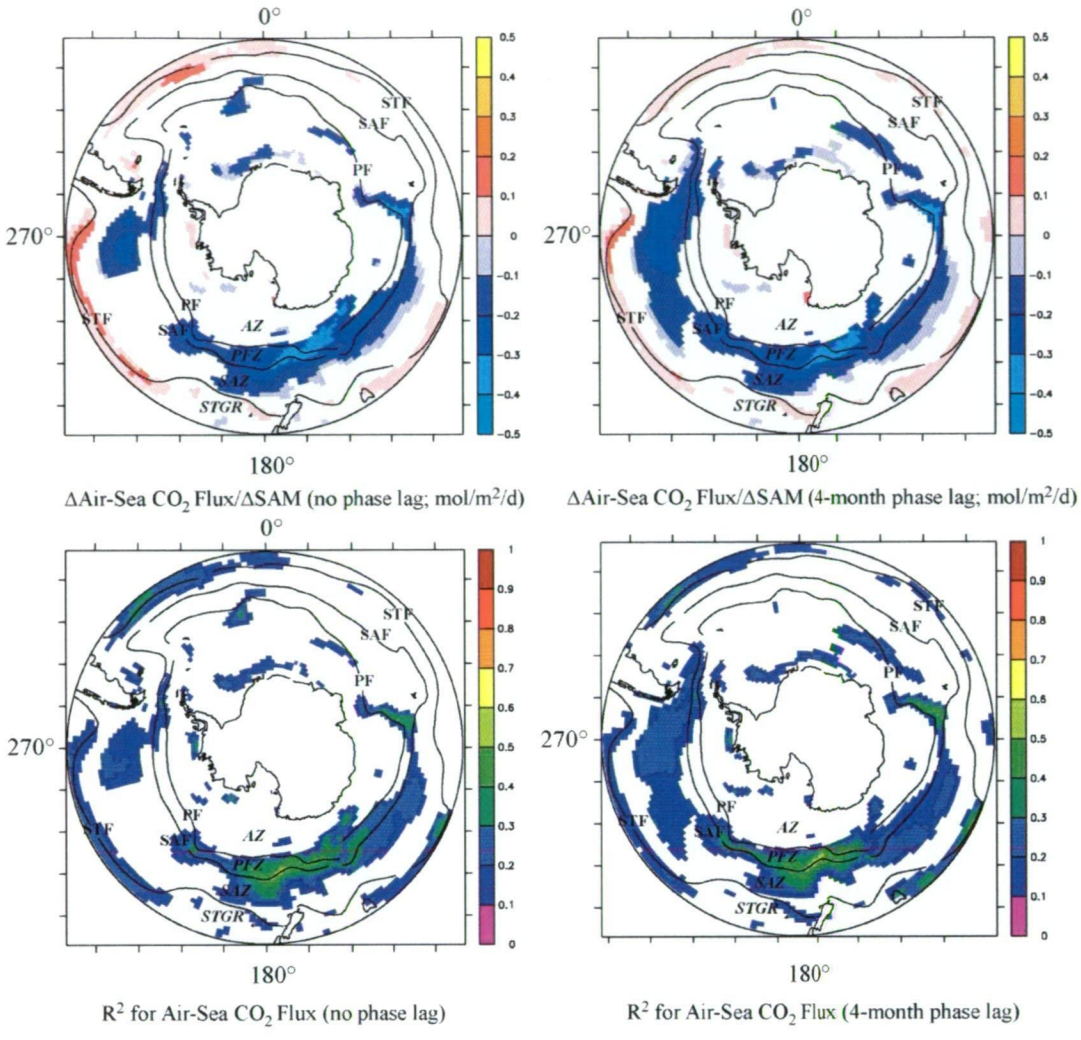

Figure 4.2. Regression (top) and R^2 (bottom) of the SAM Index against air-sea CO_2 flux, with no phase lag (left) and with a 4-month phase lag (right). Note positive represents an increased uptake. Overlain on these maps are the mean positions of the major fronts and interfrontal zones, please refer to the text for definitions. Note units are mol/m^2/day and the areas of white, in the open ocean, represent the non-statistically significant values.

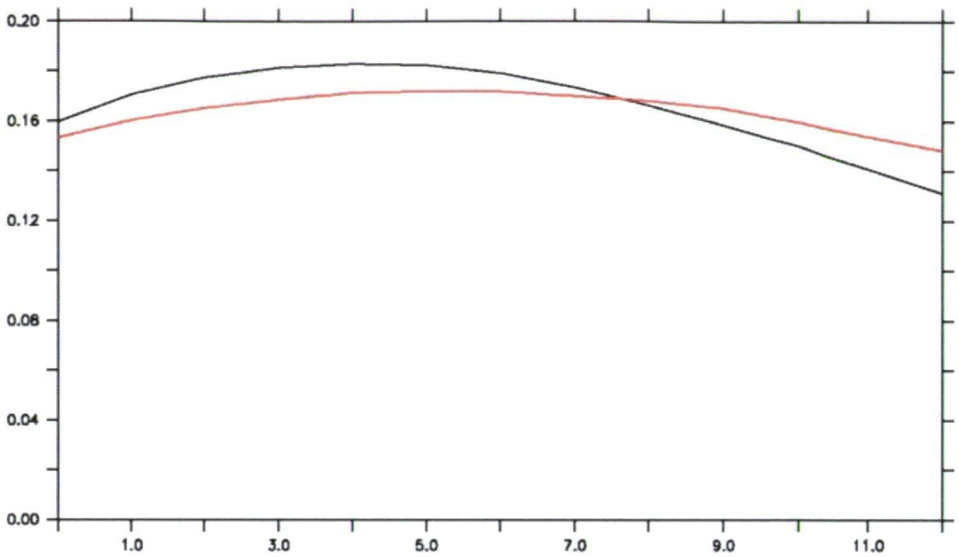

Figure 4.3. The decrease in response to the positive phase of the SAM, with different phase lags, of interannual CO_2 flux uptake in the Southern Ocean south of 40°S (in black), units are PgC/yr. Overlain on this plot in red is the phase lagged response of integrated phosphate, units are $2x10^{10}$ mol.

The phase lag did not significantly alter the spatial pattern of the air-sea flux response of CO_2, only reinforcing the magnitude of the response (Figure 4.2). The regions north and south of the mean position of the STF showed different and opposing responses. North of the mean position of the STF there was an increase in flux of CO_2 into the ocean corresponding to a well-correlated, semi-annular ring at the STF. South of the STF a decrease in the flux of CO_2 into the ocean was evident, with the strongest and most highly correlated response in the PFZ.

The integrated response of Southern Ocean air-sea CO_2 fluxes to the SAM was compared with the total interannual variability (Figure 4.4). The interannual variability was relative to an annual mean uptake of ~0.6 PgC/yr. The amount of the total interannual variance in air-sea CO_2 flux explained by the SAM in the Southern Ocean increased from 36% with no phase-lag to 47% at 4-months, with the largest response in the Pacific Ocean Sector (Table 4.1).

	% Variance explained Pacific Ocean	% Variance explained Atlantic Ocean	% Variance explained Indian Ocean	% Variance explained Southern Ocean
Gas transfer co-eff.	34	5	23	31
ΔpCO_2	22	9	20	17
Air-sea CO_2 Flux	42	17	26	47

Table 4.1 Percent of the total interannual variability variance explained by the SAM south of 40°S.

The SAM can alter Southern Ocean CO_2 fluxes through changes in the gas exchange co-efficient (K) and changes in ΔpCO_2. The response of each of these to changes in the SAM was assessed by regressing these variables against the SAM and then calculating the corresponding R^2 value with a phase lag of 4-months (Figure 4.5).

	%Variance explained Pacific Ocean	% Variance explained Indian Ocean	% Variance explained Atlantic Ocean	% Variance explained Southern Ocean
$\overline{K}\Delta pCO_2'$	93	94	94	93
$K'\overline{\Delta pCO_2}$	7	6	5	6
$K'\Delta pCO_2'$	<< 1	<< 1	< 1	< 1

Table 4.2. Percentage of the total integrated Southern Ocean response of interannual CO_2 flux explained by $\overline{K}\Delta pCO_2'$, $K'\overline{\Delta pCO_2}$ and $K'\Delta pCO_2'$, see text for explanation

A strong annular response of K to the SAM was evident in the region south of the STF (~40°S) and north of the Antarctic Divergence (~63°S). The strongest and most highly correlated (Figure 4.6) response to the SAM was seen in the Indian Ocean PFZ and in the PFZ and SAZ of the Pacific Ocean, where the integrated response to the SAM explains 20% and 22% respectively of the total variance in interannual variability of K (Table 4.2).

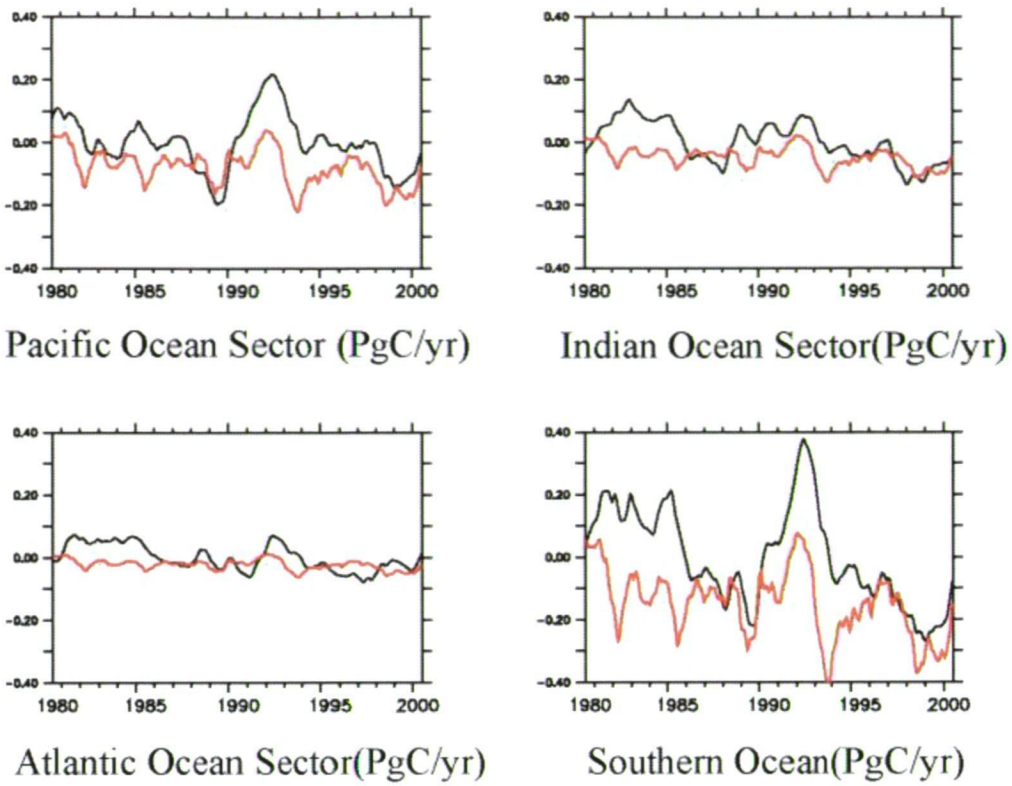

Figure 4.4. Simulated interannual variability in the Southern Ocean total CO_2 uptake (black) and the Southern Ocean CO_2 uptake explained by the SAM (red). Units are PgC/yr.

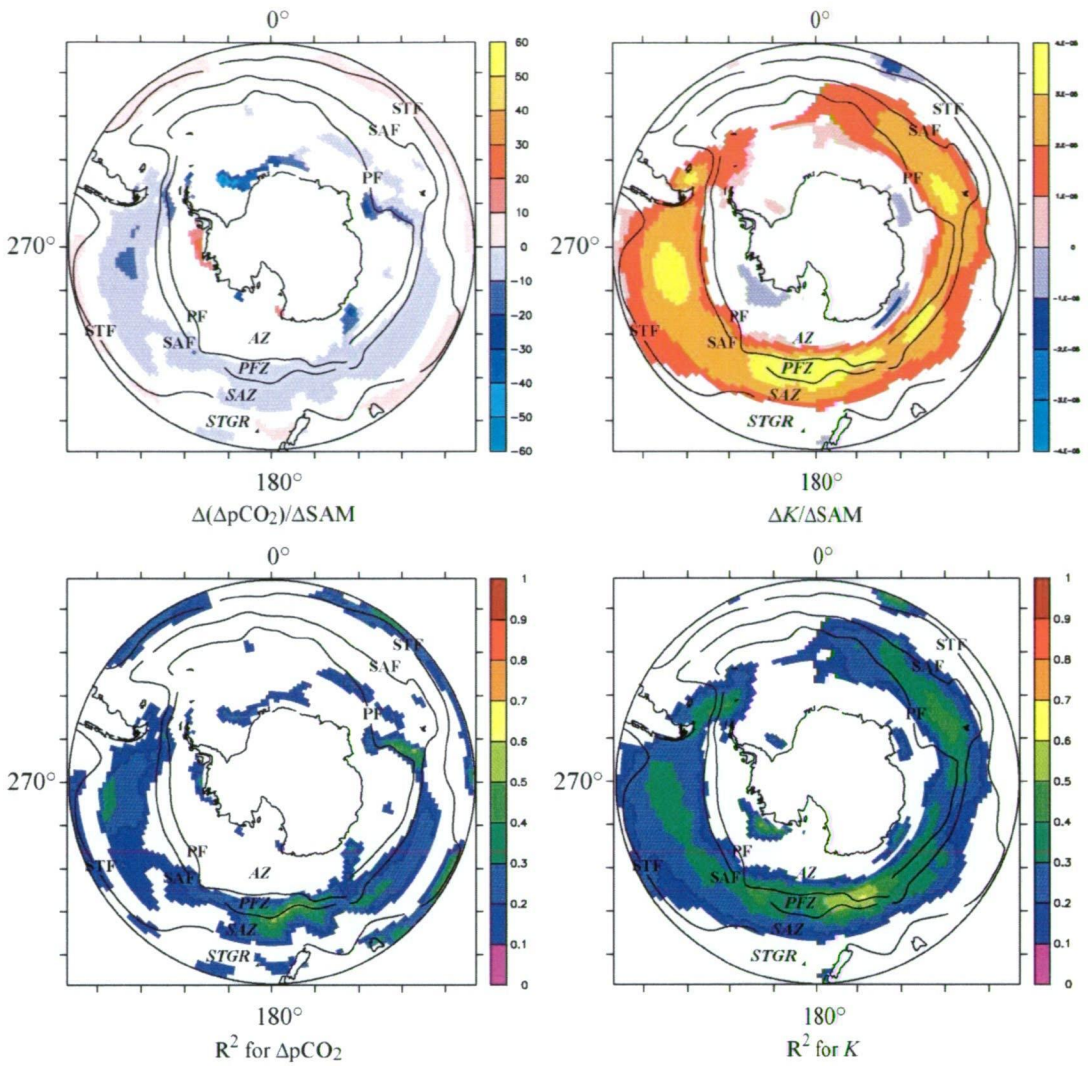

Figure 4.5. Regression and R^2 of the SAM Index against ΔpCO_2 and K with a 4-month phase lag. Overlain on these maps are the means positions of the major fronts and interfrontal zones, please refer to the text for definitions. Note the areas of white, in the open ocean, represent the non-statistically significant values.

The regression and R^2 values of ΔpCO_2 against the SAM (Figure 4.5) showed that when the SAM Index was positive, total ΔpCO_2 decreased. The obvious strong circumpolar response of K was not evident in ΔpCO_2; instead the Southern Ocean showed a very differing circumpolar response north and south of mean position of the STF. South of the STF oceanic ΔpCO_2 showed an increase relative to atmospheric values, while north of this there was a decrease in oceanic values. The exception was the region adjacent to the Antarctic coastline, where these values do not translate to a large air-sea flux because they encompass small areas and covered by sea-ice for much of the year. The explained variance maps (R^2) of ΔpCO_2 show two semi-annular rings of higher explained variance: an inner region, corresponding to the Atlantic Ocean PFZ and the Pacific PFZ; and an outer region, corresponding to the STF. The total variance in ΔpCO_2 explained by the SAM was 17% (Table 4.2). ΔpCO_2 displays more interannual variability than was explained by the SAM.

We explored how much of the total SAM response in the air-sea CO_2 fluxes was driven by changes in K and ΔpCO_2. The air-sea CO_2 flux is given by:

$$F_{AIR-SEA} = K(pCO_{2AIR} - pCO_{2SEA}) = K(\Delta pCO_{2AIR-SEA}) \quad (4.1)$$

Equation 4.1 was rewritten in terms of the temporal mean $\overline{K}$ and variability K' between 1980 and 2000.

$$F_{AIR-SEA} = (\overline{K} + K')(\overline{\Delta pCO_2} + \Delta pCO_2') \quad (4.2)$$

$$F_{AIR\_SEA} = K'\Delta pCO_2' + K'\overline{\Delta pCO_2} + \overline{K}\Delta pCO_2' + \overline{K}\,\overline{\Delta pCO_2} \qquad (4.3)$$

We calculated and regressed each of these terms of Equation 4.3 against the SAM and then divided this by the total response of air-sea CO_2 flux; this provided a means of quantifying the contribution of each term (Figure 4.6). The integrated response (Table 4.2) showed that the ΔpCO_2 response to the SAM ($\overline{K}\Delta pCO_2'$) contributed more than 90% of the total air-sea flux variability: this term was strongest in the PFZ and the AZ, particularly in the Atlantic Ocean sector. The remaining 10% of the air-sea flux variability was driven by changes in K ($K'\overline{\Delta pCO_2}$), while the other terms ($\overline{K}\,\overline{\Delta pCO_2}$ and $K'\Delta pCO_2'$) were negligible. This analysis was repeated with different temporal lags ranging from 0 to >12 months, the results showed that the relative importance of K against ΔpCO_2 decreased as the lag increased.

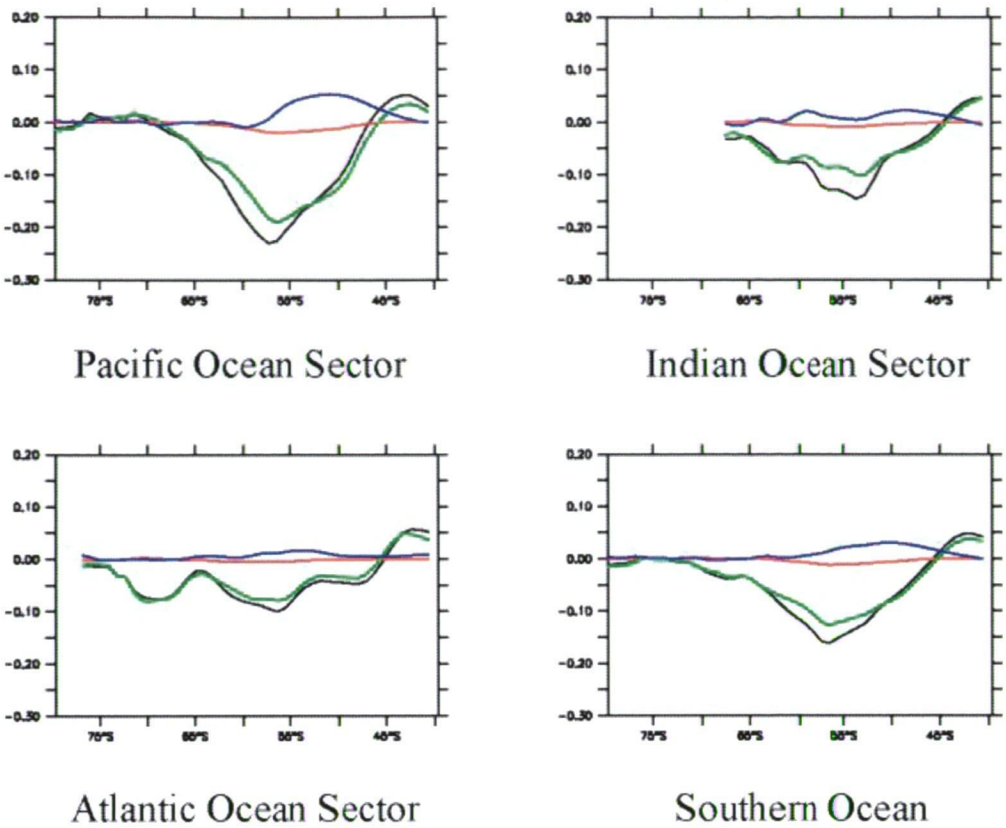

Figure 4.6. Zonally averaged component analysis of interannual variability of CO_2 air-sea flux driven by the SAM in each of the major ocean basins – total air-sea CO_2 flux response (black line) due to: $\overline{K}\Delta pCO_2'$ (green line), $K'\overline{\Delta pCO_2}$ (blue line) and $K'\Delta pCO_2'$ (red line). Units are ((mmol/m^2/day)/ΔSAM Index)

4.4.2 Component Analysis of ΔpCO_2 Variability

Our results showed that more than 90% of the total air-sea flux response was due to the changes in ΔpCO_2. In this section we attempt to understand and quantify what drives changes in ΔpCO_2 in response to the SAM. The value of ΔpCO_2 is a function of four variables: SST, sea surface salinity (SSS), TALK (Total Alkalinity) and DIC (dissolved inorganic carbon), related through the standard equations of carbonate chemistry (Dickson and Goyet, 1994).

As we sought to explore the anomalies, the response of ΔpCO_2 was written as the summation of the regression of each component onto the SAM in units of ΔpCO_2 (μatm), with a 4-month phase lag, shown below:

$$\frac{d\Delta pCO_2}{dSAM} = \frac{\partial \Delta pCO_2}{\partial SST}\frac{dSST}{dSAM} + \frac{\partial \Delta pCO_2}{\partial SSS}\frac{dSSS}{dSAM} + \frac{\partial \Delta pCO_2}{\partial TALK}\frac{dTALK}{dSAM} + \frac{\partial \Delta pCO_2}{\partial DIC}\frac{dDIC}{dSAM} \tag{4.4}$$

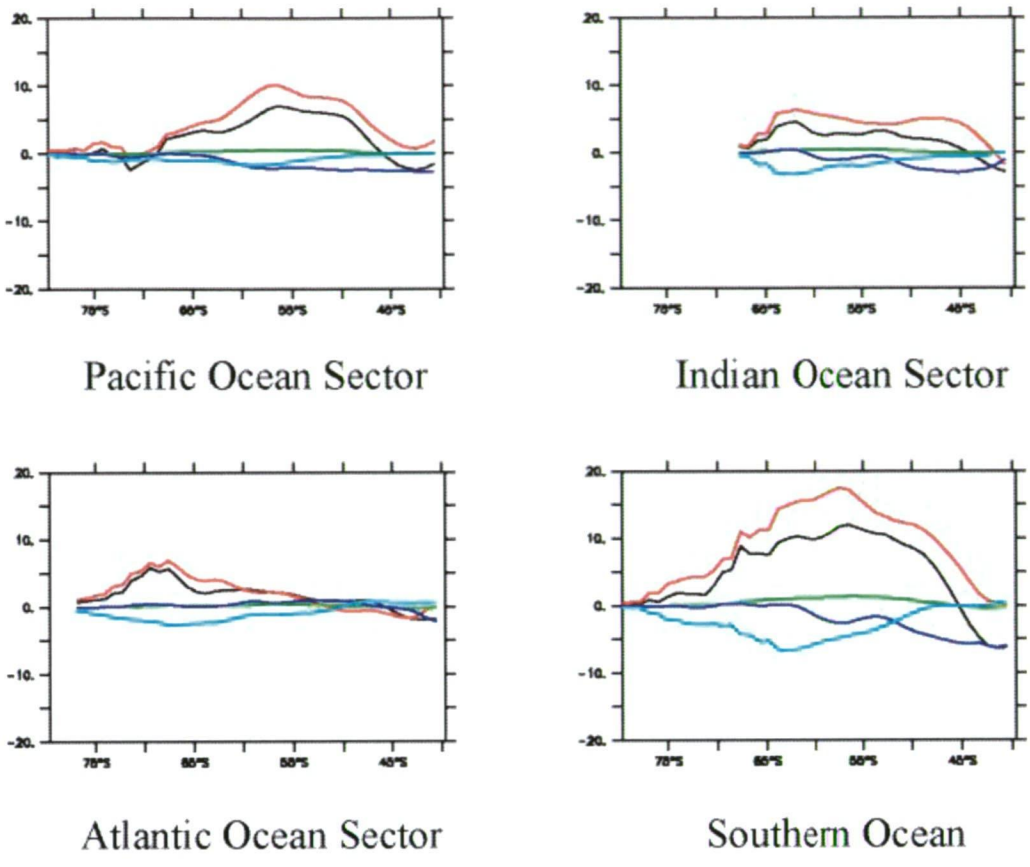

Figure 4.7. Zonally integrated component analysis of interannual variability of ΔpCO_2 driven by the SAM in each of the major ocean basins - total ΔpCO_2 (black line), ΔpCO_2 variability due to: DIC (red line), TALK (light blue line), Salinity (SSS) (green line) and SST (dark blue line); all units are $1x10^7$ µatm

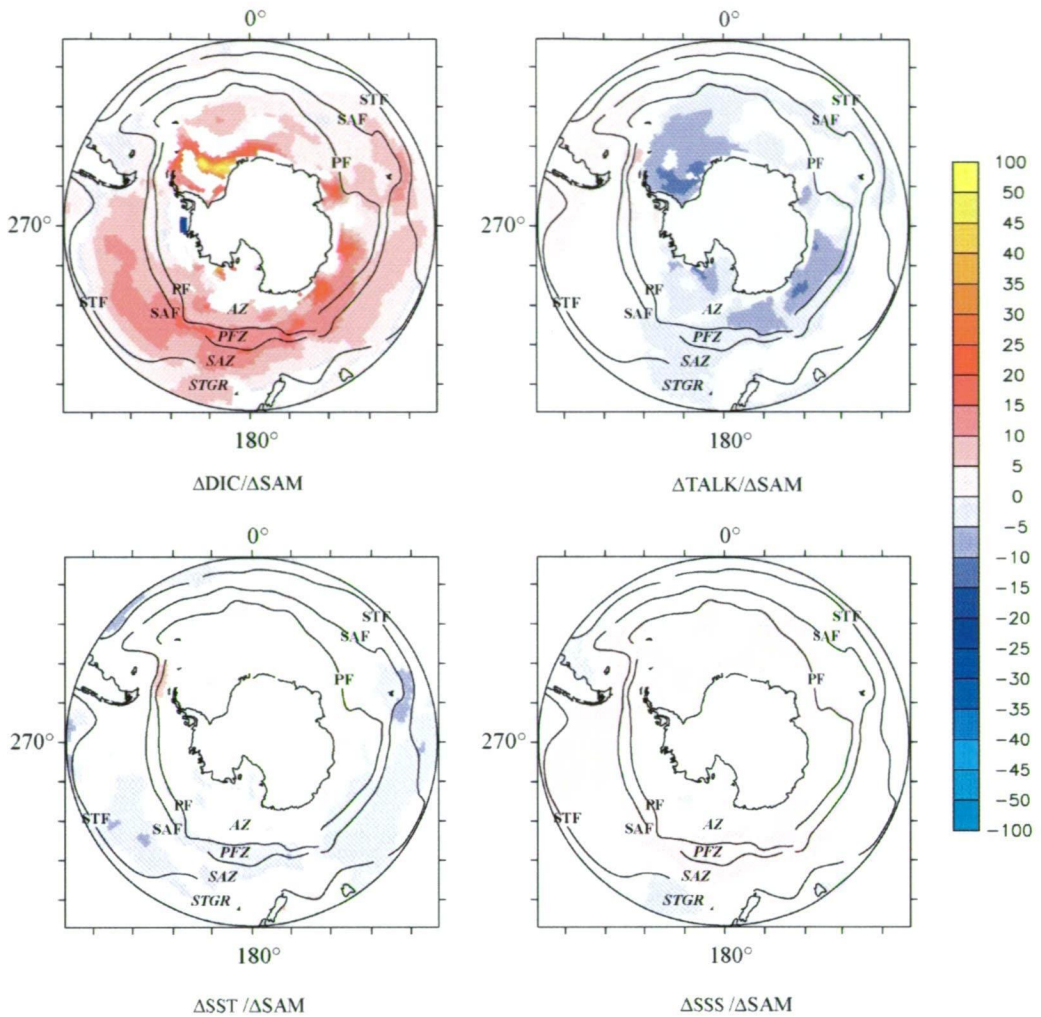

Figure 4.8. Spatial maps of the components of $\Delta pCO_2/\Delta SAM$. Overlain on these maps are the mean positions of the major fronts and interfrontal zones, please refer to the text for definitions. Note all units are µatm and the areas of white, in the open ocean, represent the non-statistically significant values

The component analysis, and associated spatial maps of ΔpCO_2 (Figures 4.7 and 4.8) demonstrated that DIC was the dominant term driving ΔpCO_2 variability. For a positive SAM Index, DIC showed a net increase, which drove an associated increase in ΔpCO_2 in surface waters south of the STF. TALK played a significant compensating role particularly in the PFZ and AZ by decreasing ΔpCO_2 values, partially offsetting the changes due to DIC. North of the STF, the net decrease in SST became the dominant process through solubility changes, causing a decrease in ΔpCO2. The decline in DIC played a minor secondary role in this region reinforcing the decrease in ΔpCO_2. Salinity did not play a large role in driving the SAM response of air-sea CO_2 fluxes in any of the ocean basins. Consistent with the previous results, the component analysis was repeated with different temporal lags ranging from 0 to >12 months and showed that the spatial pattern did not change significantly, nor did the relative importance of each of the drivers of air-sea CO_2 flux to the SAM.

4.4.3 Component Analysis of DIC and TALK

South of the STF, the major drivers of ΔpCO_2 variability due to the SAM were identified as DIC and TALK. In this section we explore what oceanic processes drove this response with a 4-month phase lag.

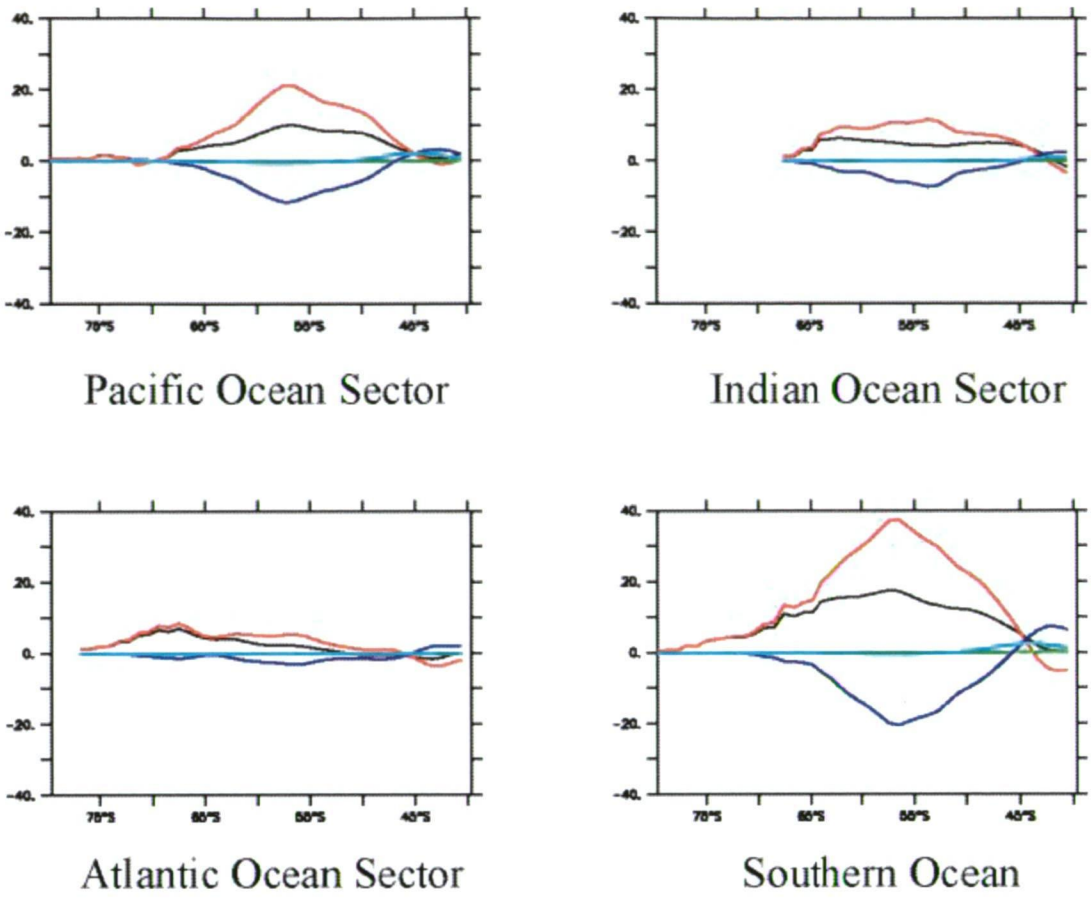

Figure 4.9. Zonally integrated component analysis of interannual variability of DIC driven by the SAM in each of the major ocean basins – total DIC (black line), DIC response due to: ocean physics (red line), air-sea flux (dark blue), dilution (green line) and export production (light blue line). Units are all $1x10^7$ µatm

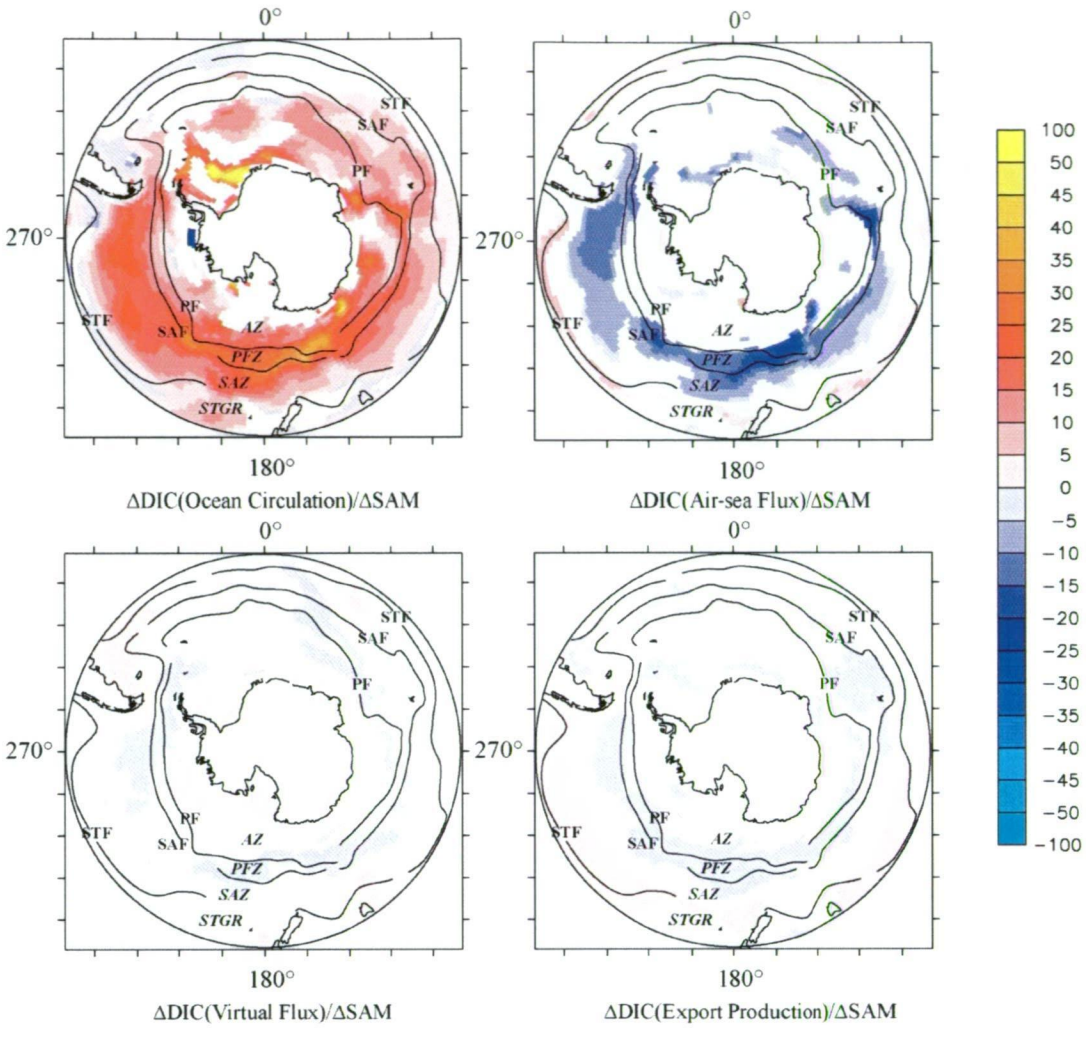

Figure 4.10. Spatial maps of the components of the ΔDIC/ΔSAM. Overlain on these maps are the mean positions of the major fronts and interfrontal zones, please refer to the text for definitions. Note all units are µatm and the areas of white, in the open ocean, represent the non-statistically significant values

Total (SAM) DIC change over the upper grid box of the model (10m) was separated into changes due to: i) ocean physics; ii) air-sea CO_2 flux; iii) freshwater dilution fluxes; and iv) export production, shown by:

$$\frac{\partial \Delta pCO_2}{\partial DIC}\frac{dDIC}{dSAM} = \frac{\partial \Delta pCO_2}{\partial Phys}\frac{dPhys}{dSAM} + \frac{\partial \Delta pCO_2}{\partial Flux}\frac{dFlux}{dSAM} + \frac{\partial \Delta pCO_2}{\partial Dilut}\frac{dDilut}{dSAM} + \frac{\partial \Delta pCO_2}{\partial EP}\frac{dEP}{dSAM}$$

(4.5)

In a similar way the change in TALK over the top 10m of the model was written as the sum of changes due to: i) ocean physics; ii) freshwater dilution fluxes; and iii) export production, shown by:

$$\frac{\partial \Delta pCO_2}{\partial TALK}\frac{dTALK}{dSAM} = \frac{\partial \Delta pCO_2}{\partial Phys}\frac{dPhys}{dSAM} + \frac{\partial \Delta pCO_2}{\partial Dilut}\frac{dDilut}{dSAM} + \frac{\partial \Delta pCO_2}{\partial EP}\frac{dEP}{dSAM} \quad (4.6)$$

The zonally integrated response, and the associated spatial maps, to the SAM of DIC and TALK and their respective components (Figures 4.9-4.13) demonstrated that the ocean dynamics dominated. The largest increase in DIC and TALK was associated with the region adjacent to the Antarctic continent. The magnitude of the changes in DIC and TALK due to ocean dynamics decreased moving northward away from the coast. The response of DIC was partially offset by changes in air-sea CO_2 fluxes, particularly in the PFZ and AZ. Export production and freshwater dilution fluxes played no significant role in driving changes in DIC and TALK in response to the SAM.

To demonstrate the strong link between the physical supply of DIC and air-sea CO_2 fluxes we use phosphate variability as a proxy physical supply. PO_4 is a good proxy for the oceanic supply of DIC as: it contains no air-sea flux term; the export production response is small since the Southern Ocean is not a phosphate limited region; and it is related to DIC via fixed stoichiometric ratios. We calculated the integrated PO_4 in the upper grid box of the Southern Ocean (Figure 4.3) and it showed that the maximum value of PO_4 occurred 5 months after the SAM maximum, 1 month later than the maximum value of air-sea CO_2 fluxes.

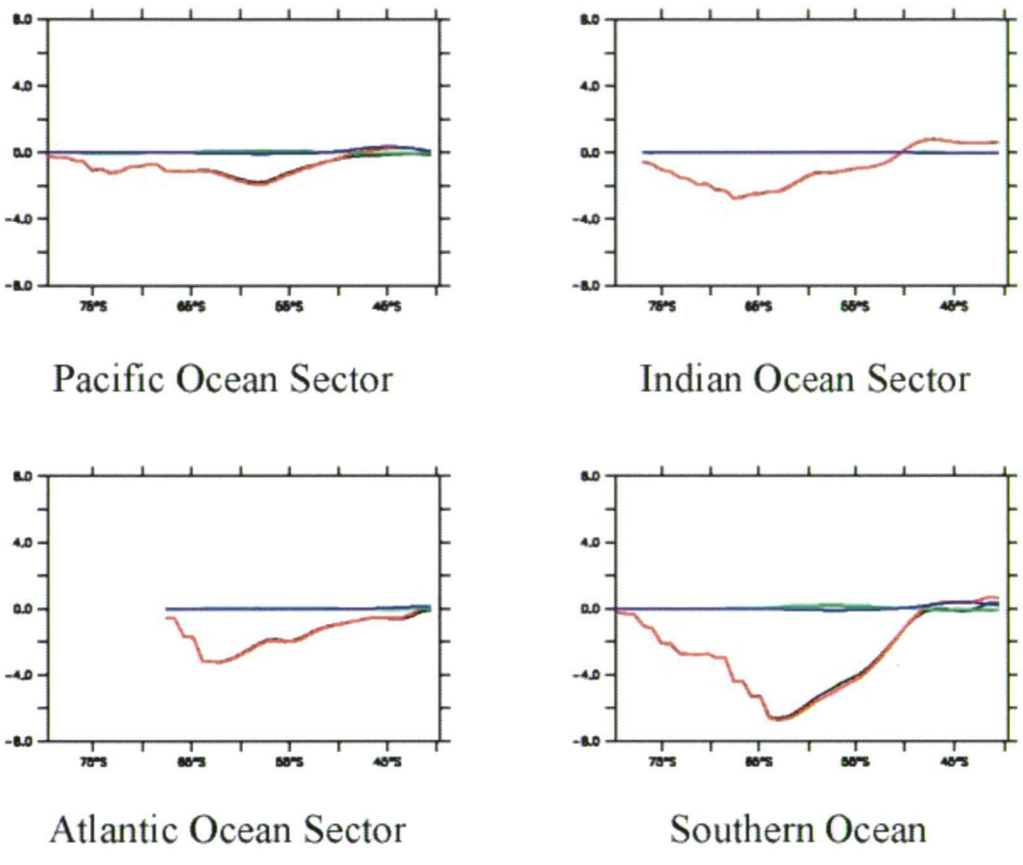

Figure 4.11. Zonally integrated component analysis of interannual variability of TALK driven by the SAM in each of the major ocean basins – total TALK (black line), TALK response due to: ocean physics (red line), dilution (dark blue line) and export production (light blue line). Units are all $1x10^{7}$ *µatm*

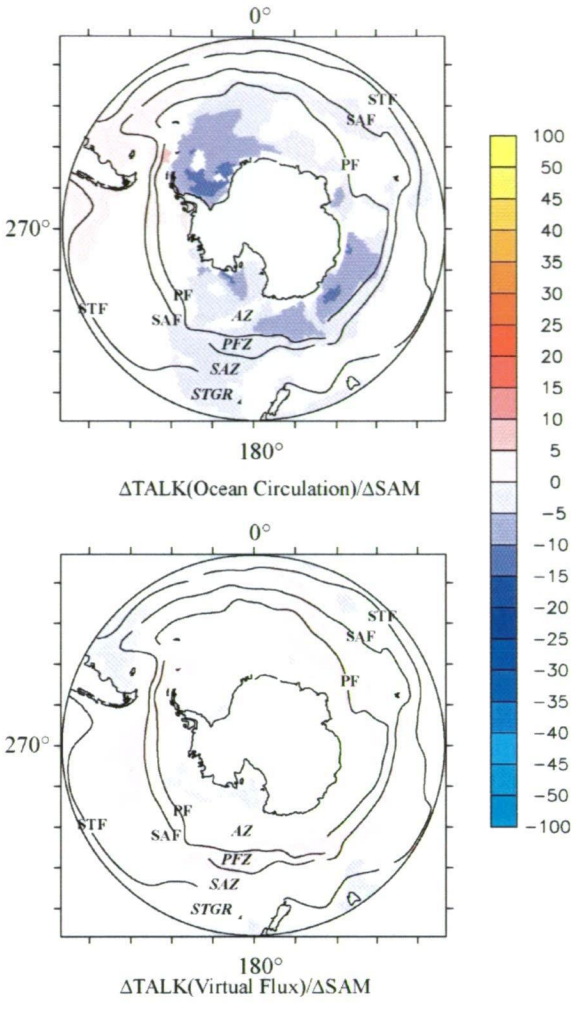

Figure 4.12. Spatial maps of the components of the ΔTALK/ΔSAM. Overlain on these maps are the mean positions of the major fronts and interfrontal zones, please refer to the text for definitions. Note all units are μatm and the areas of white, in the open ocean, represent the non-statistically significant values.

4.5. Discussion and Conclusion

We simulated the Southern Ocean interannual variability by driving a global biogeochemical ocean general circulation model with the NCEP-R1 atmospheric forcing. This experiment was performed in accordance with the protocols of NOCES/OCMIP3 that were designed to simulate variability at interannual and longer timescales (Aumont et al., 2004).

We concluded that the SAM does play an important role in driving interannual variability in air-sea CO_2 fluxes through the oceanic response, explaining 47% of the total interannual variance with a 4-month phase lag. In the positive phase of the SAM, the region south of the STF showed a net decrease in uptake of CO_2, while north of the STF there was a net increase. While these regions did have some compensating effect, when integrated over the Southern Ocean, the region south of the STF was clearly dominant, inducing a change in uptake in CO_2 of 0.18 PgC/yr per unit change in the SAM, relative to the annual mean uptake of 0.6 PgC/yr.

Our results demonstrated that while the SAM affects both K and ΔpCO_2, it was primarily (>90%) changes in ΔpCO_2 that drove the response of air-sea fluxes in the Southern Ocean. Our analysis showed that changes in ΔpCO_2 were in turn driven by changes in the concentration of DIC in Southern Ocean surface waters. South of the STF, during the positive phase of the SAM, ocean physics drove the increased supply of DIC and TALK to surface waters; the strongest response was in the AZ. The increase in ΔpCO_2 due to the supply of DIC was partially offset by increase in TALK. North of the STF during the positive phase of the SAM, surface ΔpCO_2 was decreased by solubility changes due to a decrease in SST. Neither changes in salinity, export production nor freshwater dilution fluxes played any significant role in the response of the Southern Ocean CO_2 fluxes to the SAM.

Our analysis was repeated with different temporal lags ranging from no lag to >12 months and showed that the spatial pattern did not change significantly, nor did the relative importance of the drivers of air-sea CO_2 flux response to the SAM. The only significant difference was the decrease in the relative importance of K compared to ΔpCO_2 in producing the air-sea flux variability as the lag increased.

The 4-month phase lag in the maximum response of air-sea CO_2 fluxes with respect to the SAM was due to the accumulation of DIC that results from the finite response time of air-sea CO_2 gas exchange. The phase lag between the maximum in CO_2 fluxes and the oceanic supply of DIC (PO_4; 1-month) was due to the finite time taken for ocean physics to respond to a change in the SAM and time taken to erase the accumulation of DIC (PO_4) in the upper ocean. In this way the ocean can be considered to have a memory of previous events and maybe preconditioned to other drivers of interannual variability. We note that the length of the phase lags determined may also be a function of the ocean physics implemented in our model; therefore it would be of value to repeat our analysis using other ocean biogeochemical models to explore its sensitivity to differing ocean dynamics.

The responses of ΔpCO_2 and K to the SAM were very different spatially and temporally. The response of K is instantaneous to changes in wind speed and was largest around the PFZ with the exception of the Pacific Ocean sector that showed a strong response in the SAZ consistent with the spatial pattern of the SAM (Figure 1). Conversely, the response of ΔpCO_2 is complex because the modulation of atmospheric changes by the ocean involves the cascade of energy from shorter to longer wavelengths. This modulation elicited a difference response in each of the components that drive changes in ΔpCO_2 i.e. SST, SSS, TALK and DIC.

Quantifying the importance of the SAM in driving air-sea CO_2 flux variability allowed us to qualitatively compare our results to predictions made by Hall and Visbeck (2002) and Lovenduski and Gruber (2005) on the role of the SAM in driving variability. To compare our results with Lovenduski and Gruber (2005) we recalculated the explained variance with no phase lag and with only the seasonal cycle removed (i.e. interannual + intraseasonal). The result was a reduction in the explained variance from 36% to 27%; consistent with Hall and Visbeck (2002) who suggested the oceanic response to the SAM would be on interannual and longer timescales. This recalculated value (27%) is in agreement with the 'moderate' response of air-sea CO_2 fluxes to the SAM as speculated by Lovenduski and Gruber (2005). The inclusion of the 4-month phase lag and exploring only the interannual-variability-only response nearly doubled the explained variance (47%); in agreement with the predictions of Hall and Visbeck (2002) of a net decrease in CO_2 uptake in response to the positive SAM. These results suggest that the differences between the studies of the Hall and Visbeck (2002) and Lovenduski and Gruber (2005) can be reconciled.

Our simulation showed that Export Production had little impact on the total interannual variability in the air-sea CO_2 flux response to the SAM. While it maybe true that there would be a larger Export Production response in a more complex biological model e.g. with micro-nutrient limitation, for export production to play an important role in offsetting DIC changes in response to the SAM, it would need to be at least two orders of magnitude larger (>100x). The minor role of Export Production relative to ocean physics, suggests that the use of such a model would not significantly alter our results. This weak Export Production response was consistent with the character of the Southern Ocean as a High Nutrient Low Chlorophyll (HNLC) region, i.e. as the pre-existing nutrients are replete, we would not expect an increase in the supply to cause a major increase in primary production.

As the SAM response was primarily driven by DIC supply to the upper ocean, it is suggested that the magnitude of the SAM response would be sensitive to vertical ocean stratification. Current coupled atmospheric-ocean model predictions of climate change suggest that there will be associated changes in vertical stratification at high-latitudes but they lack consensus on the magnitude and sign of this change (Sarmiento et al., 2004). What is not clear is how such changes may impact on the SAM driven oceanic supply of DIC to the upper ocean. As we cannot at present quantify the impact of changes in vertical stratification in response to climate change, this study suggests that based on the predicted behaviour of the SAM, the Southern Ocean will be a region of decreased CO_2 uptake in the future.

5. CONCLUSIONS

The Southern Ocean plays an important role in mitigating climate change by sequestering atmospheric CO_2, the level of which has continued to rise at unprecedented rates as a result of increased anthropogenic activities. The Southern Ocean is a highly variable net sink of atmospheric CO_2, but remains globally the most under-sampled ocean region for quantifying CO_2 uptake. This combination of poor sampling and large variability means that all CO_2 flux estimates contain large uncertainties and hence the carbon budget remains poorly estimated in this region.

To compensate for the lack of Southern Ocean observations, a prognostic, 3D Biogeochemical Ocean General Circulation Model (BOGCM), driven by daily NCEP R1 products, was used to simulate the Southern Ocean carbon cycle. The formulations and implementation of this model were described in detail in Chapter 2. The simulated temperature, salinity, air-sea CO_2 fluxes, ΔpCO_2 and PO_4 fields, were shown in companion with the observations. The model could not perfectly reproduce the limited observations; the model was assessed to be suitable to explore variability in air-sea CO_2 fluxes.

With the goal of reducing uncertainty in Southern Ocean CO_2 uptake, the level of sampling required to constrain the annual net uptake of CO_2 in the Southern Ocean was explored. In developing a sampling strategy, 2D Fourier transforms and signal-to-noise ratios were applied to the daily-simulated air-sea CO_2 fluxes and ΔpCO_2 between 1990-1999. Observations of oceanic pCO_2 from cruise data were used to validate the statistical properties of the model and to estimate the mesoscale variability not captured by the model resolution. The results showed that a sampling strategy of measuring 3-monthly, at every 30° in longitude and 3° in latitude was sufficient to determine the net annual Southern Ocean CO_2 uptake. Testing this strategy on the simulated air-sea fluxes, the net annual mean CO_2 uptake was estimated to be 0.6 ±0.1 PgC/yr (1990-1999).

The estimated uncertainty was dominated by the simulated interannual variability, and not by errors in the sampling or unresolved mesoscale variability. Therefore, sampling at higher resolutions in space and time would not reduce the uncertainty in the Southern Ocean annual mean uptake any further. To evaluate the uncertainty in the present sampling, the latitudinal sampling in the model was doubled to 60° to approximate the current sampling, to estimate an annual mean uptake of 0.6 ±0.2 PgC/yr (1990-1999). This demonstrated that doubling of the present Southern Ocean sampling (in longitude) would be required to constrain the net annual mean air-sea CO_2 fluxes to within the natural variability of the system.

In developing a CO_2 sampling strategy, the importance of interannual variability in driving the large non-seasonal variability in the Southern Ocean was identified. Recent studies have suggested that the Southern Annular Mode (SAM), identified as the leading mode of atmospheric variability, may drive this large interannual variability.

To explore what role the SAM played in driving Southern Ocean CO_2 fluxes between 1980-2000, the simulated the air-sea CO_2 flux and the components that drive this flux i.e. salinity, temperature, TALK, DIC, export production and the gas exchange co-efficient, were regressed against the SAM to quantify the response of each. The results showed that the SAM explained 47% of the variance in the total interannual air-sea CO_2 fluxes in the Southern Ocean (south of 40°S), with a 4-month phase lag. This region displayed decreased CO_2 uptake during the positive SAM phase and increased CO_2 uptake during the negative SAM.

The response of the Southern Ocean to the SAM was governed by changes in ΔpCO_2 and not by changes in the gas exchange co-efficient. Component analyses showed that changes in ΔpCO_2 were due to SAM-induced changes in ocean physics controlling the supply of nutrients, primarily DIC, to the upper ocean. The SAM is predicted to become stronger and more positive in response to climate change and we conclude by suggesting that this would in turn result in a net decrease in Southern Ocean CO_2 uptake.

In concluding this thesis several suggestions can be made regarding future work; these include:

- To allow validation of model data in the Southern Ocean, particularly with reference to interannual variability, at least one long-term CO_2 monitoring station should be commenced in the Southern Ocean and if possible the development of CO_2 sensors on drifters be made a priority.
- The technique developed in Chapter 3 should be applied globally or at least in other regions to develop appropriate sampling strategies that would allow the air-sea CO_2 fluxes to be constrained to within the natural variability of the system.
- Given the importance of DIC in the response of the Southern Ocean air-CO_2 fluxes at the interannual and longer time scales, the study in Chapter 3 should be repeated with a longer term model simulation to determine what sampling is required to constrain and measure longer term variability thus allowing detection of changes against a baseline.
- The study performed in Chapter 4 would be useful to repeat with a suite of BOGCMs such as those run as part of OCMIP3/NOCES with the same atmospheric forcing. Within these simulations it would be of value to explore the strength of SAM response in other ocean models with different physical circulations. This may provide insight on how the ocean may respond to future increases in the SAM.
- The study performed in Chapter 4 should be repeated using a coupled ocean–atmosphere model, run into the future, to explore how predicted changes in vertical stratification may impact on the SAM-driven oceanic supply of DIC to the upper ocean.

- The study in Chapter 4 should be repeated using a control simulation i.e. with fixed pre-industrial CO_2, to explore the role the SAM plays in both natural and anthropogenic CO_2 fluxes.
- Many other drivers of variability potentially capable of inducing large CO_2 interannual variability e.g. changes in heat flux due to volcanic activities, changes in incident radiation and nutrient limitation have not been explored in this thesis and should be pursued and quantified in future studies.

6. BIBLIOGRAPHY

ARGO Science Team. (1998). On the design and implementation of Argo: An initial plan for a global; array of profiling floats. Melbourne, Australia, GODAE International Project Office: 32.

Aumont, O., C. Le Quéré and J. C. Orr (2004). NOCES Project: Interannual HOWTO, http://www.ipsl.jussieu.fr/OCMIP/phase3/simulations/NOCES/HOWTO-NOCES.htm.

*Ballabrera-Poy, J., R. G. Murtugudde, J. R. Christian and A. J. Busalacchi (2003). "Signal-to-noise ratios of observed monthly tropical ocean color." Geophysical Research Letters **30**(12, 1645, doi:10.1029/2003GL016995).*

*Barnola, J., - M., M. Anklin, J. Porcheron, D. Raynaud, J. Schwander and B. Stauffer (1995). "CO_2 evolution during the last millennium as recorded by Antarctic and Greenland ice." Tellus Series B- Physical and Chemical Meteorology **47**: 264-272.*

*Belkin, I. M. and A. L. Gordon (1996). "Southern Ocean fronts from the Greenwich meridian to Tasmania." Journal of Geophysical Research **101**(C2): 3675-3696.*

Boyd, P. W. and S. C. Doney (2004). The Impact of Climate Change and Feedback Processes on the Ocean Carbon Cycle. Ocean Biogeochemistry: The Role of the Ocean Carbon Cycle in Global Change. M. J. R. Fasham, Springer: 157-193.

Bryan, K. (1969). "A Numerical Method for the Study of the Circulation of the World Ocean." Journal of Computational Physics(4): 347-376.

Bryan, K. and L. J. Lewis (1979). "A Water Mass Model of the World Ocean." Journal of Geophysical Research **84**: *2503-2517.*

Cai, W., P. Whetton and D. J. Karoly (2003). "The response of the Anatrctic Oscillation to increasing and stablized CO_2*."* Journal of Climate **10**: *1525-1538.*

Chaigneau, A., R. A. Morrow and S. R. Rintoul (2004). "Seasonal and Interannual evolution of the mixed layer in the Antarctic Zone south of Tasmania." Deep-Sea Research Part I, **51**(12):2047-2072

Chen, D., L. M. Rothestein and A. J. Busalacchi (1994). "A Hybrid Vertical Mixing Scheme and Its Application to Tropical Ocean Models." Journal of Physical Oceanography **24**: *2156-2179.*

Conkright, M. E., J. I. Antonov, O. Baranova, T. P. Boyer, H. E. Garcia, R. Gelfeld, D. Johnson, R. A. Locarnini, P. P. Murphy, T. D. O'Brien, I. Smolyar and C. Stephens (2002). World Ocean Database 2001. NOAA Atlas. *S. Levitus. Washington DC, US Government Printing Office.* **NESDIS 42:** *167pp.*

Conkright, M. E., J. L. Antonov, O. Baranova, T. P. Boyer, H. E. Garcia, R. Gelfeld, D. D. Johnson, R. A. Locarnini, P. P. Murphy, T. D. O'Brien, I. Smolyar and C. Stephens (2002). World Ocean Database 2001. NOAA Atlas, NESDIS 42. *S. Levitus. Washington, D. C., U. S. Government Printing Office.* **1: Introduction:** *167.*

Copin-Montégut, C. (1989). "Corrigendum to Copin-Montégut 1988 A New Formula for the Effect of Temperature on the partial pressure of CO_2 *in seawater."* Marine Chemistry **27**(27): *143-144.*

Copin-Montégut, C. (1988). "A new formula for the effect of temperature on the partial pressure of CO_2 in seawater." Marine Chemistry **25***(29-37).*

Cox, M. D. (1984). A primative equations, three dimensional model of the ocean. Princeton., N. J., GFDL: 143.

Cunningham, S. A., S. G. Alderson, B. A. King and M. A. Brandon (2003). "Transport and variability of the Antarctic Circumpolar Current in Drake Passage." Journal of Geophysical Research-Oceans **108***(C5): -.*

Dickson, A. G. and C. Goyet (1994). Handbook of methods for the analysis of the various parameters ofthe carbon dioxide system in sea water, US Department of Energy.

Doney, S. C., K. Lindsay, K. Caldiera, J.-M. Campin, H. Drange, J.-C. Dutay, M. Folllows, Y. Gao, A. Gnanadeskian, N. Gruber, A. Ishida, F. Joos, G. Madec, E. Maier-Reimer, J. C. Marshall, R. J. Matear, P. Monfray, A. Mouchet, R. G. Najjar, J. C. Orr, G.-K. Plattner, J. L. Sarmiento, R. Schlitzer, R. Slater, I. J. Totterdell, M.-F. Weirig, Y. Yamanaka and A. Yool (2004). "Evaluating global ocean carbon models: The importance of realistic physics." Global Biogeochemical Cycles **18***(GB3017): doi:10.1029/2003GB002150.*

Dutay, J.-C., J. L. Bullister, S. C. Doney, J. C. Orr, R. G. Najjar, K. Caldiera, J.-M. Campin, H. Drange, M. Follows, Y. Gao, N. Gruber, M. W. Hecht, A. Ishida, F. Joos, K. Lindsay, G. Madec, E. Maier-Reimer, J. C. Marshall, R. J. Matear, P. Monfray, A. Mouchet, G.-K. Plattner, J. L. Sarmiento, R. Schlitzer, R. Slater, I. J. Totterdell, M.-F. Weirig, Y. Yamanaka and A. Yool (2002). "Evaluation of ocean model ventilation with CFC-11: comparsion of 13 global ocean models." Ocean Modelling **4***: 89-120.*

England, M. H. (1995). "The age of water and ventilation timescales in a global ocean model." Journal of Physical Oceanography **25**: *2756-2777.*

Enting, I. G., M. L. Wigley and M. Heimann (1994). Future Emissions and concentrations of carbon dioxide: key ocean/ atmosphere/ land analyses. CSIRO Australian Division of Atmospheric Research Techinical Paper 31*: 118.*

Eppley, R. W. (1972). "Temperature and phytoplankton growth in the sea." Fish. Bull. U.S. **70**: *1063-1085.*

Etheridge, D. M., L. P. Steele, R. L. Langefelds, R. J. Francey, J. Barnola, - M. and V. Morgan, I. (1996). "Natural and anthropogenic changes in atmospheric CO_2over the last 1000 years from air in Anatrctic ice and firn." Journal of Geophysical Research **101**: *4115-4128.*

Francey, R. J., L. P. Steele, D. A. Spencer, R. L. Langefelds, R. M. Law, P. B. Krummel, P. J. Fraser, D. M. Etheridge, N. Derek, S. A. Coram, L. N. Cooper, C. E. Allison, L. Porter and S. Baly, Eds. (2003). The CSIRO (Australia) Measurement of Greenhouse Gases in the Global Atmosphere*. Baseline Atmospheric Program Australia 1999-2000. Melbourne, Australia, Bureau of Meteorology and CSIRO Atmospheric Research.*

Friedlingstein, P., J. L. Dufresne, P. Cox and P. J. Rayner (2003). "How positive is the feedback between climate change and the carbon cycle?" Tellus B*: 672-700.*

Garcia, H. E. and L. I. Gordon (1992). "Oxygen solubility in seawater: Better fitting equations." Limnology and Oceanography **37**: *1307-1312.*

*Garçon, V., F. Thomas, C. S. Wong and J.-F. Minster (1992). "Gaining insight into the seasonnal variability of CO_2 at ocean station P using an upper ocean model." Deep-Sea Research **39**: 921-938.*

*Gent, P. R. and J. C. McWilliams (1990). "Isopynal Mixing in Ocean Circulation Models." Journal of Physical Oceanography **20**: 150-155.*

*Gerdes, R., C. Koberle and J. Willebrand (1991). "The Influence of Numerical Advection Schemes on the Results of Ocean General Circulation Models." Climate Dynamics **5**: 211-226.*

Godfrey, J. S. and A. Schiller (1997). Tests of mixed-layer schemes and surface boundary conditions in an Ocean General Circulation Model, using the IMET flux data set, CSIRO Australia.

*Gong, D. and S. Wang (1999). "Definition of the Antarctic oscillation index." Geophysical Research Letters **26**: 459-462.*

Gordon, H. B., L. D. Rotstayn, J. L. McGregor, M. R. Dix, E. A. Kowalczyk, S. P. O'Farrell, L. J. Waterman, A. C. Hirst, S. G. Wilson, M. A. Collier, I. G. Watterson and T. I. Elliot (2002). The CSIRO Mk3 Climate System Model. Aspendale, Australia, CSIRO Atmospheric Research: 134.

*Gould, J., D. H. Roemmich, S. E. Wijffels, H. Freeland, M. Ignazewsky, X. Jianping, S. Pouliquen, Y. Desaubies, U. Send, R. K., K. Takeuchi, K. Kim, M. Danchenkov, P. Sutton, B. King, B. Owens and S. Riser (2004). "Argo Profiling Floats Bring New Era of In Situ Ocean Observations." EOS **85**(19).*

*Griffies, S. M. (1998). "The Gent-McWillams Skew Flux." Journal of Physical Oceanography **28**: 831-841.*

Griffies, S. M., C. Boning, F. O. Bryan, E. P. Chassignet, R. Gerdes, H. Hasumi, A. C. Hirst, A.-M. Treguier and D. Webb (2000). "Developments in ocean climate modelling." Ocean Modelling II: 123-192.

*Gruber, N., C. D. Keeling and N. R. Bates (2002). "Interannual Variability in the North Atlantic Ocean Carbon Sink." Science **298** (20 December 2002).*

*Gruber, N. and J. L. Sarmiento (2002). "Sinks for anthropogenic carbon." Physics Today, **August 2002**: 30-36*

*Hall, A. and M. Visbeck (2002). "Synchronous variability in the Southern hemisphere Atmosphere, Sea Ice, and Ocean Resulting from the Annular Mode." Journal of Climate **15**: 3043-3057.*

*Hirst, A. C., S. P. O'Farrell and H. B. Gordon (2000). "Comparison of a coupled ocean-atmosphere model with and without oceanic eddy-induced advection. Part I: Ocean spinup and control integrations." Journal of Climate **13**(1): 139-163.*

*Jabaud-Jan, A., N. Metzl, C. Brunet, A. Poisson and B. Schauer (2004). "Interannual varaibility of the carbon dioxide system in the southern Indian Ocean (20°-60°S): the impact of a warm anomaly in the austral summer 1998." Global Biogeochemical Cycles **18**(1): GB1042,10.1029/2002GB002017.*

*Kalnay, E. (1996). "The NCEP/NCAR 40-year reanalysis project." Bulletin of the American Meteorological Society **77**(3): 437-470.*

*Kanamitsu, M., E. Ebisuzaki, J. Woollen, S.-K. Yang, J. J. Hnilo, M. Fiorino and G. L. Potter (2002). "NCEP-DOE AMIP-II Reanalysis (R-2)." Bulletin of the American Meteorological Society **November**: 1631-1643.*

Keeling, R. F., B. B. Stephens, R. G. Najjar, S. C. Doney, D. Archer and M. Heimann (1998). "Seasonal variations in the atmospheric O-2/N-2 ratio in relation to the kinetics of air-sea gas exchange." Global Biogeochemical Cycles **12**(1): 141-163.

Keeling, R. F. and T. P. Whorf (2003). Atmospheric CO_2 Concentrations--Mauna Loa Observatory, Hawaii, 1958-2002 (revised July 2003), http://cdiac.esd.ornl.gov/ndps/ndp001.html *Carbon Dioxide Information and Analysis Center, Oak Ridge, TN.*

Körtzinger, A., L. Mintrop, D.W.R. Wallace, K.M. Johnson, C. Neill, B. Tilbrook, P. Towler, H.Y. Inoue, M. Ishii, G. Shaffer, R.F. Torres Saavedra, E. Ohtaki, E. Yamashita, A. Poisson, C. Brunet, B. Schauer, C. Goyet and G. Eischeid (2000). The International At-sea Intercomparison of fCO_2 Systems during the R/V Meteor Cruise 36/1 in the North Atlantic Ocean, Marine Chemistry **72**: 171 - 192.

Kraus, E. B. and J. S. Turner (1967). "A one-dimensional model of the seasonal thermocline." Tellus Part II **81**: 98-105.

Kushner, P. J., I. M. Held and T. L. Delworth (2001). "Southern Hemisphere Atmospheric Circulation Response to Global Warming." Journal of Climate **14**: 2238-2249.

Le Quéré, C., J. C. Orr, P. Monfray and O. Aumont (2000). "Interannual variability of the oceanic sink of CO_2 from 1979 through 1997." Global Biogeochemical Cycles **14**(4): 1247-1265.

Lefebvre, W., H. Goosse, R. Timmerman and T. Fichefet (2004). "Influence of the Southern Annular Mode on the sea-ice system." Journalof Geophysical Research **109**(C09005, doi:10.1029/2004JC002403).

Leonard, B. P. (1979). "A Stable and Accurate Convective Modelling Procedure based on Quadratic Upstream Interpolation." Computer Methods in Applied Mechanics and Engineering ***19****: 59-98.*

Levitus, S., J. L. Antonov, T. P. Boyer and C. Stephens (2000). "Warming of the World Ocean." Science ***287****(24 March 2000): 2225-2229.*

Louanchi, F. and M. Hoppema (2000). "Interannual variations of the Antarctic Ocean CO_2 uptake from 1986 to 1994." Marine Chemistry ***72****: 103-114.*

Louanchi, F., M. Hoppema, D. C. E. Bakker, A. Poission, M. H. C. Stoll, H. De Baar, J. W., B. Schauer, Ruiz-Pino and D. Wolf-Gladrow (1999). "Modelled and observed sea surface fCO_2 in the southern ocean: a comparative study." Tellus ***51B****: 541-559.*

Lovenduski, N. S. and N. Gruber (2005). "Impact of the Southern Annular Mode on Southern Ocean Circulation and Biology." Geophysical Research Letters ***32****(L11603, doi:10.0129/2005GL022727).*

Mahadevan, A., M. Levy and L. Memery (2004). "Mesoscale variability of sea surface pCO_2: What does it respond to?" Global Biogeochemical Cycles ***18****(1017).*

Marland, G., T. A. Boden and R. J. Andres (2005). Global, Regional, and National CO2 Emissions*. Oak Ridge, Tenn., USA, Carbon Dioxide Inf. Ann. Cent.*

Marshall, G. J. (2002). "Trends in Antarctic geopotential height and temperature: A comparsion between radiosonde and NCEP-NCAR reanalysis." Journal of Climate ***15****: 659-674.*

Marsland, S. J., N. L. Bindoff, W. G. D. and W. F. Budd (2004). "Modelling water mass formation in the Mertz Glacier Polynya and Adelie Depression." Journal of Geophysical Research ***109****(C11003): doi:10.1029/2004JC002441.*

Martin, J. H., G. A. Knauer, D. M. Karl and W. W. Broenkow (1987). "VERTEX: Carbon Cycling in the northeast Pacific." Deep-Sea Research ***34****: 267-286.*

Matsumoto, K., J. L. Sarmiento, R. M. Key, O. Aumont, J. L. Bullister, K. Caldeira, J.-M. Campin, S.C. Doney, H. Drange, J.-C. Dutay, M. Follows, Y. Gao, A. Gnanadesikan, N. Gruber, A. Ishida, F. Joos, K. Lindsay, E. Maier-Reimer, J. C. Marshall, R. J. Matear, P. Monfray, A. Mouchet, R. Najjar, G.-K. Plattner, R. Schlitzer, R. Slater, P. S. Swathi, I. J. Totterdell, M.-F. Weirig, Y. Yamanaka, A. Yool and J. C. Orr (2004) "Evaluation of ocean carbon cycle models with data-based metrics", Geophysical Research Letters ***31****, doi:10.1029/2003GL018970*

Matear, R. J. (2004). Ocean carbon cycle in a changing climate: climate change detection. The Ocean Carbon Cycle and Climate*. M. Follows and T. Oguz. Netherlands, Kluwer Academic Press.* ***40:*** *297-315.*

Matear, R. J. and A. C. Hirst (1999). "Climate change feedback on the future oceanic CO_2 uptake." Tellus ***51B****: 722-733.*

McKinley, G. A., C. Rodenbeck, M. Gloor, S. Houweling and M. Heimann (2004). "Pacific dominance to global air-sea CO2 flux variability: A novel atmospheric inversion agrees with ocean models." Geophysical Research Letters ***31****(22): -.*

*McNeil, B. I., R. J. Matear, R. M. Key, J. L. Bullister and J. L. Sarmiento (2003). "Anthropogenic CO2 uptake by the ocean based on the global chlorofluorocarbon data set." Science **299**(5604): 235-239.*

Metzl, N., C. Brunet, J.-J. A., A. Poisson and B. Schauer (2006). "Summer and Winter Air-Sea CO_2 Fluxes in the Southern Ocean." Deep-Sea Research II, in press

*Metzl, N., A. Poission, F. Louanchi, C. Brunet, B. Schauer and B. Bres (1995). "Spatio-temporal distributions of air-sea fluxes of CO_2 in the Indian and Antarctic Oceans: A first step." Tellus **47B**: 56-69.*

*Metzl, N., B. Tilbrook and A. Poisson (1999). "The annual fCO2 cycle and the air-sea CO2 flux in the sub-Antarctic Ocean." Tellus **51B**: 849-861.*

Murray, J. W., Ed. (2004). Ocean Carbonate Chemistry: The Aquatic Chemistry Fundamentals. NATO Science Series, Kluwer Academic Publishers.

*Mémery, L., M. Levy, S. Verant and L. Merlivat (2002). "The relevant time scales in estimating the air-sea CO2 exchange in a mid-latitude region." Deep-Sea Research Part Ii-Topical Studies in Oceanography **49**(11): 2067-2092.*

Najjar, R. and J. Orr (1998). Design of the OCMIP-2 simulations of chlorofluorocarbons, the solubility pump and common biogeochemistry. http://www.ipsl.jussieu.fr/OCMIP/.

Netfel, A., H. Friedli, E. Moor, H. Loctscher, H. Oeschger, U. Siegenthaler and B. Stauffer (1995). HIstorical CO2 record from the Siple ice core. Trends '93: A Compendium of Data on Climate Change. T. A. Boden, D. P. Kaiser, R. J. Sepanski and F. W. Stoss. Oak Ridge, Carbon Dioxide Inf. Anal. Cent: 11-14.

Nightingale, P. D., G. Malin, L. C. S., A. J. Watson, P. S. Liss, M. I. Liddicoat, J. Boutin and R. C. Upstill-Goddard (2000). "In-situ evaluation of air-sea gas exchange parameterizations using novel conservative and volatile tracers." Global Biogeochemical Cycles ***14***: *313-387.*

NOAA (1988). Digital Relief of the Surface of the Earth, Data Announcement 88-MG-02, National Geophysical data Center, Boulder, Colorado, U.S.A.

NOAA (2005). NCEP/NCAR Reanalysis 1: http://www.cdc.noaa.gov/cdc/data.ncep.reanalysis.html.

Obata, A. and Y. Kitamura (2003). "Interannual variability of the sea-air exchange of CO2 from 1961 to 1998 simulated with a global ocean circulation-biogeochemistry model." Journal of Geophysical Research-Oceans ***108***(C11): -.

Oke, P. and M. H. England (2004). "Oceanic Response to Changes in the Latitude of the Southern Hemisphere Subpolar Westerly Winds." Journal of Climate ***17***: *1040-1054.*

Orr, J. C., O. Aumont, L. Bopp, S. C. Doney, V. J. Fabry, R. A. Feely, M. Folllows, A. Gnanadeskian, A. Ishida, F. Joos, R. M. Key, K. Lindsay, E. Maier-Reimer, R. J. Matear, P. Monfray, A. Mouchet, R. G. Najjar, G.-K. Plattner, C. L. Sabine, J. L. Sarmiento, R. Schlitzer, R. Slater, I. J. Totterdell, M.-F. Weirig, Y. Yamanaka and A. Yool (2005). "Anthropogenic ocean acidification over the twenty first century and its impacts on calcifying organisms." Nature ***437***(29 September).

Orsi, A. H., T. Whitworth and W. D. Nowlin (1995). "On the meridional extent and fronts of the Antarctic Circumpolar Current." Deep-Sea Research I ***42***(5): *641-673.*

Pacanowski, R. C. (1996). The MOM 2 Version 2, Documentation, User's Guide and Reference Manual, GFDL/NOAA, Princeton, USA.

Pacanowski, R. C. and S. M. Griffies (1999). The MOM 3 Manual. NOAA/Geophysical Fluid Dynmaic Laboratory Technical Report No. 4. Princeton, USA.

Pacanowski, R. C. and S. G. H. Philander (1981). "Parametrization of Vertical Mixing in Numerical Models of Tropical Oceans." Journal of Physical Oceanography ***11****: 1443-1451.*

Peylin, P., P. Bousquet, C. Le Quéré, S. Sitch, P. Friedlingstein, G. McKinley, N. Gruber, P. J. Rayner and P. Ciais (2005). "Multiple constrains on regional CO2 flux variations over land and oceans." Global Biogeochemical Cycles ***19****(GB1011): doi:10.1029/2003GB002214.*

Prentice, I. C., G. D. Farquhar, M. J. R. Fasham, M. L. Goulden, M. Heinmann, V. J. Jaramillo, H. S. Kheshgi, C. Le Quéré, R. J. Scholes, D. W. R. Wallace and co-authors (2001). The carbon cycle and atmospheric CO_2. Climate change; the scientific basis, the contribution of WGI of the IPCC to the IPCC Third Assesment Report (TAR). J. T. Houghton and D. Yihui. Cambridge, UK, Cambridge University Press.

Price, J., R. Weller and R. Pinkel (1986). "Diurnal cycling: observations and models of upper ocean response to diurnal heating, cooling and wind mixing." Journal of Geophysical Research ***91****: 8411-8427.*

Rayner, P. J., I. G. Enting, R. J. Francey and R. Lagenfelds (1999). "Reconstructing the recent carbon cycle from atmospheric CO_2, delta^{13}C and O_2/N_2 observations." Tellus ***51B****: 213-232.*

Redfield, A., B. Ketchum and F. Richards (1963). The influence of organisms on the composition of the sea water. The Sea. *M. Hill. New York, Interscience.* **2:** *26-77.*

Redi, M. H. (1982). "Ocean Isopycnal Mixing by Coordinate Rotation." Journal of Physical Oceanography **12***(1154-1158).*

Reynolds, R. W. and T. M. Smith (1994). "Improved global sea surface temperature analyses using optimal interpolation." Journal of Climate **7***: 929-948.*

Rintoul, S. R., C. W. Hughes and D. Olbers (2001). The Antarctic Circumpolar Current System. Ocean Circulation and Climate. *S. G., J. Church and J. Gould. Barcelona, Academic Press. 77.*

Rintoul, S. R. and T. W. Trull (2001). "Seasonal evolution of the mixed layer in the Subantarctic Zone south of Australia." Journal of Geophysical Research **106***(C12): 31,447-31,462.*

Rogers, J. C. and H. van Loon (1982). "Spatial variability of sea level pressure and 500mb height anomalies over the Southern Hemisphere." Monthly Weather Review **110***(1375-1392).*

Roy, T., P. J. Rayner, R. J. Matear and R. Francey (2003). "Southern hemisphere ocean CO_2 uptake: reconciling atmospheric and oceanic estimates." Tellus **55B***: 701-710.*

Rödenbeck, C. S., S. Houweling, M. Gloor and M. Heimann (2003). "CO_2 flux history 1982-2001 infered from atmospheric data using a global inversion of atmospheric transport." Atmospheric Chemistry and Physics **3***: 1919-1964.*

*Sabine, C. L., R. A. Feely, N. Gruber, J. L. Bullister, R. Wanninkhof, C. S. Wong, D. W. R. Wallace, B. Tilbrook, F. J. Millero, T.-H. Peng, A. Kozyr, T. Ono and A. F. Rios (2004). "The Oceanic Sink for Anthropogenic CO_2." Science **305**: 367-371.*

*Sabine, C. L. and R. M. Key (1998). "Controls on f(CO2) in the South Pacific." Marine Chemistry **60**(1-2): 95-110.*

*Sarmiento, J. L., N. Gruber, M. A. Brzezinski and J. P. Dunne (2004). "High-latitude Controls of Thermocline Nutrients and Low Latitude Biological Productivity." Nature **427**: 56-60.*

*Sarmiento, J. L., R. Slater, R. T. Barber, L. Bopp, S. C. Doney, A. C. Hirst, J. Kleypas, R. J. Matear, U. Miklolajewicz, P. Monfray, V. Soldatov, S. A. Spall and R. Stouffer (2004). "Response of Ocean Ecosystems to Climate Warming." Global Biogeochemical Cycles **18**(GB3003): doi:10.1029/2003GB002134.*

*Schiller, A., S. E. Wijffels and G. A. Meyers (2004). "Design requirements for an Argo Float Array in the Indian Ocean inferred from observing system simulation experiments." Journal of Atmospheric and Oceanic Technology **21**(10): 1598-1620.*

*Siegenthaler, U. and J. L. Sarmiento (1993). "Atmospheric carbon dioxide and the ocean." Nature **365**: 119-125.*

*Sloyan, B. M. and S. R. Rintoul (2001). "Circulation, Renewal and Modification of Antarctic Mode and Intermediate Water." **Journal of Physical Oceanography** **31**(4):1005-1030*

*Sokolov, S. and S. R. Rintoul (2002). "Structure of Southern Ocean fronts at 140E." Journal of Marine Systems **37**: 151-184.*

*Speer, K. G., S. R. Rintoul and B. M. Sloyan (2000). "The Diabatic Deacon Cell." Journal of Physical Oceanography **30**: 3212-3222.*

Suess, E. (1980). "Particulate organic carbon flux in the ocean-surface, productivity and oxygen utilization." Nature(280): 260-263.

Sweeney, C., T. Takahashi, A. Gnanadeskian, R. Wanninkhof, R. A. Feely, G. Friedrich, F. Chaves, N. Bates, J. Olafsson and J. L. Sarmiento (2002). Spatial and Temporal Variability of Surface Water pCO_2 and Sampling Strategies (Appendix D). A Large-Scale CO_2 Observing Plan: In Situ Oceans and Atmosphere (LSCOP).

Sweeney, C., T. Takahashi, R. Wanninkhof (2000) Spatial and temporal variability of surface water pCO2 and sampling strategies. Report prepared for the NOAA Advisory Meeting for Sea-air CO2 Flux Program, October 8-10, Boulder, Colorado

*Takahashi, T., R. A. Feely, R. F. Weiss, R. H. Wanninkhof, D. W. Chipman, S. C. Sutherland and T. T. Takahashi (1997). "Global air-sea flux of CO_2: An estimate based on measurements of sea-air pCO_2 difference." Proceedings of the National Academy of Sciences of the United States of America **94**(16): 8292-8299.*

*Takahashi, T., S. C. Sutherland, C. Sweeney, A. Poisson, N. Metzl, B. Tilbrook, N. Bates, R. Wanninkhof, R. A. Feely, C. Sabine, J. Olafsson and Y. Nojiri (2002). "Global sea-air CO2 flux based on climatological surface ocean pCO2 and seasonal biological and temperature effects." Deep-Sea Research II **49**(1601-1622).*

Takahashi, T. and C. Sweeney (2002). Errors in Sea-Air CO2 Flux Due to Time-Space Ocean Sampling Strategies for Sea-Air pCO2 Difference. A Large-Scale CO2 Observing Plan: In Situ Oceans and Atmosphere (LSCOP).

*Thompson, D. W. J. and S. Solomon (2002). "Interpretation of Recent Southern Hemisphere Climate Change." Science **296**(3 May).*

Tilbrook, B. (2005). Observational measurements of pCO_2 in the Australian Sector of the Southern Ocean, CSIRO Marine and Atmospheric Research.

*Trull, T. W., S. G. Bray, S. J. Manganini, S. Honjo and R. Francois (2001). "Moored sediment trap measurements of carbon export in the Subantarctic and Polar Frontal Zones of the Southern Ocean, soth of Australia." Journal of Geophysical Research **106**(C12): 31489-31509.*

*Trull, T. W., S. G. Bray, S. J. Manganini, S. Honjo, and R. Francois (2001). Moored sediment trap measurements of carbon export in the Subantarctic and Polar Frontal Zones of the Southern Ocean, south of Australia, Journal of Geophysical Research, **106**, 31489-31509*

*Trull, T. W., S. R. Rintoul, M. Hadfield and E. R. Abraham (2001). "Circulation and seasonal evolution of polar waters south of Australia: Implications for iron fertilizations for the Southern Ocean." Deep-Sea Research II **48**: 2439-2466.*

Visbeck, M. and A. Hall (2004). "Reply." Journal of Climate.

Volk, T. and M. I. Hoffert (1985). "Ocean Carbon Pumps: Analysis of relative strenghts and efficencies in ocean-driven circulation."

Walsh, J. (1978). A data set on northern hemisphere sea ice extent, 1953-1976, Glaciological Data, World Data Center for Glaciology (Snow and Ice).

Wang, X. and R. J. Matear (2001). "Modeling the upper ocean dynamics in the Subantarctic and polar Frontal Zones in the Australian sector of the Southern Ocean." Journal of Geophysical Research ***106****(C12): 31511-31524.*

Wanninkhof, R. (1992). "Relationship between wind speed and gas exchange over the ocean." Journal of Geophysical Research ***97****(C5): 7373-7382.*

Watson, A. J. and J. C. Orr (2003). Carbon Dioxide Fluxes in the Global Ocean. Ocean Biogeochemistry: The Role of the Ocean carbon Cycle in Global Change. M. J. R. Fasham. Heidelberg, Springer.

Weiss, R. F. and B. A. Price (1980). "Nitrous Oxide Solubility in Water and Seawater." Marine Chemistry ***8****: 347-359.*

Wetzel, P., A. Winguth and E. Maier-Reimer (2005). "Sea-to-air CO2 flux from 1948 to 2003: A model study." Global Biogeochemical Cycles ***19****(2): -.*

Yamanaka, Y. and E. Tajika (1996). "The role of vertical fluxes of particulate organic material and calcite in the oceanic carbon cycle: Studies using a ocean biogeochemical general; circulation model." Global Biogeochemical Cycles ***10****: 361-382.*

Zwally, H. J., C. J., C. Parkinson, W. Campbell, F. Carsey and P. Gloerson (1983). Antarctic Sea Ice, 1973-1976: Satellite Passive Microwave Observations, NASA.